# First International MRE Workshop in Berlin

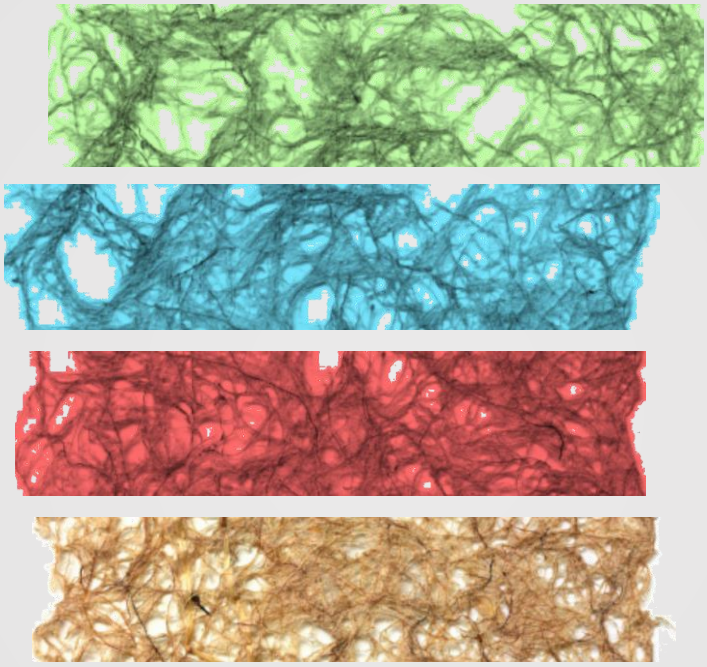

Charité Berlin, Germany

September 28-29, 2017

Program

Illustration on front page: Tissue III, taken from Ursi Schiegnitz (Moos)

# International MRE workshop, September 28-29, 2017

# 1st meeting in Berlin, Germany

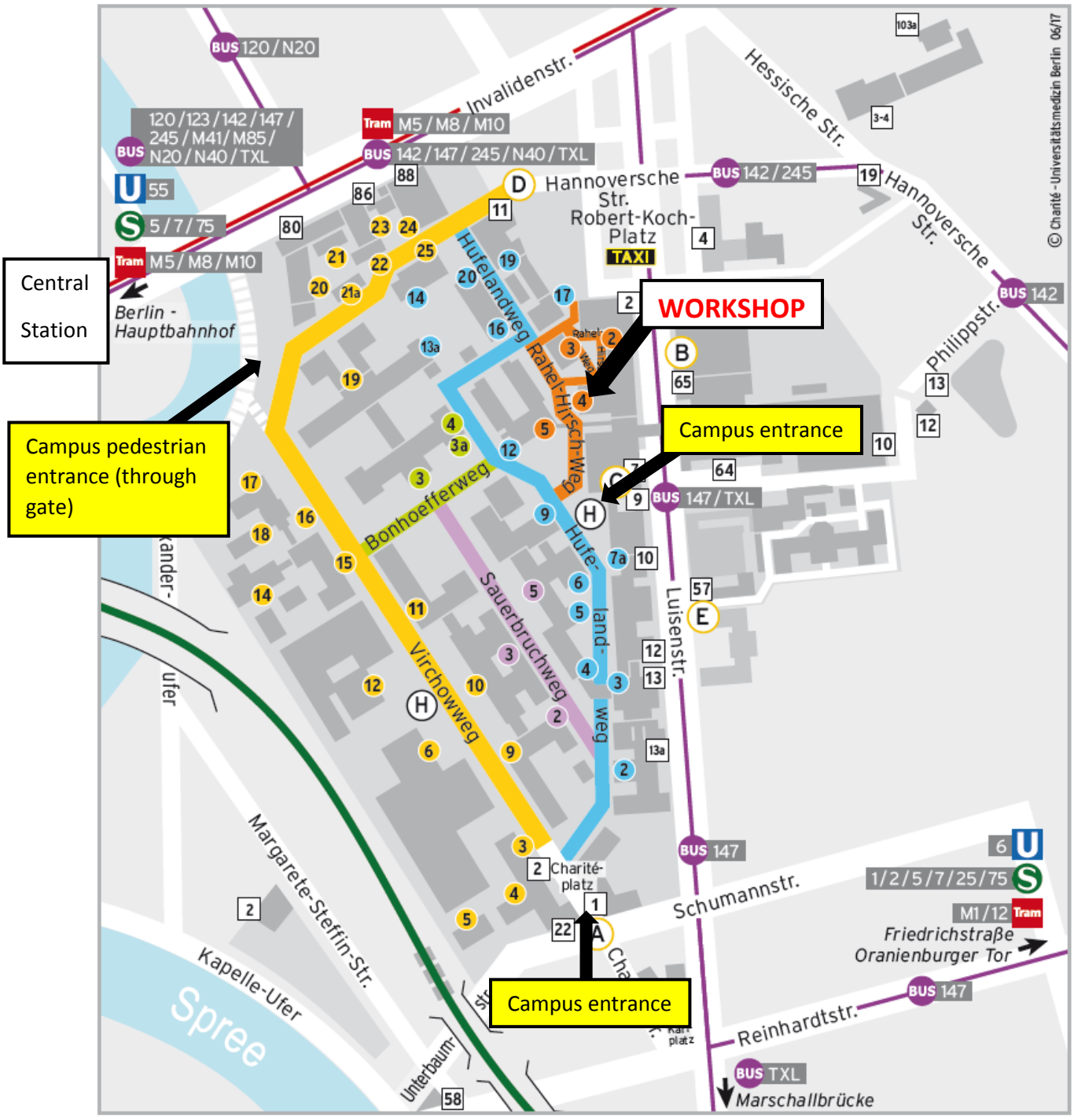


Charité Campus Mitte,

Rahel-Hirsch-Weg 4,

Workshop registration: 3th Floor (‘Ebene 4’ in Charité concepts)

Lecture Hall of Dermatology Clinic (‘Hautklinik’)

Take the stairs on the right after entering the building

**The first MRE International Workshop in Berlin is sponsored by:**




# Table of contents

# Foreword

Dear workshop participant,

A warm welcome to the first international MRE workshop, which we are very glad to host here at Charité – Universitätsmedizin Berlin! This event is organized by members of the MRE study group of the International Society for Magnetic Resonance in Medicine (ISMRM) to bring together researchers interested in MR elastography, medical imaging and biophysics to stimulate their exchange of knowledge, ideas and experiences. The realm of elastography is an exciting field of research that has emerged over the past years into a cutting-edge modality for both clinical scientists who seek quantitative biomarkers to improve diagnosis and basic scientists who strive to translate mechanobiology into a new in-vivo imaging contrast. The success of MRE wouldn't have been possible without the tireless commitment of countless engineers, computer scientists, physicists and mathematicians worldwide who developed MR elastography into a reproducible, high-resolution imaging modality for biophysical parameter mapping. Still, many challenges remain, in areas including but not limited to tissue anisotropy, moving organs, poroelastic properties, MRE sequences, optimization of and/or new approaches for actuators and image processing routines, etc. In the next couple of days some of these topics will be presented; and we hope our workshop will contribute to basic and clinical translational research to advance MRE technology and provide higher precision, better reproducibility, and improved clinical applicability.

Our workshop embraces scientists from different fields – as reflected by the multidisciplinarity of MRE – however, we particularly welcome young scientists who bear the enthusiasm and fresh thinking of next-generation MRE experts! Therefore, we are happy to continue with our workshop after the first BIOQIC day, which will be held on Wednesday Sept-27. BIOQIC Day gathers the first cohort of PhD students of the newly established research training group (Graduiertenkolleg) BIOphysical Quantitative Imaging towards Clinical diagnosis. Many of these young scientists have overlapping research interests with MRE. Since BIOQIC focusses on quantitative and biophysical measurements of soft-tissue properties, MRE delivers one very important class of parameters which is related to the mechanical interactions within tissues across multiple scales. We are looking forward to stimulating talks, discussions and demonstrations of how mechanical tissue interactions can be turned into a quantitative, physics-based imaging contrast. The biological and biophysical foundations of this new contrast will be highlighted by our keynote lecturers Kristian Franze (Thursday) and Paul Janmey (Friday). Many thanks to both of them and to all other presenters who together will create a stimulating and open atmosphere for scientific exchange during our workshop. We are confident that this spirit will further shape our field into a unique and versatile scientific landscape of manifold disciplines from math to diagnostic medicine.

To make your stay in Berlin an unforgettable event, we invite you to the museum of natural history, for a special guided tour on Wednesday, Sep-27, right after the BIOQIC presentations. On Thursday, Sept-28, all participants are cordially invited for a complimentary buffet dinner offered in the Swiss ambiance of the restaurant Nola's am Weinberg. Live music will be played by the Acoustic Image Quartet, which at least by its name, has ties to our field of research. We hope that you will enjoy the first international MRE workshop, that you receive many fresh ideas, and that you have stimulating discussions with new and established colleagues from many countries around the world!

The organizers

Ingolf Sack
Judith Bergs
Dieter Klatt
Curtis Johnson
Armando Manduca
Arunark Kolipaka
Ziying Yin

# Program - First International MRE workshop, Charité – Berlin

## Thursday 28/09/2017

| | |
|---|---|
| **8:30-9:00** | Welcome and introduction – Ingolf Sack / Judith Bergs |
| **9:00-9:45** | Keynote lecture by Kristian Franze - Brain mechanics controls neuronal growth<br>*University of Cambridge, Cambridge, UK* |
| **9:45-10:00** | **Coffee break** |
| **10:00-10:30** | Opening talk - Armando Manduca - MR elastography: standardizing terminology and setting guidelines<br>*Mayo Clinic, Rochester, USA* |
| **10:30-10:45** | Mathilde Bigot et al. - New 3D-printed elastography bench for MR study of engineered tissue and histology<br>*CREATIS – site CPE, Villeurbanne, France* |
| **10:45-11:00** | Darryl Hwang et al - MREAnaylsis: Software for ROI Stiffness Quantification and Reporting<br>*University of Southern California, Los Angeles, USA* |
| **11:00-11:30** | **Coffee break - posters and demonstrations** |
| **11:30-11:45** | Itamar Terem et al. - Revealing sub-voxel motions of brain tissue using phase-based Amplified MRI<br>*Stanford University, Palo Alto, USA* |
| **11:45-12:00** | Cristobál Bertoglio et al. - Robust flow reconstruction and quantitative post-processing from Phase-Contrast MRI<br>*Johann Bernoulli Institute, University of Groningen, Groningen, The Netherlands* |
| **12:00-12:15** | Pauline Lefebvre et al. - Optimal control theory applied to MR Elastography<br>*CREATIS, Villeurbanne, France* |
| **12:15-12:30** | Simon Chatelin et al. - Identification of the viscoelastic properties in magnetic resonance elastography by coupling a finite element model and a gradient method<br>*ICube, University of Strasbourg – CNRS, Strasbourg, France* |
| **12:30-13:30** | **Lunch break** |
| **13:30-13:45** | Daniel Fovargue et al. - Heterogeneous Multifrequency Direct Inversion in MR Elastography: A Preliminary Comparison of Finite-Difference and Finite-Element Based Approaches<br>*King's College London, London, UK* |
| **13:45-14:00** | Matthew McGarry et al. - Reconstruction of high-resolution MR elastography motion data using nonlinear inversion<br>*Thayer School of Engineering at Dartmouth, Hanover, USA* |
| **14:00-14:15** | Cemre Arıyürek et al. - OSS-Weighted Averaging in Multifrequency Inversion for MR Elastography<br>*National Magnetic Resonance Research Center, Bilkent University, Ankara, Turkey* |
| **14:15-14:30** | Elijah Van Houten et al. - Power-Law Multi-Frequency MR Elastography of the human brain via Non-Linear Inversion Reconstruction<br>*Université de Sherbrooke, Québec, Canada* |
| **14:30-15:00** | **Coffee break - posters and demonstrations** |
| **15:00-15:15** | Keith Paulsen - Spatially Resolved Damping Ratio Imaging with Non-Linear Inversion MRE in Gel-Tofu Phantoms<br>*Thayer School of Engineering at Dartmouth, Hanover, USA* |

| | |
|---|---|
| **15:15-15:30** | Anthony Romano et al. - Mild TBI Studies Using Mixed Model Inversions *Naval Research Laboratory, Washington, DC, USA* |
| **15:30-15:45** | Helen Marshall - Magnetic Resonance Elastography (MRE) Reproducibility Study in the Same Participants at Field Strengths of 1.5 , 3 and 7 Tesla<br>*University of Edinburgh, Edinburgh, UK* |
| **15:45-16:00** | Keith Paulsen - Imaging visual cortex activity with intrinsic poro-MR elastography<br>*Thayer School of Engineering at Dartmouth, Hanover, USA* |
| **16:00-16:15** | **Coffee break** |
| **16:15-16:30** | Philip Bayly et al. - Measurement of anisotropy in computer simulations and in porcine brain white matter ex vivo by MR elastography<br>*Washington University in Saint Louis, Saint Louis, MO, USA* |
| **16:30-16:45** | Faisal Fakhouri et al.- Magnetic Resonance Elastography of the Lung<br>*The Ohio State University, Columbus, USA* |
| **16:45-17:00** | Jelizaveta Sudakova et al. - Shear wave dispersion probes fractal dimension of 3D vascular trees<br>*St Thomas Hospital, London, UK* |
| **17:00-18:00** | Hands-on demonstrations of MRE and time harmonic ultrasound elastography |
| **From 19:00** | **Dinner and social get-together** |

**Friday 29/09/2017**

| | |
|---|---|
| **9:00-9:45** | Keynote lecture by Paul Janmey - Non-linear elasticity and relaxation in cells, tissues and biopolymer networks<br>*University of Pennsylvania, Philadelphia, USA* |
| **9:45-10:00** | **Coffee break** |
| **10:00-10:15** | Aaron Anderson et al. - Mechanical Properties of the Healthy Aging Human Brain<br>*University of Illinois at Urbana-Champaign, Urbana, USA* |
| **10:15-10:30** | Curtis Johnson et al. - Double Dissociation of Structure-Function Relationships in Memory and Fluid Intelligence Observed with Magnetic Resonance Elastography<br>*University of Delaware, Newark, USA* |
| **10:30-10:45** | Gloria Fabris - Characterization of pediatric brain viscoelasticity using magnetic resonance elastography<br>*Stevens Institute of Technology, Hoboken, USA* |
| **10:45-11:00** | Lucy Hiscox et al. - Hippocampal viscoelasticity and episodic memory performance in healthy older adults<br>*University of Edinburgh, Edinburgh, UK* |
| **11:00-11.30** | **Coffee break** - **posters and demonstrations** |
| **11:30-11:45** | Anthony Romano et al. - Moderate to Severe TBI Studies Using Mixed Model Inversions<br>*Naval Research Laboratory, Washington, DC, USA* |
| **11:45-12:00** | Dieter Klatt - Early-stage analysis of murine models of Familial Alzheimer's disease: Preliminary results<br>*UIC Bioengineering, Chicago, USA* |

| | |
|---|---|
| **12:00-12:15** | Arvin Arani et al. - An initial experience with high resolution, high frequency, brain MRE with a high performance compact 3T scanner<br>*Mayo Clinic, Rochester, USA* |
| **12:15-12:30** | Huiming Dong et al. - Comparison of Gradient Recalled Echo and Spin-Echo Echo Planar Imaging Sequences in In Vivo Aortic MRE<br>*The Ohio State University Wexner Medical Center, Columbus, USA* |
| **12:30-13:30** | **Lunch break** |
| **13:30-13:45** | Michiel Simons et al. - The Effect of Muscle Loading on Muscle Stiffness<br>*Edinburgh Imaging Facility, University of Edinburgh, Edinburgh, UK* |
| **13:45-14:00** | Gwenaël Pagé et al. - Assessing tumor mechanical properties and blood perfusion with MRE and FAIR MRI at different strain levels<br>*UMR 1149 Inserm, Paris, France* |
| **14:00-14:15** | Michael Perrins et al. - MRE Study of Muscle Recovery Following Time Spent in an Intensive Care Unit (ICU)<br>*Edinburgh Imaging Facility, University of Edinburgh, Edinburgh, UK* |
| **14:15-14:30** | Jonathan Vappou et al. - Monitoring of High Intensity Focused Ultrasound (HIFU) ablations in real time using interventional MR Elastography (MRE)<br>*ICube laboratory, CNRS-Université de Strasbourg, Strasbourg, France* |
| **14:30-14:45** | **Coffee break** |
| **14:45-15:00** | Michael Perrins et al. - Evidence from MRE that Muscle Engagement Strategy Influences Occurrence of Oedema Following an Exercise Induced Muscle Damage (EIMD) Protocol<br>*Edinburgh Imaging Facility, University of Edinburgh, Edinburgh, UK* |
| **15:00-15:15** | Michiel Simons et al. - Change in Mechanical Properties and Cross Sectional Area (CSA) of Thigh Muscles Following Total Knee Replacement (TKR) Surgery<br>*Edinburgh Imaging Facility, University of Edinburgh, Edinburgh, UK* |
| **15:15-15:30** | Jing Guo et al. - MR elastography for assessing hepatic fibrosis and steatosis in pediatric non-alcoholic fatty liver disease<br>*Charité-Universitätsmedizin Berlin, Berlin, Germany* |
| **15:30-16:00** | Discussion panel with focus on upcoming MRE events |
| **16:00-18:00** | Hands-on demonstrations of MRE and time harmonic ultrasound elastography |

## Poster contributions

1. Angela Ariza de Schellenberger et al. *Charité-Universitätsmedizin Berlin, Berlin, Germany* - Viscoelasticity of rat liver tissue in native, lysed and decellularized states measured by 0.5 T tabletop MRE
2. Gergely Bertalan et al. *Charité-Universitätsmedizin Berlin, Berlin, Germany* - Tomoelastography of the mouse brain
3. Gloria Fabris et al. *Stevens Institute of Technology, Hoboken, USA* - Correlating relative myelin content and dissipative properties of human brains: an in-vivo MRI study
4. Koki Ishii et al. *Chiba University, Chiba, Japan* - Development of a Tissue-Mimicking Visco-elastic Phantom for Quantitative Assessment of MRE
5. Kisoo Kim et al. *CNRS-Université de Strasbourg, Strasbourg, France* - Multislice interventional MR Elastography using simultaneous image refocusing (SIR)
6. Harish Palnitkar et al. *UIC Bioengineering, Chicago, USA* - An investigation of the relationship between the grid dimensions and wave shapes of an anisotropic fiber phantom: preliminary results
7. Frank Sauer et al. *University of Leipzig, Leipzig, Germany* - MR Elastography on polymer networks: a proof of concept for collagen gels
8. Felix Schrank et al. *Charité-Universitätsmedizin Berlin, Berlin, Germany* - Heparin as MRE phantom material with viscoelastic powerlaw properties similar to soft biological tissues

# Abstracts
# First International MRE Workshop in Berlin
# Berlin, Germany
# September 28-29, 2017

**00** **Keynote Lecture: Brain mechanics controls neuronal growth**

Kristian Franze
*Department of Physiology, Development and Neuroscience, University of Cambridge, UK*

During development and pathological processes, cells in the central nervous system (CNS) are highly motile. Despite the fact that cell motion is driven by forces, our current understanding of the mechanical interactions between CNS cells and their environment is very limited. We here show how nanometer deformations of CNS tissue caused by piconewton forces exerted by cells contribute to regulating CNS development and pathologies. In vitro, growth and migration velocities, directionality, cellular forces as well as neuronal fasciculation and maturation all significantly depended on substrate stiffness. Moreover, when grown on substrates incorporating linear stiffness gradients, glial cells migrated towards stiffer, while axon bundles turned towards softer substrates. In vivo atomic force microscopy revealed stiffness gradients in developing brain tissue, which axons followed as well towards soft. Interfering with brain stiffness and mechanosensitive ion channels in vivo both led to similar aberrant neuronal growth patterns with reduced fasciculation and pathfinding errors. Importantly, CNS tissue significantly softened after traumatic injuries. Ultimately, mechanical signals not only directly impacted neuronal growth but also indirectly by regulating neuronal responses to chemical guidance cues, strongly suggesting that neuronal growth is not only controlled by chemical signals – as it is currently assumed – but also by the tissue's local physical properties.

**01** **Keynote Lecture: Non-linear elasticity and relaxation in cells, tissues and biopolymer networks**

Paul Janmey
*Department of Physiology, Institute for Medicine and Engineering, University of Pennsylvania*

The stiffness of tissues in which cells are embedded has effects on cell structure and function that can act independently of or override chemical stimuli. Most measurements of tissue stiffness report elastic moduli measured at a single frequency and at a low strain, but tissues and the cells within them are subjected to strains that often exceed the range of linear viscoelasticity. Rheologic measurements of liver, brain, and adipose tissues over a range of shear, compressive, and elongational strains show that the viscoelastic response of these tissues differs from that of synthetic hydrogels that have similar elastic moduli when measured in the linear range. The shear moduli of soft tissues generally decrease with increasing shear or elongational strain, but they strongly increase under uniaxial compression. In contrast, networks of crosslinked collagen or fibrin soften under compression, but strongly increase shear modulus when deformed in extension. The mechanisms leading to the unusual strain-dependent rheology of soft tissues and fibrous networks do not appear to be explained by current models of polymer mechanics, but appear to relate to local and global volume conservation within the networks and tissues.

**02 Opening Talk: MR elastography: standardizing terminology and setting guidelines**

Armando Manduca
A. Manduca[1], P. Bayly[2], R. Ehman[1], T. Royston[3], I. Sack[4], R. Sinkus[5], B. van Beers[6], A. Kolipaka[7]
*[1]Mayo Clinic, Rochester, MN, USA; [2]Washington University, St. Louis, MO, USA; [3]University of Illinois at Chicago, Chicago, IL, USA; [4]Charité – Universitätsmedizin Berlin, Berlin, Germany; [5]King's College – London, London, England; [6]Université Paris Diderot, Paris, France; [7]Ohio State University, Columbus, OH, USA.*

**Background and aims:** Magnetic resonance elastography (MRE) is a phase-contrast based MRI technique that can measure displacement due to propagating mechanical waves, from which various mechanical material properties such as shear modulus can be calculated. It is motivated by the clinical importance of palpation, which though very useful is subjective and can reach only certain parts of the body. MRE can be thought of as quantitative, non-invasive palpation.

MRE is increasing in clinical importance; it has become widespread in the diagnosis and staging of liver fibrosis, may soon become useful in tumor surgery planning, and many other areas being researched. The research applications of MRE also continue to increase, and the number of MRE papers per year is increasing rapidly. However, many groups are reporting MRE results in terms of different parameters, and many types of acquisitions and processing techniques are in use. There is some confusion (particularly among clinicians) as to the meaning of certain terms, or how to interpret certain types of MRE results.

The ISMRM MRE study group, at its founding in 2015, set up an MRE Guidelines Committee, composed of the authors of this abstract. One task that this committee set for itself was the drafting of a white paper, as a service to the MRE community, which would attempt to clarify and (to some extent) standardize MRE terminology and practice. For example, results in different MRE papers are expressed in terms of many different quantities: shear modulus (possibly complex), storage modulus, magnitude of the complex shear modulus, shear stiffness (defined in different ways), wave speed, propagation, loss modulus, attenuation, loss tangent or loss factor, phase angle, damping ratio, attenuation, and penetration rate. This list is not exhaustive and does not even include additional quantities related to fits to specific assumed material models. The density of soft tissue is usually taken to be 1000 kg/m$^3$ (except for the lung), but true values are typically closer to 1050 kg/m$^3$ and vary slightly across tissues, and occasional papers use values other than 1000 kg/m$^3$. Papers are sometimes published without giving all the details necessary to fully replicate or interpret the experiment, with little sense of the reproducibility of the measurement, or with no assessment or discussion of the effect of noise or discretization on the reported values. The above are only a few examples of issues we believe should be addressed to help advance the field.

The purpose of the white paper is therefore to (a) explain sometimes confusing MRE terminology to those not familiar with it, (b) discuss some practices and terms that we believe should be standardized, (c) try to define "good practices" for practitioners of MRE, and (d) discuss some practices and terms that we believe should be discouraged.

The latest draft of this paper is currently circulating among the coauthors for additional comments, and some recommendations are still being finalized. The intent is to submit this paper within three months to Magnetic Resonance in Medicine. Anyone with specific issues or questions they feel should be addressed by such a paper is welcome to contact any member of the committee with their suggestions.

**03** **New 3D-printed elastography bench for MR study of engineered tissue and histology**

Mathilde Bigot[1], Fabien Chauveau[2], Hugo Dorez[1], Céline Mandon[3], Christophe Marquette[3], Kevin Tse Ve Koon[1], Pauline Lefebvre[1], Denis Grenier[1], Hamza Raki[1-4], Olivier Beuf[1], Simon A. Lambert[1]

*[1]Univ. Lyon, INSA-Lyon, Université Claude Bernard Lyon 1, UJM-Saint Etienne, CNRS, Inserm, CREATIS UMR 5220, U1206, FF-69000, LYON, France ; [2]Lyon Neuroscience Research Center, Centre National de la Recherche Scientifique UMR5292, Institut national de la Santé et de la Recherche Médicale, Université Lyon 1, Lyon, France ; [3]Université Lyon 1, CNRS, INSA, CPE-Lyon, ICBMS, UMR 5246, 43 Boulevard du 11 Novembre 1918, 69622 Villeurbanne Cedex, France; [4]Buc, FR, General Electric Healthcare.*

**Background/Aims:** To study viscoelastic parameters of small ex vivo or engineered tissue sampes, Magnetic Resonance Elastography (MRE) has been used during the last few years [1], [2]. It should enable a cautious sample-handling and be performed with a high spatial resolution. We describe here an elastography bench responding to those criteria.

**Methods:** The setup is designed to image small samples (Fig.1). This requires an MRI coil with a high uniformity and filling factor to maximize the signal to noise ratio (SNR). Moreover, the sample must be placed in the center of the coil and in contact with the mechanical transducer. Here, the sample holder is designed to slide into a 3D-printed support in which is included a Helmholtz coil tuned with two capacitor trimmers. Matching of the Helmholtz coil is done inductively using a circular coaxial coupling loop tuned at 200MHz. The sample holder is stopped at the center of the coil, guaranteeing the best RF uniformity and SNR. A cactus needle pierces the sample and is actuated by an MRI-compatible piezoelectric driver at 600Hz. Two samples were used to test the bench. The first one is made of polymerized fibrinogen (Sigma-F8630), which is used for engineered tissue. To limit motion of the sample, it was surrounded by a stiffer gel (DTM 133460). We also used a healthy rat brain embedded in agarose (Sigma A9414). The two embedding gels have well characterized mechanical properties and can serve as reference. Acquisition of a FLASH and a MRE-compatible RARE sequence were made with a Bruker 4.7T scanner. Reconstruction of the viscoelastic parameters was done using an adapted method from Sinkus et al. [3].

**Results:** A voxel of 0.312x0.312x0.625mm3 with an SNR of 82.8 and 63.6 were obtained with the FLASH sequence, for the rat brain (Fig.2) and the phantom (Fig.3), respectively. Mean displacement amplitude for the RARE sequence was evaluated at 1.5µm and 5.6µm. Storage modulus representing elasticity was 1.8kPa and 1.4kPa. The gel surrounding the sample had an elasticity of 2.6kPa.

**Conclusions:** Setup was easy to handle. It can be easily adapted to any MRI system. SNR is high and the induced mechanical displacement is enough to reconstruct viscoelastic parameters and highlight differences in elasticity between the commercial gel and the fibrinogen sample. Ex vivo results in brain are in agreement with literature [4].

**Acknowledgement:** This work was supported by the LABEX PRIMES (ANR-XX-LABX-0063) of Université de Lyon, within the program « Investissements d'Avenir » (ANR-11-IDEX-0007) operated by the French National Reasearch Agency (ANR). PEPS CNRS "Balanced".

**References:** [1] Boulet T. et al., J. Neurosci. Methods, 201: 296-306, 2011. [2] Guertler C. et al., Proc. ISMRM, 1377, 2017. [3] Sinkus, R. et al., CR Mécanique, 2010. [4] Millward, J. et al., J. Neuroimmunol., 275: 102,2014.

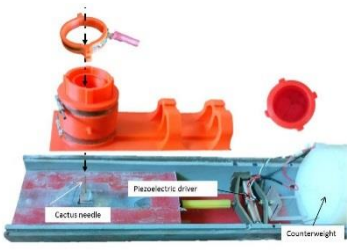


**Figure 1:** Photography of the different parts of the MR Elastography setup and the sample holder, on the right side

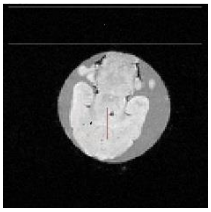

**Figure 2:** 3D FLASH Coronal image of a rat brain embedded in agarose. Red and white rectangles are ROIs for SNR measurement

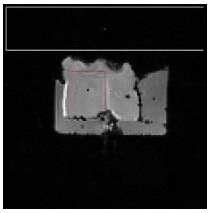

**Figure 3:** 3D FLASH Axial image of a homogenous fibrinogen phantom, embedded in candle gel. Red ans white rectangles are ROIs for SNR measurement

**04 MREAnaylsis: Software for ROI Stiffness Quantification and Reporting**

D.H. Hwang[1], S.L. Palmer[1]

*[1]Department of Radiology, Univ. Southern California, 1500 San Pablo St., Los Angeles, CA,USA.*

**Background:** Magnetic Resonance Elastography (MRE) is an emerging imaging modality gaining acceptance in both research and clinical use. Currently, multiple image sets are generated on the magnetic resonance (MR) scanners which need to be analyzed in parallel for the correct assessment of regions of interest (ROIs). There is a lack of user friendly post-processing software for elastography analysis.

**Aims:** i) to provide an intuitive graphic user interface (GUI) for the selection of ROIs, ii) to automatically combine the information from the multiple image volumes to refine user defined ROIs and iii) to provide multiple reporting options for the post-processed results.

**Methods:** MREAnaylsis is a custom Matlab[1] GUI designed to allow users to mark and quantify a ROI. Elastography generates two volumes which are crucial to the accurate interpretation of the images reconstructed on the scanner: stiffness map and confidence interval map. Ideally, a user would set the confidence interval threshold thereby excluding portions of low confidence from the final ROI. The software MREQuant[2] has visual representation of below threshold confidence interval, but requires the user to manually sculpt around these areas for accurate quantitation.

MREAnaylsis simplifies the procedure by allowing the user to draw an ROI independent of the confidence threshold. The user-defined ROI is merged with the confidence interval map allowing for the final ROI to include all voxels the user defines which meet or exceed the minimum confidence threshold.

Another feature included into the software is multiple reporting mechanisms. There are 4 file formats which data is reported, comma separated value file, MS Word file, DICOM (jpeg for PACS viewing), and DICOM-SR.

**Results:** MREAnalysis was used by 2 experience abdominal radiologist, 1 third year medical student, and an experienced radiology technician to quantify 280 scans (140 patients with two elastography sequences). The study showed consistent values across all readers.

**Conclusions:** MREAnalysis is an intuitive software program which allows users a simple method of creating ROIs and quantifying stiffness for elastography volumes acquired on the MR scanner. It accommodates both researchers and clinicians by allowing the user multiple reporting options.

**References:** [1] Mathworks, Natick, MA, USA. [2] Mayo Clinic, Rochester, MN. USA.

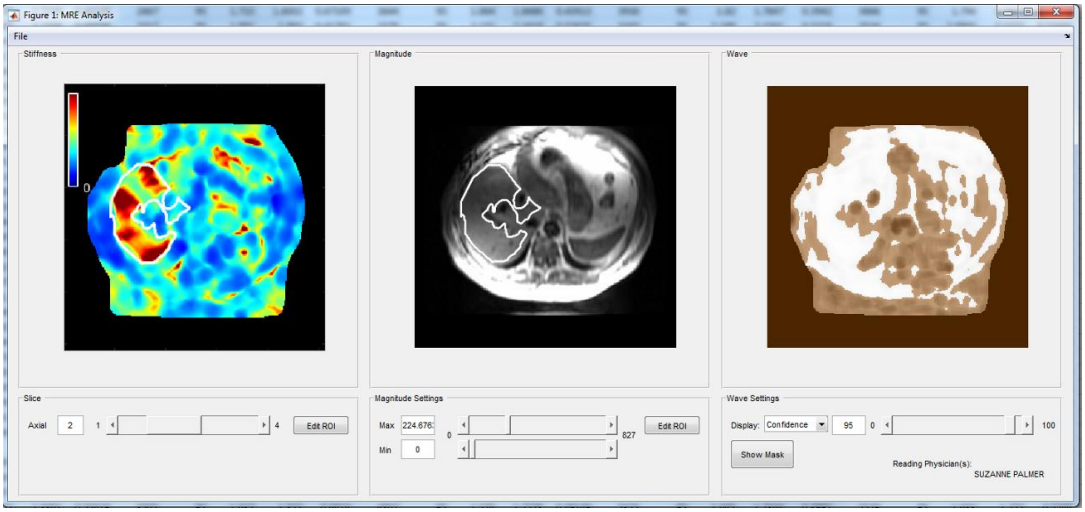


**Figure 1:** MREAnalysis GUI.

**05** **Revealing sub-voxel motions of brain tissue using phase-based Amplified MRI**

Itamar Terem[1], Wendy Ni[1], Maged Goubran[1], Mahdi Salmani Rahimi[1], Julian Maclaren[1], Greg Zaharchuk[1], Michael Moseley[1], Mehmet Kurt[2], Samantha Holdsworth[1]

*[1]Lucas Center for Imaging, Department of Radiology, Stanford University, Stanford, U.S.A.; [2]Stevens Institute of Technology, Hoboken, New Jersey, United States.*

**Introduction:** Amplified Magnetic Resonance Imaging (aMRI) was introduced as a new brain motion detection and visualization method [1]. The aMRI approach used a video-processing algorithm, Eulerian Video Magnification (EVM) [2], to amplify cardio-ballistic motion in retrospectively cardiac-gated MRI data. We introduce a new aMRI method based on phase-based video motion processing [3]. We validate phase-based aMRI using digital phantoms and show the potential for accurate displacement measurements.

**Method:** Image acquisition: Scans were performed on volunteers at 3T (GE MR750) using an 8-channel head coil. A mid-sagittal slice of a normal brain (adult volunteer 29yr/F) was acquired using a 2D cardiac-gated bSSFP sequence (cine MRI), using the following parameters: matrix size=2242, flip angle=45°, TR/TE=3.6/1.3ms; FOV=22mm2; slice-thickness=4mm, acceleration factor 2, 6 views/segment, scan time ~1min, and retrospective re-binning to 150 cardiac phases/frames. Motion amplification: With cine MRI images as input, phase-based aMRI decomposes the images using a linear steerable pyramid [3]. The phase for each spatial component is temporally band pass-filtered, multiplied by an amplification parameter, added to the original phase components, and then reconstructed, resulting in a movie with amplification of motion within the desirable frequency range. Here, we used an ideal narrowband filter with pass band 0–5Hz and amplification parameter α=10. Simulations: Two Gaussian-filtered 2D digital phantoms, a vertical bar (mimicking CSF around the midbrain and spinal cord) with width d and a disc (mimicking the cerebellum) with radius r, were simulated in MATLAB [4]. The phantom moved with 1D displacement $\Delta x=\Delta x0*\sin(2n\pi t/150)$. Rician noise and sinusoidal intensity variations were added to emulate partial volume effect (PVE). Amplification factor calculated as peak amplified displacement divided by Δx0.

**Results & Discussion:** Table 1 lists ideal behaviors: 1) linear dependence of amplified displacement on true displacement (i.e. constant amplification), 2) independence of amplification on temporal frequency, phantom size, Rician noise, and PVE. Non-ideal behavior: slight dependence on phantom shape (standard deviation of the amplification was ~5% of the mean). Figure 1 shows the temporal normalized variance maps for different temporal harmonic bands. The method enables to extract brain displacements for each temporal frequency separately. As can be seen: https://web.stanford.edu/~iterem/phasebased_aMRI_Fig1.mov.

**Conclusion:** Phase-based aMRI can quantify accurate displacement measurements at various temporal frequencies of the brain due to heart pulsation and could complement. From phantom simulations, we found: 1) phase-based MRI can magnify motions on the order of micrometers 2) accurate quantification of amplified motion is possible using phantoms emulating brain structures. We hope to compare the extracted biomechanical properties through aMRI with corresponding MRE measurements.

**Acknowledgements:** This work was supported by a Philips-Stanford sponsored research collaboration.

References: [1] Holdsworth S, et al. 2016. MRM. [2] Rubinstein M, et al. 2012. ACM Trans Graph. [3] Rubinstein M, et al. 2013. ACM Trans Graph. [4] Ni W, et al. 2016. ISMRM.

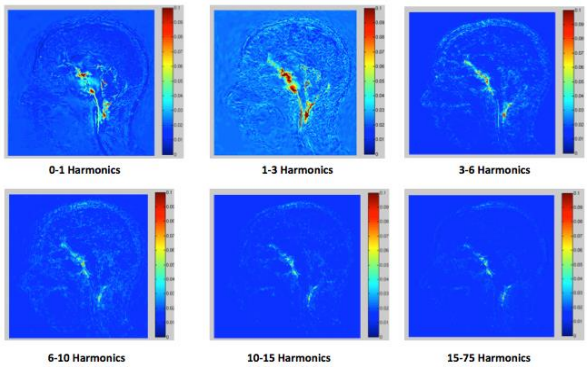


**Figure 1:** Temporal normalized variance maps for different harmonics bands. This enables the future displacement measurements for each temporal frequency separately

| Purpose of Simulations | Parameter Space | Results | Desired |
|---|---|---|---|
| Dependence on varying alpha | α: [0-10] | Linear correlation with r squared = 0.999 | ✔ |
| Dependence on varying initial displacement | $\Delta x_0$: [0-0.95] mm | Linear correlation with r squared = 0.999 (indicating constant amplification parameter) | ✔ |
| Dependence on varying harmonics | n: [0-10] | Different harmonics were amplified equally | ✔ |
| Dependence on varying disk size | d: [1.875-30] mm | Different phantom sizes were amplified equally | ✔ |
| Dependence on varying bar size | t: [3.75-60] mm | Different phantom sizes were amplified equally | ✔ |
| Dependence on varying background contrast | Intensity multiplier: [0.1-1] | Different intensities were amplified equally | ✔ |
| Dependence on varying Rician noise | Rician noise parameter s: [0-0.01] | Different noise parameter were amplified equally | ✔ |
| Investigate coupling between motion and partial volume effect (PVE) | n: [0-4] $\Delta I_0$: [0-0.2] | Amplification parameter is independent on partial volume effect | ✔ |

**Table 1:** Phantom simulations results showing that phase-based aMRI demonstrated ideal behavior. This enables future quantitation and accurate displacement measurement

**06 Robust flow reconstruction and quantitative post-processing from Phase-Contrast MRI**

C. Bertoglio[1,2] H. Carrillo[2] D. Nolte[2] A. Osses[2] C. Uribe[3]

*[1]Johann Bernoulli Institute, Rijksuniversiteit Groningen, Groningen, The Netherlands; [2]Center for Mathematical Modeling, Universidad de Chile, Santiago, Chile; [3]Center for Biomedical Imaging, Pontificia Universidad Católica de Chile, Santiago, Chile*

**Background:** Flow imaging in MRI is subjected to velocity aliasing what limits the quality of the reconstruction in complex flows of varying magnitudes and directions. Moreover, 4D Flow is increasingly being used to reconstruct hemodynamic pressure gradients.

**Aims:** In this talk we will discuss methods dealing with: i) dual-VENC velocity estimation strategies able to use VENC values smaller than the actual velocity and ii) to present and analyze new estimators of pressure gradients in blood vessels from 4D-Flow data.

**Methods:** For aim i), we introduce a non-linear least-squares approach for estimating the velocities, which leads to natural choices of VENC values that avoid aliasing. For aim ii), we reformulate some pressure estimation methods that may have some theoretical advantages. In both cases, we verify the methods using synthetic (simulated) data and then validate them from phantom (experimental data).

**Results:** In aim i), we are able with dual-VENC non-symmetric gradient acquisitions (i.e. 1 reference phase image and 2 phase images with encoding gradients of different magnitudes) to obtained un-aliased velocities for VENC>=vel_true/3. In aim ii) we are able to obtain improved estimates of pressure drops in the synthetic examples and comparably good estimates in the real data examples.

**Conclusions:** Introducing more complex mathematical formulations but still resulting in computationally tractable tools can help to considerably improve reconstruction and quantification in Flow MRI.

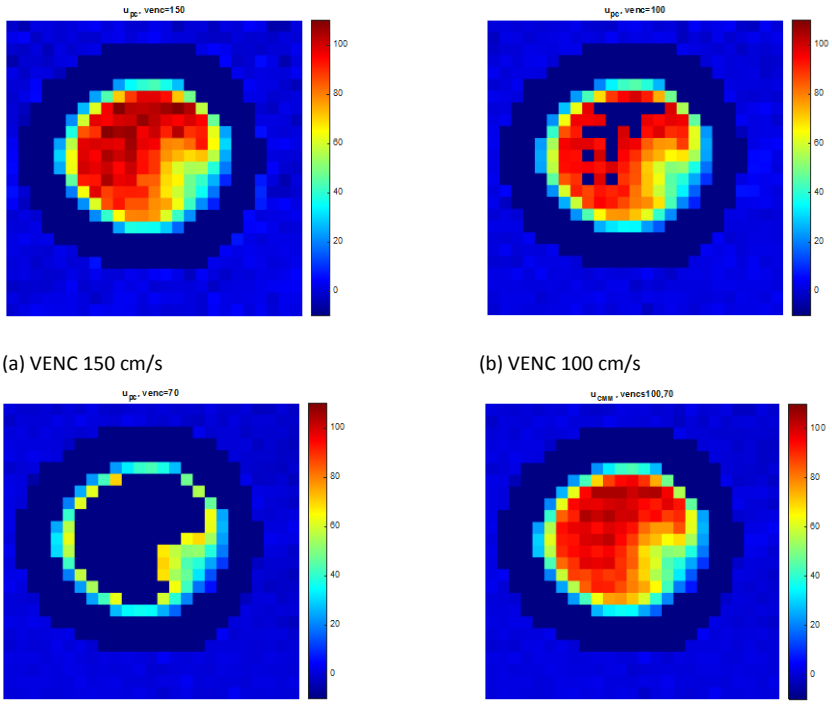


(a) VENC 150 cm/s

(b) VENC 100 cm/s

(c) VENC 70 cm/s

(d) Dual-VENC 100 and 70 cm/s

**Figure:** Through-plane velocity reconstructions from PCMRI data in an experimental phantom. (a)-(c) Standard single-VENC PCMRI reconstructions. The peak velocity is about 110 cm/s, hence aliasing appears for VENC 100 and 70 cm/s. (d) Dual-VENC velocity estimation using VENC 100 and 70 cm/s.

## 07 Optimal control theory applied to MR Elastography

P.M. Lefebvre[1], K. Tse Ve Koon[1], H. Ratiney[1], D. Grenier[1], E. Brusseau[1], S.A. Lambert[1], S.J. Glaser[2], D. Sugny[3], O. Beuf[1], E. Van Reeth[1]

*[1]Univ. Lyon, CREATIS; CNRS UMR5220; INSERM U1206; INSA-Lyon; UJM; Univ. Lyon 1, Villeurbanne, France; [2]Department of Chemistry, TU München, Germany; [3]ICB, CNRS UMR6303, Université de Bourgogne, France*

**Background:** Standard MRE uses periodic motion encoding gradients (MEG) and synchronized harmonic mechanical excitation[1], typically applied at the same frequency. However, gradient commutations are physically limited by the slew rate of the gradient system and MEG lengthen the echo time of the acquisition. In this paper, a new encoding approach is proposed[2], without oscillating MEG.

**Aims:** i) to propose a new encoding method, which directly encodes the wave propagation using a specific RF-pulse, generated with Optimal Control (OC) theory, and a constant gradient, ii) to validate the proposed approach through phantom experiments with a comparison with conventional MRE.

**Methods:** OC theory[3] is a powerful pulse design tool that computes the RF-pulse ($\omega_x$,$\omega_y$) to optimize the trajectory of the macroscopic magnetization **M** (whose evolution obeys the Bloch equations) so that it reaches a given target-state[4]. In the context of MRE, the goal is to design a RF-pulse that leads the final magnetization to a given final state in the transverse plane. Mimicking conventional MRE, our objective is to obtain a sinusoidal distribution of the spins phase over a wavelength in the interval [0;2π[ at the end of the RF-pulse. The cost-function writes: $C(\omega_x,\omega_y)=\sum_{s=0}^{Nspins-1} ||\boldsymbol{M}_s^{\perp}(t_f)-\boldsymbol{M}_{s,TS}^{\perp}||^2$, with $N_{spins}$ the spin number discretized on a wavelength, and $\mathbf{M}_{s,TS}^{\perp}$ the target-state vector (in transverse plane): $\boldsymbol{M}_{s,TS}^{\perp}= (cos(\pi*cos(s*2\pi/N_{spins}))\ \ sin(\pi*cos(s*2\pi/N_{spins})))$. In order to discriminate spins position along a wavelength, we decide to apply a constant gradient $G_z$ in the harmonic motion direction z during the RF-pulse. It induces a variation of the magnetic field perceived by oscillating spins: $\Delta B_0(x,z,t)=G_z(z+A\ sin(-2\pi f_e t+2\pi x/\lambda))$ with $A$ the wave amplitude, $\lambda$ its wavelength, $x$ the wave propagation direction, and $f_e$ the excitation frequency. Depending on their position $s$ along the wavelength, spins are assigned a different target-state with $\Delta B_0(x,z,t)$ being the discriminating factor. An example of optimized RF-pulse is presented in Fig.1.

Conventional and OC-MRE experiments were performed on a plastisol phantom[5], excited with a piezoelectric actuator and imaged with a gradient-echo sequence using a Bruker 4.7T MRI system. For OC-MRE, a gradient-echo sequence was modified to replace the excitation pulse by the simultaneous application of the OC-designed pulse and the constant gradient $G_z$, equal to 150 mT/m here. TE was equal to 14.4 ms for conventional MRE and 1.9 ms for OC-MRE and TR = 5 s in both cases. The amplitude of the MEG in conventional MRE was 258 mT/m, and FOV = 4 x 4 cm.

**Results:**. An example of resulting phase images of the wave propagation is presented on Fig.2, showing comparable results between the two MRE approaches. Shear storage (G') and loss (G'') moduli have been calculated from phase images with an Helmholtz inversion algorithm. Mean values in a user-defined ROI at 500 Hz were found to be G'=26.7+/-1.78 kPa and G''=4.31+/-1.34 kPa for conventional MRE and G'=27.8+/-2.10 kPa and G''=4.41+/-1.63 kPa for OC-MRE.

**Conclusions:** Results presented here show that simultaneous RF-excitation and motion encoding is possible with OC-based RF-pulses. This strategy allows image acquisition with minimal echo-time and relaxes constraints on having oscillating MEG. This avoids gradient commutations that are physically limited and therefore restricts applications requiring high frequencies[6]. Future works will investigate high-frequency OC-MRE, UTE MRE and apply OC-MRE to in vivo experiments.

**References:** [1] Muthupillai R, et al., Science, 269(5232) : 1854-7, 1995. [2] P.M. Lefebvre, E. Van Reeth et al., Journal of Magnetic Resonance, 281:82-93, 2017. [3] L. S. Pontryagin, CRC Press, 1987. [4] E. Van Reeth, et al., Journal of Magnetic Resonance, 279:39-50, 2017. [5] P.M. Lefebvre et al., IEEE 38th conference of the EMBS, pp.1216-19, 2016. [6] O. Lopez et al. Journal of Magnetic Resonance Imaging, 25(2):310-20, 2007.

**Acknowledgments:** Support from the ANR-DFG research program Explosys (Grant No. ANR-14-CE35-0013-01; GL203/9-1). This work was performed within the framework of the LABEX PRIMES (ANR-11-LABX-0063/ ANR-11-IDEX-0007).

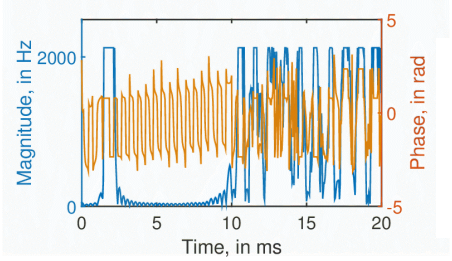


**Figure 1:** RF pulse resulting from OC theory applied to the MRE problem.

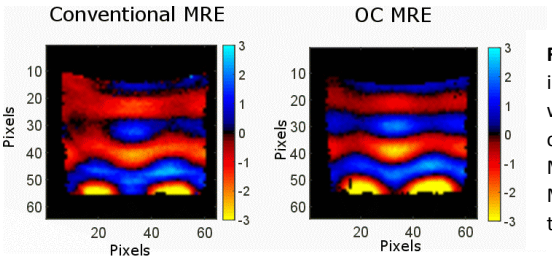


**Figure 2:** Phase image obtained with conventional MRE and OC MRE at one time step.

**08 Identification of the viscoelastic properties in magnetic resonance elastography by coupling a finite element model and a gradient method**

S. Chatelin[1,3] , I. Charpentier[1], M. Bilasse[1,2], J. Vappou[1,3]

*[1]ICube, University of Strasbourg, UMR 7357 CNRS, 1, place de l'hôpital, Strasbourg, France; [2]ECAM Strasbourg-Europe, 2 rue de Madrid, Schiltigheim, France; [3]IHU, Institute of Image Guided Surgery, 1, place de l'hôpital, Strasbourg, France*

**Background:** Finite element (FE)-based inversion methods allow for accurate reconstruction of the biomechanical properties in Magnetic Resonance Elastography (MRE) [1-3]. Thanks to the possibility of accounting for complex mechanical properties, such approaches offer major perspectives for quantitative, biomechanical applications of MRE.
**Aims:** The objective of this study is to investigate an automatic differentiation-based gradient method of a dedicated biomechanical model for the investigation of viscoelastic properties in MRE. The proposed approach focuses on the accurate characterization of viscoelastic properties using a FE description of wave propagation.
**Methods:** The first step consisted in developing a realistic numerical model of harmonic shear wave propagation with a limited amount of computational power and memory. Based on the first-order shear deformation theory (FSDT) for moderately thick viscoelastic heterogeneous structures, a 2D finite element formalism has been developed and compared to analytical formulations of wave propagation, to a numerical 3D model from a commercial FE software, and to experimental MRE data. As a first step, the proposed FE model mimics experimental cylindrical wave propagations obtained with the protocol described by [4]. At this time, the proposed model focuses on a known local source for the waves that has to be applied through the whole thickness of the model. The model is then differentiated using an Automatic Differentiation (AD) tool to compute an accurate gradient-based data assimilation approach and to solve the inverse problem. The method is applied for the identification of elasticity and viscosity: (i) in a 3D FE phantom generated using a commercial software (Comsol Multiphysics) ($|G^*|$ = 5kPa, $tan(\delta)$ = 0.1218) with a soft viscoelastic inclusion ($|G^*|$ = 2.5kPa, $tan(\delta)$ = 0.2231, ø = 40mm) ; (ii) in an experimental 8% gelatin phantom with a soft inclusion (ø = 40mm), in which cylindrical shear waves ($f_0$ = 100Hz) were generated from a vibrating needle and encoded in the slice direction using a spoiled gradient echo sequence with motion-sensitizing gradients (1.5T *Magnetom Aera Siemens*; $T_E/T_R$ = 7ms/10ms; slice thickness = 10mm; matrix = 128×128; FOV = 350mmx350mm; 1 slice) [4]. The identification process is applied on the phase image regridded in 16x16 in a 118mmx118mm region of interest. The mechanical properties obtained with the proposed method are compared to measurements using rotational rheometry for both the phantom and the inclusion.
**Results:** This study shows that the proposed FSTD FE model allows simulating cylindrical, harmonic shear wave propagation in 2D in viscoelastic media at significantly reduced computer costs. Shear wave patterns from the numerical (**Figure 1.a**) and experimental phantoms (**Figure 2.a**) are represented next to the shear wave patterns simulated by the proposed 2D FE model using the optimal viscoelastic parameters (**Figures 1.b** and **2.b**, respectively).
**Conclusions:** These preliminary results illustrate the feasibility of the proposed approach. Viscoelastic parameters could be identified on a non-uniform phantom at low computational cost. Moreover, the AD-based gradient method offers the opportunity to account for complex mechanical properties, - such as anisotropy, hyperelasticity or porosity – by adapting the FEM accordingly. At this time, one of its major limitation is that the source of the waves has to be known and to be applied through the whole thickness of the model. The next step consists in optimizing the computational process to reduce further computer costs, allowing application of the method to images with higher resolution.

**References:** [1] Van Houten et al., MRM, 42(4):779-86, 1999. [2] Oberai et al., Inverse Problems, 19(2): 297-313, 2003. [3] Wang et al., J Biomed Imaging, 406854, Epub, 9, 6:1-:6:9, 2009. [4] Corbin et al., MRM, 75(3): 1110-8, 2015.

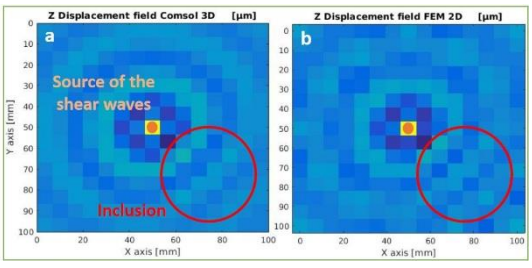


**Figure 1:** Wave pattern from 3D *Comsol* FE model (a) and from our 2D FE model with the identified mechanical parameters (b).

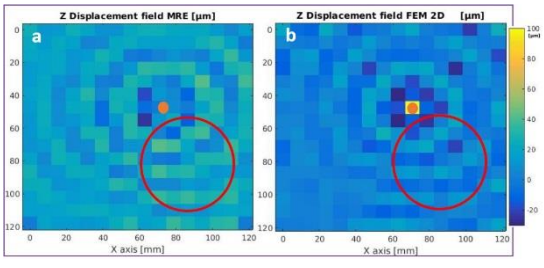


**Figure 2:** Wave pattern from experimental MRE (a) and from our 2D FE model with the identified mechanical parameters (b).

## 09 Heterogeneous Multifrequency Direct Inversion in MR Elastography: A preliminary Comparison of Finite-Difference and Finite-Element Based Approaches

Daniel Fovargue[1], David Nordsletten[1], Ralph Sinkus[1], Jürgen Braun[2], Ingolf Sack[2], and Eric Barnhill[2]
*[1]Imaging Sciences and Biomedical Engineering, King's College London, London, UK; [2]Radiological Science and Medical Informatics, Charité, Berlin, Germany*

**Introduction:** Interest has grown in MRE inversion methods that do not neglect the stiffness gradient, that is, do not assume "local homogeneity". Multifrequency inversions are of related interest as additional frequencies may make direct heterogeneous inversions more tractable. A comparison of two heterogeneous multifrequency reconstruction methods (a finite difference (FD) approach [1] and a finite element method (FEM) approach [5]) fixing all other factors is anticipated to yield valuable information on the next generation of MRE inversion methods.

**Methods:** A two-frequency (40 & 50 Hz) multifrequency liver simulation and a retrospectively investigated cohort of 4 abdominal MRE acquisitions from healthy volunteers, acquisitions described in [3], were used in the study. The *in vivo* abdominal acquisitions were phase-unwrapped using a Laplacian-based method [2] and denoised using complex dual-tree wavelets [6] with soft thresholding and VisuShrink threshold estimation [4]. A 4th order Butterworth high-pass filter with normalized frequency cutoff of $\omega = 0.05$ was used to isolate the shear wave.

Assuming isotropy, incompressibility, and the removal of pressure, the time-harmonic linear elasticity equations to invert to find stiffness are $\rho\omega^2 u + \nabla \cdot (G\nabla u + (\nabla u)^T) = 0$ , (1) where u are time-harmonic wave displacements and $G$ is the complex-valued shear modulus. The FD reconstruction utilizes difference stencils for all derivatives of (1) and constructs a matrix system to solve globally for the spatially variable $G$. The FEM solves the weak form of (1) where the test functions are chosen to be zero on the boundary which removes corresponding terms. Standard construction of FEM matrices, using quadratic hexahedral elements, leads to a discretized system and this is solved via least squares and with Tikhonov regularization. As a control, a "Helmholtz" inversion was also used, which assumes local homogeneity of stiffness and reconstructs stiffness voxel-wise based on FD approximations of the Laplacian of u.

**Results:** In the simulated liver data (not shown), both approaches reconstruct stiffness within expected variation from the known value. fig:ab-images shows example images from each of the three pipelines for the simulated liver and *in vivo* abdomen: (a) locally-homogeneous Helmholtz, (b) FD, (c) FEM. The true images differ in range and these images have been scaled to show similar high and low values. Liver, spleen, kidney, and spinal disc all show clear spatial resolution in all reconstructions, however value ranges differ. fig:ab-values shows mean liver stiffness. The three methods show different ranges, but agree in relative values.

**Discussion:** The three reconstruction methods show good resolution of the relevant anatomical organs, however they showed unexpected divergence in value ranges. All aspects of filtering and denoising are held fixed and this shows that changes in stiffness ranges and relative evaluation of organs may depend on numerical choices in the inversion stage. Future work will more deeply investigate the relations between these mathematically diverse methods and their relationships to acquisition and pre-processing choices.

**Acknowledgements:** This project has received funding from the European Unionâ™s Horizon 2020 research and Innovation programme under grant agreement No 668039 and the European Unionâ™s Seventh Framework Programme for research, technological development and demonstration under grant agreement no FP7-ICT-2011-9-601055.

**References:** [1] Barnhill et al. ISMRM 2017 1382 [2] Barnhill et al. 2014 MRM 73(6) [3] Dittmann et al 2016 MRM 30 [4] Donoho et al JRSS-B, 301-369 [5] Fovargue et al ISMRM 2017 1368 [6] Selesnick et al. 2005 IEEE SPM 22(6)

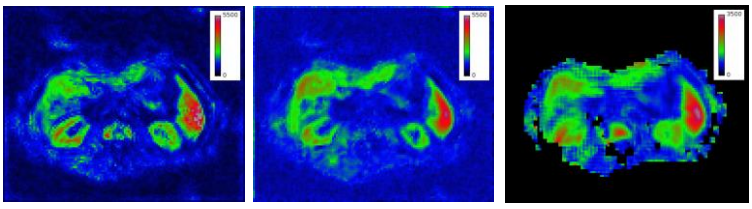

(a) (b) (c)

**Figure 1:** Liver images for (a) Helmholtz inversion, (b) FD method, (c) FEM method.

| Subj. | Helm. | FD | FEM |
|---|---|---|---|
| 1 | 1542 | 1926 | 1172 |
| 2 | 1740 | 2120 | 1294 |
| 3 | 1567 | 1874 | 1212 |
| 4 | 1568 | 1868 | 1241 |

**Figure 2:** Liver values by subject for Helmholtz, FD and FEM methods.

**10 Reconstruction of high-resolution MR elastography motion data using nonlinear inversion**

Matthew McGarry[1,2], John B. Weaver[1,3], Keith D. Paulsen[1,3], Curtis L. Johnson[4]

*[1]Thayer School of Engineering, Dartmouth College, Hanover NH, USA; [2]Department of Bioengineering, Columbia University, New York, USA; [3]Department of Radiology, Dartmouth-Hitchcock Medical Center, Lebanon NH, USA; [4]Department of Bioengineering, University of Delaware, Newark DE, USA*

**Background:** MRE sequence development has been pushing toward higher resolution sequences and faster acquisition times to maximize the amount of data that can be collected in an imaging session. In our externally actuated MRE work to date, we have generally used the same parameters in the nonlinear inversion (NLI) process for both phantom and in vivo studies in the interests of a standardized protocol and to allow subsequent studies to be compared[1,2]. These parameters were chosen for stability and repeatability for estimations of larger brain regions with 2.0 mm isotropic data, and did not necessarily emphasize spatial resolution in recovered properties. Recently, there has been substantial interest in measuring properties of small brain structures[3,4,5], along with a substantial improvement in motion data quality and resolution; thus, renewed study into the achievable resolution of NLI mechanical property reconstruction is needed. NLI resolution is determined by numerous factors, including the data resolution and quality, finite element mesh resolutions[1], regularization parameters[2], and optimization approach.

**Aims:** Investigate the achievable resolution of NLI brain MRE with high resolution motion data by tuning the existing regularization weightings and optimization parameters.

**Methods:** MRE data was collected from a healthy subject at 2.0, 1.6 and 1.25 mm isotropic spatial resolutions of under 50Hz external actuation in a single session with common field-of-view[6]. The NLI inversion parameters with the most influence are the number of conjugate gradient (CG) iterations per subzone iteration, spatial filter (SF) width, and total variation minimization (TV) weighting. Various combinations of these parameters were applied during inversion, and the resulting property images were visually assessed for convergence, artifacts, instability, and correspondence to anatomical structures.

**Results:** Decreasing the width of the SF kernel, decreasing TV weighting, and increasing the number of CG iterations per subzone improved resolution (figure 1), at a cost of potential instability. Using the highest motion data resolution and balancing all three NLI effects produced a property image with an effective resolution of around 3 mm, where anatomical structures are evident in the real shear modulus image (figure 2). Higher resolution motion data allowed lower regularization levels to be applied while maintaining stability to achieve higher resolution property images. CSF regions remain problematic due to model-data mismatch; soft prior regularization will still be helpful close to fluid spaces[2,5].

**Conclusions:** High resolution, high quality motion data combined with advanced NLI reconstruction can achieve effective resolution approaching 3 mm from single-frequency MRE data. Further studies involving repeated examinations of the same subject will characterize the reproducibility of the high resolution estimates of small brain structures for potential clinical applications.

**References:** [1] McGarry et al., Med Phys (2012); [2] McGarry et al. IEEE Trans Med Imag (2013); [3] Schwarb et al., Neuroimage (2016), [4] Schwarb et al., Neuroimage (2017), [5] Johnson et al. Hum Brain Mapp (2016); [6] Johnson et al., ISMRM (2016)

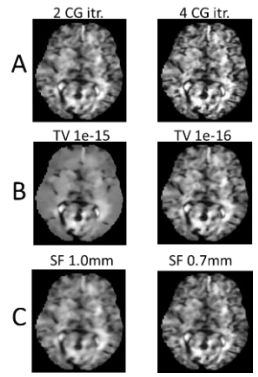


**Figure 1:** Improved resolution with: A: more CG iterations, B: lower TV weight , and C: smaller SF width.

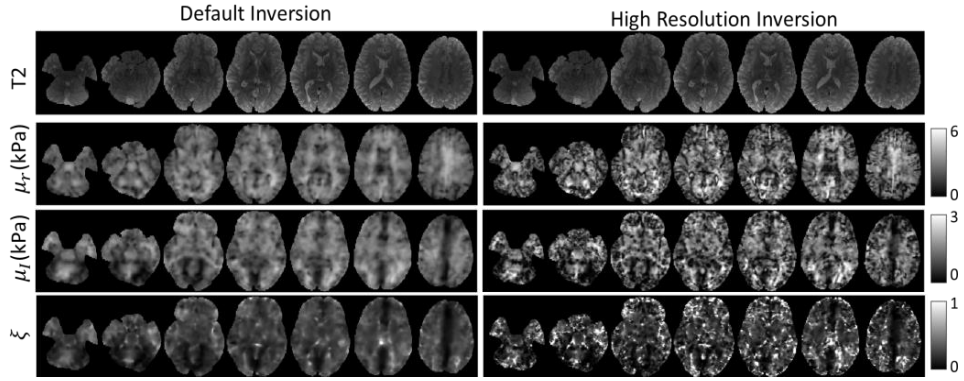


**Figure 2:** Comparison of standard NLI parameters (Left: SF 1.5mm, no TV, 2 CG iterations per zone), and high resolution parameters (Right, SF 0.7mm, TV 5e-17, 4 CG iterations per zone) for 1.25 mm motion data resolution. Rows show T2 MRI image, real shear modulus, $\mu_r$, imaginary shear modulus $\mu_I$, and damping ratio, $\xi$, for a selection of image slices.

## 11 OSS-Weighted Averaging in Multifrequency Inversion for MR Elastography

Cemre Ariyurek[1, 2], Bilal Tasdelen[1, 2], Arif Sanli Ergun[3], Yusuf Ziya Ider[1], Ergin Atalar[1, 2]
*[1]Department of Electrical and Electronics Engineering, Bilkent University, Ankara, Turkey; [2]National Magnetic Resonance Research Center (UMRAM), Ankara, Turkey; [3]Department of Electrical and Electronics Engineering, TOBB-University of Economics and Technology, Ankara, Turkey*

**Background:** Inversion techniques in multifrequency MR elastography (MMRE) are useful for compensating the influence of amplitude nulls on the elastograms and to reconstruct frequency-independent stiffness maps [1, 2]. In the inversion, the elastograms reconstructed for different frequencies are combined by amplitude-weighted averaging. The shear strain is directly related to the shear modulus. Hence, it was shown that strain-SNR is more important to decide on the quality of the data than motion-SNR for reconstructing elastography maps [3]. Therefore, combining the elastograms at different frequencies using octahedral shear strain (OSS) weighted averaging instead of amplitude-weighted averaging may give more reliable maps.
**Aims:** To compare OSS-weighted and amplitude-weighted averaging for multifrequency inversion.
**Methods:** For multifrequency inversion, k-MDEV [2] was implemented, which uses amplitude-weighted averaging to combine shear wave speed maps at different frequencies. Here, as a second multifrequency inversion technique, we used OSS-weighted averaging instead of amplitude-weighted averaging, where other steps of inversion were same with k-MDEV. We tested these two multifrequency inversion techniques on MRE phantom data provided by Charité - Universitätsmedizin Berlin, Germany on the ISMRM MRE study group webpage, also reported in [1, 2].
**Results:** The wave speed maps at different frequencies are shown in Figure 1. Figure 2 demonstrates combined wave speed maps according to amplitude-weighted averaging and OSS-weighted averaging.
**Discussion and Conclusion:** In Figure 2, the lower left inclusion is more visible and the background has less wave artifacts in OSS-weighted averaging compared to amplitude-weighted averaging. For instance, wave artifacts are visible in the wave speed map at 70 Hz, as seen in Figure 1, which are also observed in amplitude-weighted averaging inversion result but successfully suppressed in OSS-weighted averaging inversion result. Moreover, OSS-weighted averaging gives better results on the boundaries. It is concluded that using OSS-weighted averaging could be more advantageous over amplitude-weighted averaging. As a future work, the reconstructions should be validated on human experimental data.

**References:** [1] Papazoglou S, Hirsch S, Braun J, Sack I. Multifrequency inversion in magnetic resonance elastography. Phys Med Biol 2012;57:2329–2346 McCurry M et al., Elastojournal, 41(3): 724-33, 2015. [2] Tzschatzsch H , Guo J, Dittmann F, Hirsch S, Barnhill E, Johrens K, Braun J, Sack I. Tomoelastography by multifrequency wave number recovery from time-harmonic propagating shear waves. Med Image Anal2016;30:1–10 [3] McGarry MDJ, Van Houten EEW, Perrinez PR, Pattison AJ, WeaverJB, Paulsen KD. An octahedral shear strain-based measure of SNR for3D MR elastography. Phys Med Biol 2011;56:N153–N164

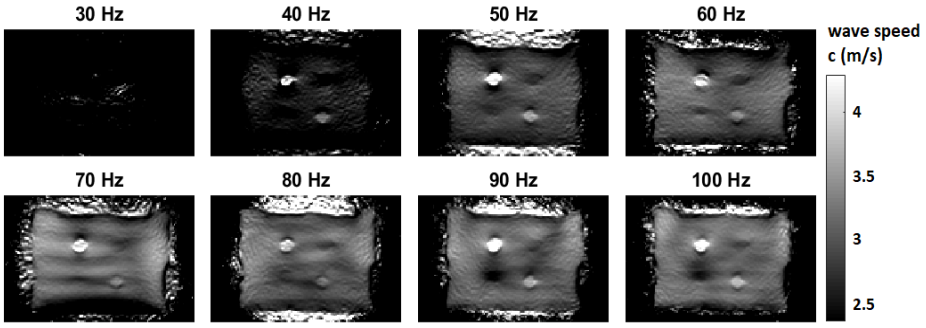


**Figure 1:** The wave speed maps at different frequencies.

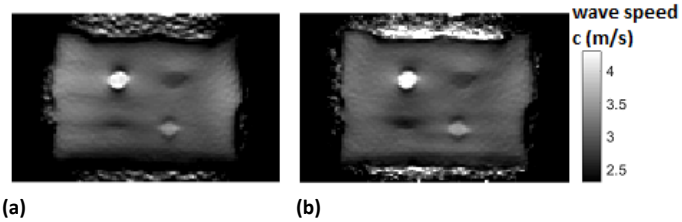


**Figure 2:** The wave speed maps
for the phantom data: (a) Amplitude-weighted, (b) OSS-weighted inversion.

**12 Power-Law Multi-Frequency MR Elastography of the human brain via Non-Linear Inversion Reconstruction.**

Elijah E.W. Van Houten[1], J. Testu[1], M.D.J. McGarry[2], F. Dittmann[3], J.B. Weaver[4,5], K.D. Paulsen[4,5], I. Sack[3]
*[1]Department of Mechanical Engineering, University of Sherbrooke, Sherbrooke, Canada; [2]Department of Biomedical Engineering, Columbia University, New York, United States; [3]Department of Radiology, Charité-Universitätsmedizin Berlin, Germany;[4]Thayer School of Engineering, Dartmouth College, Hanover, United States; [5]Department of Radiology, Dartmouth-Hitchcock Medical Center, Lebanon, United States*

**Background:** The interest in viscoelastic parameters obtained from MR Elastography has grown continuously since the development of the method, and preliminary results have indicated the potential of these damping properties as biomarkers for a number of targets, including the liver and the brain [1]. Viscous property characterization has now begun to seek to identify the parameters describing the spectral tissue response across a range of frequencies through power-law (PL) models that can be related to multi-scale effects in both scattering [2] and fluid-solid interactions [3].
**Aims:** i) To develop a multi-frequency reconstruction method based on a power-law model (PL-MF MRE) for the storage and loss modulus ii) To test the application of the PL-MF MRE reconstruction on in-vivo data sets and iii) To verify the resulting PL parameters against values obtained from regression of mon-frequency reconstructions.
**Methods:** Experiments were conducted on a 1.5-T Siemens MAGNETOM Sonata using single-shot spin-echo EPI with trapezoidal flow-compensated MEGs in all three directions [4]. The actuator employed was similar to the head rocker system described by Sack *et al.* [5] with the setup detailed by Guo *et al.* [6]. Full 3D displacement fields at 15, 20, 25, 30, 35, 40 and 50 Hz were used first for a series of mono-frequency reconstructions which were fit to independent power law models for the storage and loss modulus, $\mu_R = \theta_R \cdot \omega^{\alpha R}$ and $\mu_I = \theta_I \cdot \omega^{\alpha I}$, through a logarithmic regression [7]. These same displacement fields were then provided to a PL-MF MRE algorithm using non-linear inversion (NLI) based on finite element solutions of the linear, time-harmonic viscoelasticity equations. Total variation (TV) regularization was applied during the PL-MF MRE reconstruction process to counteract decreased stability of the inversion given the strict application of the PL model.
**Results:** As reported in Testu *et al.* [7], mono-frequency reconstructed properties were generally well described by a power-law model, except in the region of the *falx cerebri*. The TV stabilized PL-MF MRE reconstruction provided similar PL parameters to the regression results (see Figure 1), with image definition clearly improved through the incorporation of multiple displacement fields into the NLI algorithm.
**Conclusions:** This preliminary demonstration of a PL-MF MRE method able to match the PL parameters obtained from regression analysis of mono-frequency reconstruction results provides an important step toward accurate and verifiable quantification of the dispersive, multi-scale nature of soft-tissue.

**References:** [1] Sack I *et al.*, PMB, 45(6): 1649, 2000. [2] Sinkus R *et al.*, MRM, 58(6): 1135-1144, 2007. [3] Parker K, PMB, 59(15): 4443, 2014. [4] Dittmann F *et al.*, MRM, 76(4): 1116-1126, 2016. [5] Sack I *et al.*, NMR in BioMed, 21(3): 265-271, 2008. [6] Guo J *et al.*, PLoS ONE, 8(8): 1-10, 2013. [6] Testu J *et al.*, JMBBM, 74: 333-341, 2017.

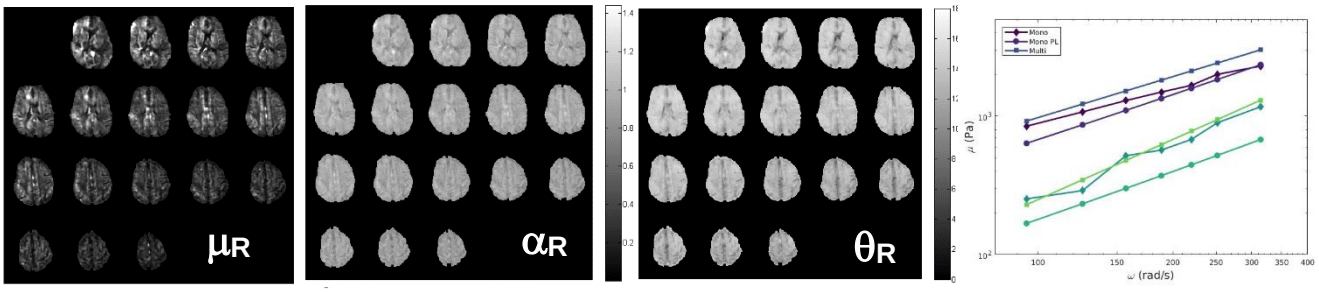


**Figure 1:** PL-MF MRE results (left to right): storage modulus reconstructed from the PL-MF parameters at 30 Hz ($\mu_R = \theta_R \cdot (2\pi \cdot 30)^{\alpha R}$); PL exponent for the storage modulus; PL scalar for the storage modulus; comparison of average values (storage modulus above, loss modulus below) from the individual mono-frequency reconstructions (mono), the regression analysis (mono PL) and PL-MF MRE (multi).

**13 Spatially Resolved Damping Ratio Imaging with Non-Linear Inversion MRE in Gel-Tofu Phantoms**

Ligin M. Solamen[1], Matthew D. McGarry[1], Likun Tan[1] John B. Weaver[1,2], and Keith D. Paulsen[1,3]
*[1]Thayer School of Engineering, Dartmouth College, 14 Engineering Drive, Hanover, NH USA [2]Department of Radiology, Dartmouth Hitchcock Medical Center, 1 Medical Center Drive, Lebanon NH, USA. [3]Norris Cotton Cancer Center, 1 Medical Center Drive, Lebanon NH, USA*

**Background:** Magnetic resonance elastography (MRE) using a viscoelastic model recovers images of the complex-valued shear modulus, which captures both elastic stiffness and viscous attenuation effects. Although the majority of studies to date have focused on stiffness related parameters, recent and ongoing studies have demonstrated that the relative viscosity, or damping ratio, of brain tissue is a sensitive indicator of brain function. Sack et al. provided evidence that the damping ratio reveals information about brain tissue organization [1], and recently, Schwarb et al. reported a strong correlation between the damping ratio of the hippocampus and relational memory function in healthy adults, [2], as well as a correlation of aerobic fitness and hippocampal damping ratio [3]. The spatial accuracy of most MRE methodologies have been tested in simple phantoms with stiffness contrast, but to date no comprehensive phantom-based evaluation of the spatial accuracy of tissue viscosity imaging has been presented, despite frequent use of region-specific viscous properties in clinical studies.
**Aims:** This work evaluates the spatial resolution of non-linear inversion (NLI) MRE damping ratio images in gel-tofu phantoms containing inclusions and interfaces with damping ratio contrast.
**Methods:** The high mobile fluid content of tofu gives a greater relative viscosity than agar, where the fluid is more tightly bound in the polymerized structure. A damping ratio inclusion phantom was fabricated with a soft tofu background and four cylindrical 0.75% agar inclusions of varying diameter (15mm, 12mm, 10mm, and 8mm). A damping ratio interface phantom was also constructed from a soft tofu triangular prism encased in 0.65% agar. Both phantoms were actuated using a shear plate at 60Hz and 100Hz, and the resulting displacements were imaged at 2 mm resolution on a 3T Philips Achieva MRI. The damping ratio inclusion phantom was scanned in three different orientations to study reproducibility of the MRE images for different motion fields. Independent mechanical testing using dynamic mechanical analysis was also performed on samples of the phantom materials.
**Results:** The NLI reconstruction results indicated that the achievable spatial resolution of the damping ratio imaging is around 10 mm with CNR values greater than 1 (Fig. 1). The edge spread function of the interface phantom gave an edge response distance (90% to 10% transition in property change) of 12 mm.
**Conclusions:** This study provides the first phantom-based evidence of accurate imaging of damping ratio contrast in MRE. Results suggest that structures smaller than 10mm may require higher resolution data and/or soft prior regularization to recover accurate damping ratio estimates.

**References**: [1] I. Sack, K. Jöhrens, J. Würfel, and J. Braun, "Structure-sensitive elastography: on the viscoelastic power law behavior of in vivo human tissue in health and disease," *Soft Matter*, vol. 9, no. 24, pp. 5672–5680, 2013. [2] H. Schwarb, C. L. Johnson, M. D. McGarry, and N. J. Cohen, "Medial temporal lobe viscoelasticity and relational memory performance," *NeuroImage*, vol. 132, pp. 534–541, 2016. [3] Schwarb, Hillary, et al. "Aerobic fitness, hippocampal viscoelasticity, and relational memory performance." *NeuroImage* 153 (2017): 179-188.

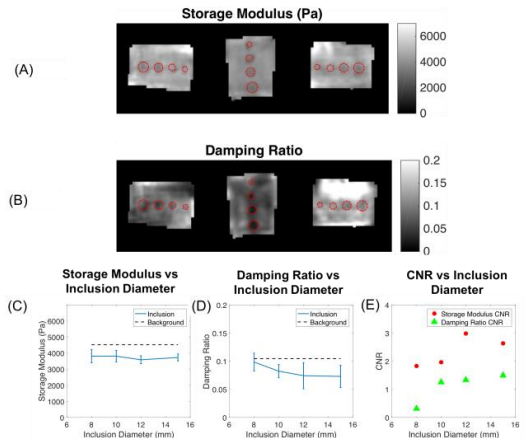


**Figure 1:** Damping ratio inclusion phantom. (A) Storage modulus and (B) Damping ratio images from three scanning orientations (C) Storage modulus (Pa) versus inclusion diameter. (D) Damping ratio values versus inclusion diameter compared to average background value. (E) Storage modulus and damping ratio CNR for inclusions.

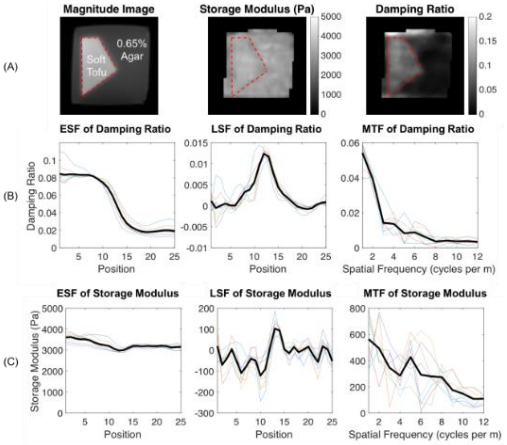


**Figure 2:** Damping ratio interface phantom (A) Viscoelastic property images, where the red contour indicates the soft tofu region. (B) and (C) Edge spread function (ESF) for the damping ratio and and storage modulus, respectively.

## 14 Mild TBI Studies Using Mixed Model Inversions

Anthony Romano[1], William Szymczak[1], Ziying Yin[2], and John Huston III[2]
*[1]Naval Research Laboratory, Acoustics Division, Washington, DC USA; [2]Department of Radiology, Mayo Clinic College of Medicine, Rochester, MN USA*

**Background:** Previously, in collaboration with Charite-Universitatsmedizin, Berlin, Germany, we introduced Waveguide Elastography[1] (WGE) which utilized a fusion of Magnetic Resonance Elastography (MRE), Diffusion Tensor Imaging (DTI), and an anisotropic inversion algorithm for the evaluation of the stiffness coefficients of white matter in the human brain using an Orthotropic model. Here, we utilize a Mixed-Model Inversion[2] (MMI) strategy which uses fractional anisotropy (FA) as a thresholding metric to differentiate between isotropic and anisotropic regions of the brain, thereby dictating whether an isotropic or anisotropic inversion should be implemented. For FA values <~0.2, an isotropic inversion was indicated[3], and for FA values ~>0.2, an Orthotropic inversion was indicated[1]. This allowed for proper segmentation of the differing brain regions such that the appropriate inversion algorithm could be utilized.
**Aims:** The aims of this work are i) to implement the MMI strategy in the evaluation of the elastic properties of both healthy controls and patients who present with mild TBI (mTBI) and ii) to demonstrate the alterations to the brain structures as a result of insult/injury.
**Methods:** As a proof of concept demonstration below, MRE at 60 Hz excitation and DTI were performed using a Compact 3T GE scanner on the brains of a healthy 21 year old male and a 19 year male who had suffered mTBI due to a hockey injury. The MMI was applied to the data and the isotropic/anisotropic stiffness coefficients were superposed on diffusion ellipsoids provided by the eigenvalues of the DTI data[4].
**Results:** When compared to the healthy control, there was diffuse axonal injury (DAI) in the mTBI patient with obvious hemorrhagic focus. In the image below, the hemorrhagic focus had a shear stiffness, C44, on the order of 4kPa, while in the relative sagittal planes, the gray matter was lower in stiffness in the patient (~2kPa) when compared to the healthy control (~3kPa). The stiffness, C44, over the entire brains, however, were quite similar with an average of 5.054 ± 0.386 kPa in the white matter of the control and 5.063 ± 0.385 kPa in the patient. In the gray matter regions, stiffness in the control was 2.333 ± 0.067 kPa and 2.333 ± 0.063 kPa in the patient. The patient had a higher fraction of white matter (52.1%) when compared to the control (46.8%) which may be attributed to differing volumes of the individual brains.
**Conclusions:** These preliminary studies indicate that the MMI, in concert with diffusion ellipsoids, provides encouraging metrics based on differences in material parameters for differentiation between healthy controls and mTBI patients. This work supported by Timothy Bentley, ONR Code 34, Warfighter Protection.

**References:** [1] Romano A.J. et al., MRM, 68, 1410-1422, 2012. [2] Romano A. J. et al., NCA TBI Research Symposium, 2017; [3] Romano A. J. et al., IEEE UFFC,47 (6): 1575-1581, 2000. [4] Basser P.J. ,NMR Biomed; Vol. 8: 333-344, 1995.

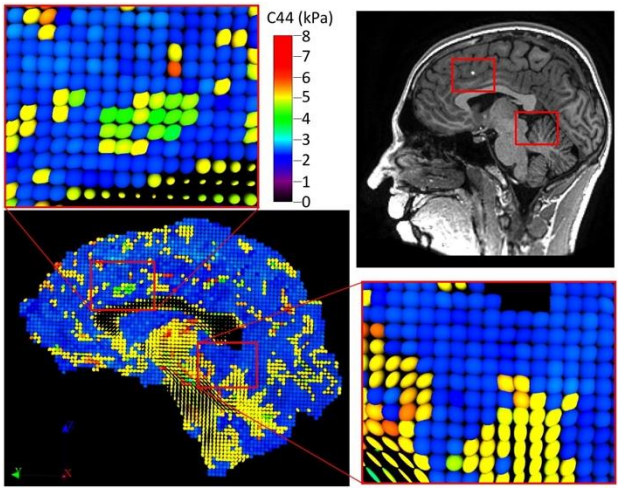


**Left image**, Diffusion ellipsoids colored by shear stiffness coefficient, C44, and T1 saggital slice of mTBI patient showing hemorrhagic focus of DAI.

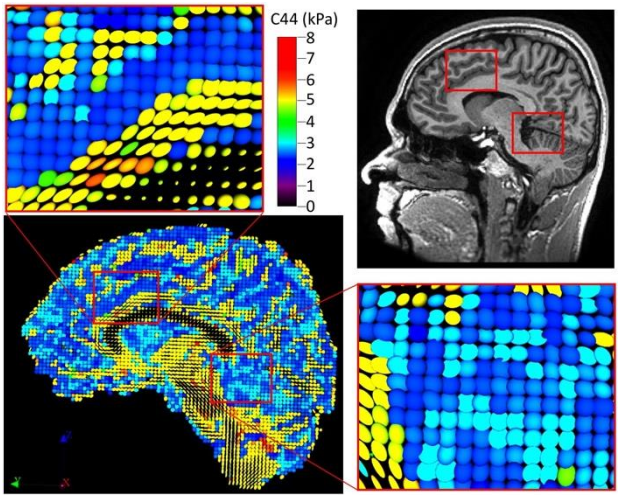


**Right image**, Diffusion ellipsoids colored by shear stiffness coefficient, C44, and T1 saggital slice of healthy control.

**15 Magnetic Resonance Elastography (MRE) Reproducibility Study in the Same Participants at Field Strengths of 1.5 , 3 and 7 Tesla**

Helen Marshall[1,2], Lucy Hiscox[1,3], Michael Perrins[1,2], Eric Barnhill[4], Ingolf Sack[4], Jurgan Braun[4], Tim Herrmann[5], Johannes Bernarding[5], Edwin van Beek[1] and Neil Roberts[1]

*[1]Edinburgh Imaging Facility, Queen's Medical Research Institute, University of Edinburgh, Edinburgh, United Kingdom, [2]Centre for Inflammation Research, Queen's Medical Research Institute, University of Edinburgh, Edinburgh, United Kingdom, [3]Alzheimer's Scotland Dementia Research Centre, University of Edinburgh, Edinburgh, United Kingdom [4]Department of Radiology, Charité – Universitätsmedizin Berlin, Berlin, Germany [5]Institute for Biometrics and Medical Informatics, Otto von Guericke University Magdeburg, Magdeburg, Germany*

**Background:** Previous work has reported that Magnetic Resonance Elastography (MRE) is a reliable method for assessing liver stiffness, with only small variations between measurements obtained using MR systems from different manufacturers, with different field strengths and pulse sequences[1]. MRE of the brain at field strengths of 1.5 and 7T have shown consistent brain stiffness estimates at multiple frequencies[2]. The effects of field strength have previously been investigated using adapted version Multi-Frequency Dual Elasto Visco (MDEV) inversion[3] and to our knowledge this is the first study to investigate the reproducibility and consistency of complex shear modulus, |G*| measures (Figure 1) in the same subjects at 1.5, 3 and 7T using unaltered MDEV[4,5].

**Aims:** To investigate the reproducibility of complex shear modulus |G*| estimates obtained for the same subjects at 1.5T, 3T and 7T.

**Methods:** Eighteen healthy participants (n=18; 36.4±12.7 years old) were studied on 1.5T, 3T and 7T MRI systems at MRE actuation frequencies of 30, 40 and 50Hz. Images were analyzed through multi-frequency MDEV post-processing[4]. The 1.5 and 3T datasets were acquired at 2mm isotropic resolution and the 7T data were acquired at 1mm isotropic resolution. The MATLAB imresize function was used to down-sample the 7T dataset to additionally provide images with 2mm isotropic resolution at this field strength. Binary Masks for each subject were generated with FLIRT, FSL[6] to obtain an average measurement of |G*| for the global cerebrum.

**Results:** Repeated measures ANOVA revealed a significant difference in |G*| between all field strengths ($p<.001$), mean values were 1.33±0.14kPa, 1.45±0.16kPa, 0.82±0.11kPa and 0.80±0.11kPa for 1.5, 3, 7T and 7T down-sampled datasets respectively. However intraclass correlation (ICC) estimates and their 95% confidence intervals, calculated in SPSS[7], revealed good to excellent reliability and strong correlations across all groups (Figure 2) comparisons: i) 1.5T by 3T ($\alpha$ = 0.71; $p$ = .007), ii) 1.5T by 7T ($\alpha$ = 0.81; $p$ = .001), iii) 3T by 7T ($\alpha$ = 0.80; $p$= .001), and finally iv) 7T by 7T down-sampled ($\alpha$ = 0.99; $p$ < .001).

**Conclusions:** This study shows brain stiffness estimates |G*| strongly correlate across varying field strengths and frequencies as assessed with MDEV, however mean stiffness values between field strengths were significantly different. This differs from previous work using adapted MDEV processing where average stiffness estimates were not significantly different, but strong intraclass correlation was still observed[5]. Multifrequency MRE of the brain is a viable technique clinically, however field strength variations between scanners must be acknowledged when considering absolute values.

**References:** [1] Trout et al, Radiology, 2016 [2] Hamhaber et al, JMRI, 2010), [3] Barnhill et al, ISMRM; Singapore, 2016 [4] Papazoglou et al, MRM, 2006, [5] Braun et al., NeuroImage 2014 [6]FMRIB Analysis Group, University of Oxford, 2012 [7] SPSS Inc, Chicago IL, 2016

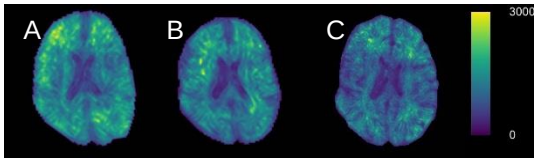


**Figure 1:** Elastograms for the same subject at (A) 1.5T (B) 3T and (C) 7T

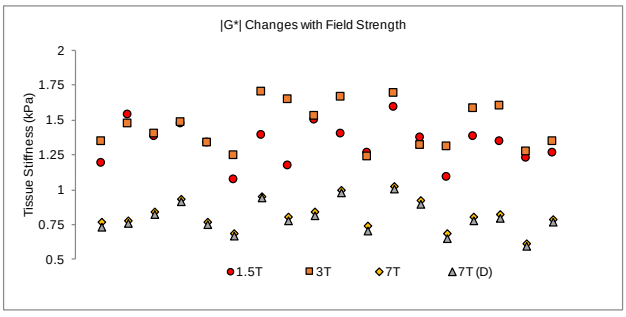


**Figure 2:** |G*| values for individual participants at 1.5, 3 and 7 T

**16 Imaging visual cortex activity with intrinsic poro-MR elastography**

Ligin Solamen[1], Reihaneh Forouhandehpour[2], Matthew D. McGarry[1], Elijah E.W. Van Houten[3], J.B. Weaver[1,4], K.D. Paulsen[1,5]

*[1]Thayer School of Engineering, Dartmouth College, 14 Engineering Drive, Hanover, NH USA [2]Department of Diagnostic Radiology, University of Sherbrooke, 3001 12th Avenue North, Sherbrooke, Quebec, Canada [3]Department of Mechanical Engineering, University of Sherbrooke, 2500, boulevard de l'Université, Sherbrooke, Quebec, Canada [4]Department of Radiology, Dartmouth-Hitchcock Medical Center, Lebanon, NH USA [5]Norris Cotton Cancer Center, 1 Medical Center Drive, Lebanon NH, USA*

**Background:** Recent interest in functional imaging via MR Elastography (fMRE) has shown evidence of mechanical changes during cerebral activity [1,2]. Given the critical role of blood flow in the gold standard functional MRI (fMRI) methods, *e.g. BOLD*, the role of hemodynamics in the viscoelastic property changes observed in fMRE is of interest. One potential approach for separating the structural and fluid components that underlie the effective viscoelastic properties of brain tissue at higher frequencies [3] is low frequency MR poro-elastography [4,5] via intrinsic activation [6].

**Aims:** i) To develop a protocol for intrinsic fMRE imaging using a visual stimulus ii) To test the detection of changes in the poroelastic properties in the region of the visual cortex during visual stimulation iii) To compare results from poroelastic and viscoelastic fMRE to better understand the role of hemodynamics during cerebral activity in the future.

**Methods:** Visual stimulus for the primary visual cortex (V1) was provided during the MR imaging protocol via the *Psychophysics Toolbox* for *Matlab*. After a high-resolution T1 image, a 5 minute BOLD sequence was used with 30 second repeated ON and OFF intervals. Once the location of V1 was identified, intrinsic brain displacements were measured by cardiac gated flow measurement similar to Weaver *et al.* [6] during 3 repeated ON and OFF cycles, with each ON or OFF interval lasting just over 4 minutes (3X2X4 = 24 minutes imaging time). Poro-elastography reconstructions were then performed on the measured displacement fields, and mean and the pooled variance values for each pixel were generated from the 3 repeats (ON and OFF). From these simple statistics, the contrast to noise ratio (CNR) of observed differences between the ON and OFF states were calculated for each of the poroelastic properties, i.e. shear modulus ($\mu$), $\lambda$-modulus and hydraulic conductivity ($\kappa$).

**Results:** Figures 1-6 show the CNR of difference images (ON-OFF) for the reconstructed shear modulus and hydraulic conductivity for two volunteer subjects. The first few inferior slices cover the primary visual cortex and the CNR difference tend to be negative in this region, suggesting greater shear modulus values when visual stimulation is absent.

**Conclusions:** Reconstructed poroelastic properties show localized changes in the region of the primary visual cortex. Further investigation will look into the effects of number of repetitions, image duration and type of stimulation used on the statistical power of poro-elastography fMRE results.

**References:** [1] Patz S et al., J Acoust Soc AM, 141: 3492, 2017. [2] Schwarb H et al., Neuroimage, 132: 534-541, 2016. [3] McGarry M et al., Med Phys, 42(2): 947-957, 2015. [4] Perriñez P et al., IEEE Trans Med Imag, 29(3) : 746-755, 2010. [5] Pattison AJ et al., Mech Biol. Syst Mater, 2: 41-48, 2011. [6]

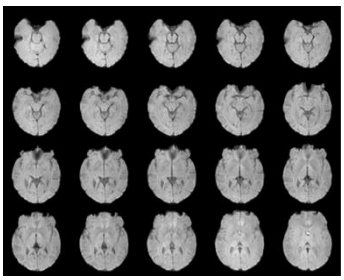

**Figure 1:** Axial magnitude image for subject A

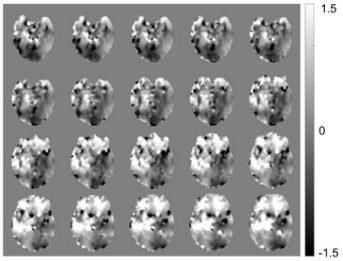


**Figure 2:** CNR image for the differences in shear modulus ($\mu$) of visual stimulation ON and OFF from subject A.

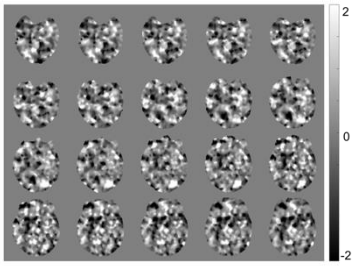


**Figure 3:** CNR difference image for hydraulic conductivity ($\kappa$) of visual stimulation ON and OFF for subject A.

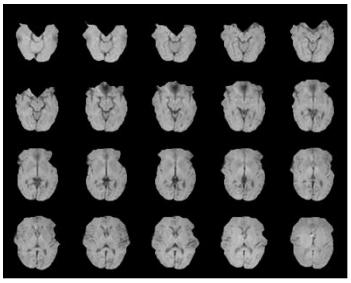

**Figure 4:** Axial magnitude image for subject B.

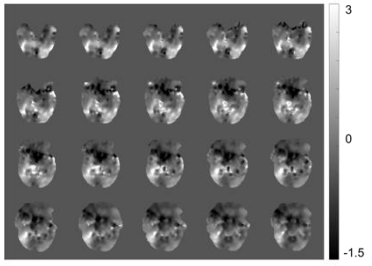


**Figure 5:** CNR image for the differences in shear modulus ($\mu$) of visual stimulation ON and OFF from subject B.

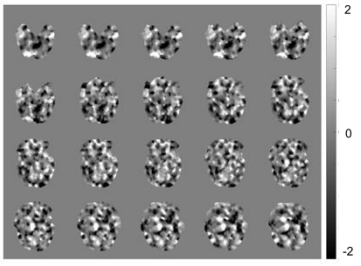


**Figure 6:** CNR difference image for hydraulic conductivity ($\kappa$) of visual stimulation ON and OFF for subject B.

## 17 Measurement of anisotropy in computer simulations and in porcine brain white matter *ex vivo* by MR elastography

P.V. Bayly, J.L. Schmidt, D.J. Tweten, R.J. Okamoto
*Mechanical Engineering and Materials Science, Washington University in Saint Louis, MO, USA.*

**Background:** Many soft tissues are mechanically anisotropic, due to underlying fibrous structure. Magnetic resonance elastography (MRE) can be used to characterize this anisotropy. The simplest anisotropic material model, valid for tissues with one dominant fiber direction, $\vec{a}$, is nearly-incompressible, transversely isotropic (NITI), elastic material, with three parameters [1-3]: **baseline shear modulus** ($\mu = \mu_2$), **shear anisotropy** ($\phi = \frac{\mu_1}{\mu_2} - 1$), and **tensile anisotropy** ($\zeta = \frac{E_1}{E_2} - 1$). For a propagation direction, $\vec{n}$, there are two shear wave modes: pure transverse or "slow" (polarization $\vec{m}_s$), and quasi-transverse or "fast" (polarization $\vec{m}_f$) (Fig. 1). The speed of a plane shear wave in uniform NITI material depends on (i) the angle, $\theta$, between propagation and fiber directions, (ii) the polarization (slow or fast), and (iii) the parameters $\mu$, $\phi$, and $\zeta$.

**Slow**: $c_s^2 = \frac{\mu}{\rho}(1 + \phi\cos^2(\theta))$ **[Eq1]**; **Fast**: $c_f^2 = \frac{\mu}{\rho}(1 + \phi\cos^2(2\theta) + \zeta\sin^2(2\theta))$ **[Eq2]**

To estimate all three material parameters, both wave modes, in multiple propagation directions are needed [2]. To estimate only $\mu$ and $\phi$, only slow shear waves are required, still at multiple directions [3].

**Aims:** (i) to demonstrate the effect of NITI material parameters on shear wave propagation in simulations; (ii) to estimate all parameters in simulations, and iii) estimate shear anisotropy in brain white matter *ex vivo*.

**Methods: Simulation:** Frequency-domain simulations of shear waves (100 Hz) in a uniform 50-mm cube of NITI material ($\mu = 1$ kPa, $\phi = 1$, $\zeta = 2$) were performed in COMSOL™ (Burlington, MA) finite element (FE) software. Data in 1 mm voxels were analyzed in MATLAB (Natick, MA) using local direct inversion to estimate wave speeds. Equations Eq1 and Eq2 were used to solve for parameters. **Experiment**: slow shear waves were excited by a central rod and imaged by MRE in discs of fresh porcine brain embedded in gelatin. Axis ratios and local wavelengths of elliptical shear waves were compared to results from simulations with known $\mu$ and $\phi$; parameters were estimated from simulations that had minimum error relative to experiment.

**Results:** Wave speeds in simulations were within 10% of theoretical predictions (Eq1, Eq2), and parameter estimates were: $\mu = 1.08$ kPa, $\phi = 0.82$, $\zeta = 1.64$ ($R^2$=0.94). In porcine brain white matter, shear modulus $\mu$ =1.04 $\pm$ 0.12 kPa (at 100 Hz), $\mu$ =1.94 $\pm$ 0.29 kPa (at 200 Hz), and $\mu$ =2.88 $\pm$ 0.34 kPa (at 300 Hz) and shear anisotropy $\phi$ =0.27 $\pm$ 0.09 (at 100 Hz), $\phi$ =0.29 $\pm$ 0.14 (at 200 Hz) and $\phi$ =0.34 $\pm$ 0.13 (at 300 Hz).

**Conclusions:** Accurate estimates of NITI parameters are possible, with sufficient, high-quality data. White matter in the porcine brain *ex vivo* is mildly anisotropic in shear, with directional differences of 30-35%.

**References:** [1] Guo et al., MRM,75:1537-45, 2016. [2] Tweten et al., MRM, (in press). [3] Schmidt et al., J Biomech 49:1042-9, 2016.

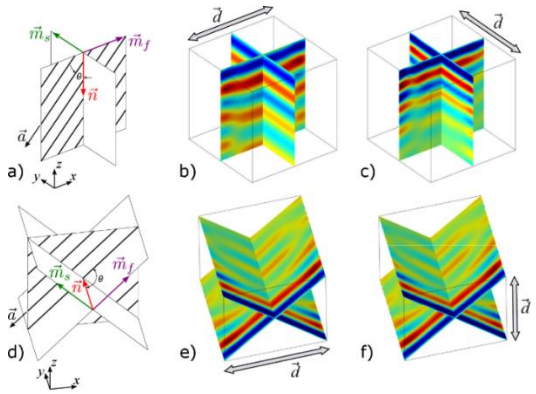


**Figure 1:** Schematic diagrams (a,d) and simulations (b-c, d-e) showing fiber orientiation ($\vec{a}$), propagation ($\vec{n}$), and polarization directions of slow ($\vec{m}_s$) and fast ($\vec{m}_f$) shear waves in anisotropic (NITI) material. Actuation direction ($\vec{d}$) is shown by outlined arrows. Note that when actuation direction corresponds to fast wave polarization (b), speed is higher and wavelength is longer than when actuation corresponds to slow wave polarization (c).

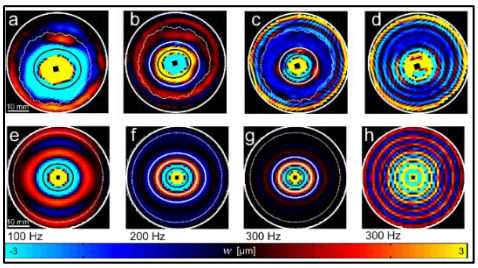


**Figure 2**: Shear waves excited by a central rod in cylinder samples of brain tissue (experiment, top row) and anisotropic (NITI) FE model (simulation, bottom row). (a-c) MRE images of shear wave propagation in WM at (a) 100 Hz, (b) 200 Hz, and (c) 300 Hz. Shear-wave fronts are fitted by ellipses (black or white). Tissue sample is outlined by dotted white line. (d) Shear-wave propagation in an image slice containing only gelatin at 300 Hz. (e-g) Shear wave propagation in FE simulations with similar mechanical properties to the experiment: (e) 100 Hz, $\mu_2$ = 1100 Pa, $\phi$ = 0.30; (f) 200 Hz, $\mu_2$ = 1600 Pa, $\phi$ = 0.45; (g) 300 Hz, $\mu_2$ = 2300 Pa, $\phi$ = 0.35. (h) Shear-wave propagation in the isotropic/gelatin portion of the FE model at 300 Hz.

## 18 Magnetic Resonance Elastography of the Lung.

F.S. Fakhouri[1,2], A. Kolipaka [1,2,3]

*[1]Department of Biomedical Engineering, The Ohio State University, Columbus, OH, 43210, USA. [2]Department of Radiology, The Ohio State University Wexner Medical Center, Columbus, OH, 43210, USA.[3]Department of Internal Medicine-Division of Cardiology, The Ohio State University Wexner Medical Center, Columbus, OH, 43210, USA.*

**Background:** Lungs continuously experience various mechanical stresses caused by the natural physiology of breathing. It is known that lungs mechanical properties change with different diseases. In general, if lungs become stiffer or softer than normal range, its normal physiology will be negatively affected[1].

**Aims:** The aim of this study is to provide a baseline of normal lung shear stiffness at both residual volume (RV) and total lung capacity (TLC) by using principal frequency analysis (PFA)[2].

**Methods:** 9 healthy volunteers were scanned using a spin echo – echo planer imaging (SE-EPI) MRE sequence on a 1.5T MR scanner (Avanto, Siemens Healthcare, Erlangen, Germany) to obtain 5 axial slices of the right lung. A passive pneumatic driver was placed on top of the apex of the right lung. Only right lung was considered for imaging because of the heart motion on the left side. In this scan a single breath hold of 26 seconds was involved for each MRE acquisition at RV and TLC scans with an EPI factor of 9. The scan parameters included field-of-view (FOV) of 40 cm, slice thickness of 10 mm, acquisition matrix of 128x64, TE of 11.6 ms (T2 of the lung = 40 ms) and a TR of 400 ms (T1 of the lung = 1100 - 1300 ms at 1.5T) to allow the longitudinal magnetization to recover[1]. The MEG frequency was 250 Hz, and an external motion of 50Hz was applied.

Lung density scans were performed by using a basic gradient recalled echo (GRE) sequence with four different TEs of 1.07 (minimum TE), 1.5, 2, and 2.5 ms to calculate $T_2$* decay, from which the initial signal of the lung was estimated. After obtaining the initial signal of the lung, the lung density was calculated in reference to a Gadolinium doped water phantom that was placed on the volunteer's chest while scanning[1,3-4].

Effective lung shear stiffness (without considering the lung density) and actual lung shear stiffness (with considering the lung density) at both RV and TLC were calculated by using PFA method (MATLAB, Math Works, Natick, MA)[2]. The directional filter cutoff was 8-40 pixels/wave for RV and 4-40 pixels/wave for TLC. Filter cutoff values were selected based on number of pixels manually measured in a full wavelength.

**Results:** The nine healthy volunteers had effective mean shear stiffness (i.e. when lung density is assumed to be 1g/cm$^3$) value of 3.43±0.39 kPa and 13.9±1.37 kPa for RV and TLC, respectively. The actual mean shear stiffness value calculated based on measured lung density was 0.66±0.12 kPa and 1.01±0.29 kPa for RV and TLC, respectively. Furthermore, volunteers' lung density had a mean value of 0.1962±0.049 g/cm$^3$ and 0.0732±0.023 g/cm$^3$ at RV and TLC, respectively.

**Conclusions:** Lung MRE can be performed in a breathhold using a SE-EPI sequence without any noble gas inhalation. Lung shear stiffness varies across respiratory cycle. The lung is softer at RV and stiffer at TLC due to its deflation and inflation with air, respectively. Also lung density changes across the respiratory cycle. The lung have higher density at RV due to less air volume content, and have lower density at TLC due to higher air volume content.

**References:** [1] Mariappan YK et al., J Magn Reson Imaging, 40(5):1230-7, 2014. [2] McGee KP et al., Phys. Med. Biol, 56(14):4291-4309, 2011. [3] Theilmann RJ et al., J Magn Reson Imaging, 30(3):527-34, 2009. [4] Holverda S et al., J Magn Reson Imaging, 34(1):220-4, 2011.

**Acknowledgement:** Department of Biomedical Technology, King Saud University, Riyadh, The Kingdom of Saudi Arabia is providing scholarship to F.S. Fakhouri. NIH-R01HL124096 for funding.

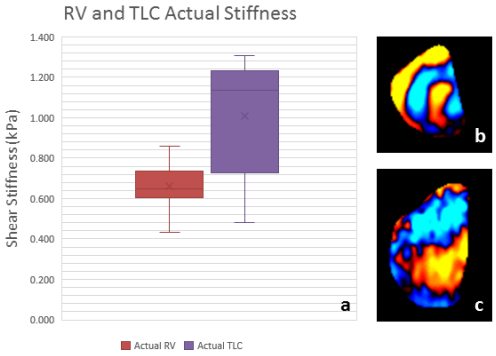


**Figure 1:** (a) Shows a box plot for both RV and TLC. The actual mean shear stiffness of RV and TLC is 0.66±0.12 kPa and 1.01±0.29 kPa, respectively. (b) and (c) show a snap shot of a wave image for a given slice at RV and TLC, respectively in which the wavelength in TLC is longer than RV.

| | RV | | | TLC | | |
|---|---|---|---|---|---|---|
| | Effective Stiffness | Actual Stiffness | Lung Density | Effective Stiffness | Actual Stiffness | Lung Density |
| 1 | 3.07±0.22 | 0.86±0.06 | 0.28 | 12.09±0.91 | 1.31±0.99 | 0.11 |
| 2 | 2.85±0.18 | 0.68±0.04 | 0.24 | 12.81±0.47 | 1.14±0.04 | 0.09 |
| 3 | 3.67±0.22 | 0.43±0.03 | 0.12 | 12.08±1.26 | 0.48±0.05 | 0.04 |
| 4 | 3.23±0.21 | 0.64±0.04 | 0.2 | 14.53±1.28 | 0.73±0.06 | 0.05 |
| 5 | 4±0.19 | 0.68±0.03 | 0.17 | 14.74±0.28 | 1.09±0.02 | 0.07 |
| 6 | 3.42±0.19 | 0.59±0.03 | 0.17 | 15.32±0.75 | 0.73±0.04 | 0.05 |
| 7 | 3.38±0.13 | 0.62±0.02 | 0.18 | 15.86±0.21 | 1.27±0.02 | 0.08 |
| 8 | 3.28±0.26 | 0.71±0.06 | 0.24 | 13.52±0.8 | 1.17±0.07 | 0.09 |
| 9 | 3.98±0.16 | 0.65±0.03 | 0.16 | 14.18±0.38 | 1.2±0.03 | 0.09 |

**Table1:** Shows effective and actual mean shear stiffness in kPa for 5 slices for all of the volunteers at RV and TLC. Also the table shows the lung densities in g/cm$^3$ for all of the volunteers at RV and TLC.

## 19 Shear wave dispersion probes fractal dimension of 3D vascular trees

J. Sudakova[1], J. de Arcos[1], H. Sverre [2], D. Nordsletten[1], R. Sinkus[1]
*[1]Department of Biomedical Engineering, King's College London, London, UK; [2]Department of Informatics, University of Oslo, Oslo, Norway*

**Background:** A recent theory relates macroscopically observable power-law dispersion of shear waves to underlying structural fractality [1,2].This is an alternative loss mechanism to absorption in the medium, here, dispersion properties are the result of coherent multiple reflections of the shear waves on the underlying scattering structure that is embedded in an otherwise isotropic and purely elastic medium [3]. The geometrical properties, and in particular the fractal dimension, of the scattering structure dictate the slope of the power-law. The theory was tested on randomly dispersed mono-size microspheres (∅10mm) leading to intrinsic fractality below a certain characteristic length due to fluctuations in the density [4].
**Aims:** i) experimentally validate that apparent dispersion properties of shear waves depend on the fractality of 3D vascular trees, and ii) explain those results in the framework of multiple reflections using the concept of lag-time distribution for the description of the medium. The ultimate aim is to use this method to characterize tumour vasculature.
**Methods:** 3D structures were printed from a translucent high definition hard plastic (VisiJet EX2000) according to the model proposed in [5]. Individual trees (Fig.1A) were assembled to four different forests (Fig.1B) where each tree had a random organization, but the same fractal dimension $d_f$. The series of random numbers for tree generation was identical among forests, only varying the branching ratio to determine $d_f$ [5] (Fig.1C). Forests were embedded in a quasi-dispersionless ultrasound gel and MRE experiments were performed in the 20-70 Hz frequency range, resulting in an effective shear wave length ranging from 15-29 mm, whereby probing on average an entire tree (Fig.1A). High resolution T2-weighted images were obtained for each forest (Fig.2A). Efficient wave penetration throughout the entire phantom (Fig.2B) allows correct reconstruction of the apparent shear wave speed *c*. Shear wave speeds were reconstructed according to published methods and effective power-law exponents of *c* extracted from linear fits to data represented on a log-log scale [1].
**Results:** Fig.2C shows the measured slope $y$ of the apparent shear wave speed as a function of the fractal dimension $d_f$ of the forests. As expected, for increasing $d_f$ – i.e. an approach towards Euclidean properties with $d_f = 2$ – we observe a drop of the slope, i.e. the material becomes less dispersive and returns to classical behaviour [1]. The case $d_f = 2$ corresponds to a flat pair-correlation function of the scattering structure, as confirmed by numerical simulations. Deviations from Euclidean properties ($d_f < D$) lead to a significant measurable increase in *y*, as confirmed by the data. The data for $d_f = 2$ in Fig.2C is taken from the dispersion properties of the bare ultrasound gel without any forest.
**Conclusions:** Multiple coherent scattering of shear waves on structures well below the wavelength lead to apparent macroscopically observable dispersion that can be explained within the context of the ODA theory [3] when considering the propagative part [1]. Our data demonstrate that the fractal dimension of the scattering structure can be measured via the slope of the shear wave speed dispersion. This result paves the way towards a non-invasive clinical assessment of tumour vasculature since the endothelium exhibits enough rupture in shear stiffness compared to the ECM to cause shear wave reflections [6]. Currently we are performing detailed simulations for all different tree configurations with varying $d_f$ to investigate whether the extended ODA theory can explain the details of Fig.2C.

**References:** [1] Lambert SA et al., Phys. Rev. E 115, 094301 (2015). [2] Garnier J, Sølna K, Multiscale Model. Simul, 7-3, 1302–1324 (2009). [3] O'Doherty RF, Anstey NA, Geophys. Prospect. 19, 430 (1971). [4] Hamburger D et al., Phys. Rev. E 53, 3342 (1996). [5] Zamir M, J. theor. Biol. 212, 183-190 (2001). [6] Juge L et al., NMR Biomed 28(12), 1763-71 (2015).

**Acknowledgements:** This project has received funding from the European Union's Horizon 2020 research and Innovation programme under grant agreement No 668039 and the European Union's Seventh Framework Programme for research, technological development and demonstration under grant agreement no FP7-ICT-2011-9-601055.

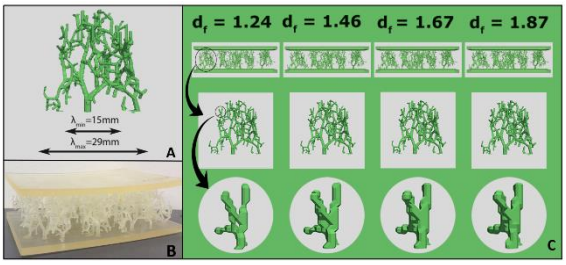


**Figure 1:** (A) A 3D vascular tree. (B) Different fractal dimension forests were built joining individual trees. (C) Variation in branching ratio between forests result in different fractal dimensions.

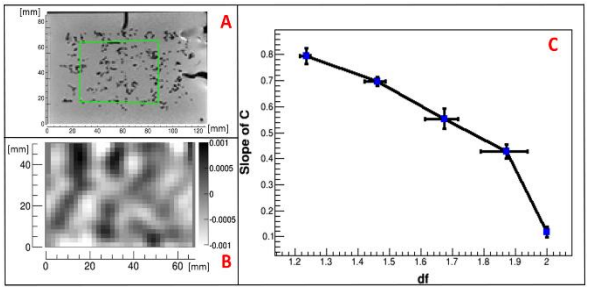


**Figure 2:** (A) Branches (in black) generate an MR signal void in the background ultrasound gel. (B) Curl in z-direction of the 3D wave field within a large region of interest positioned over several trees (green box in Fig.2A) for a driving frequency of 20 Hz. (C) Slope dependency of speed c on fractal dimension $d_f$ of the forests

**20 Mechanical Properties of the Healthy Aging Human Brain**

A.T. Anderson[1,2], C.L. Johnson [3], B.P. Sutton[2,4], E.E.W. Van Houten[5], J.G. Georgiadis[6]

*[1]Mechanical Science & Engineering Department, University of Illinois at Urbana-Champaign, Urbana, IL, USA; [2]Beckman Institute for Advanced Science & Technology, University of Illinois at Urbana-Champaign, Urbana, IL, USA; [3]Department of Biomedical Engineering, University of Delaware, Newark, DE, USA; [4]Bioengineering Department, University of Illinois at Urbana-Champaign, Urbana, IL, USA; [5]Département de génie mécanique, Université de Sherbrooke, Sherbrooke, Québec, Canada; [6]Biomedical Engineering Department, Illinois Institute of Technology, Chicago, IL, USA.*

**Background:** Previous studies using MR Elastography have shown the mechanical properties of the healthy aging human brain change with age [1-3], but not all areas by the same amount [4]. This study will attempt to characterize normal aging (senescence) of human by incorporating diffusion tensor imaging (DTI) and multi-excitation MRE [5] towards identifying important anisotropic differences.

**Aims:** i) to extend the understanding of anisotropic mechanical properties of human brain microstructure with age ii) to quantify anisotropic differences in the aging human brain using multi-excitation MRE and iii) to identify where MRE is more sensitive than DTI

**Methods:** The experiment from a previous study [5] was repeated on ten "young" (24-32 years old) and twelve "young-old" (55-76 years old) males. The MR experiment included: high-resolution anatomical MPRAGE, diffusion tensor imaging (DTI), anterior-posterior (AP) excitation MRE, and left-right (LR) excitation MRE. Nonlinear inversion estimated heterogeneous, isotropic viscoelastic properties[6].

**Results:** The reconstructed isotropic material property maps for a young and young-old subject are shown in Figure 1. The whole brain averages, see Figure 2, have population averages of: young—G' = 2.22 [kPa], G'' = 0.91 [kPa] and young-old—G' = 2.09 [kPa], G'' = 0.86 [kPa].

**Conclusions:** These preliminary results for the whole brain material properties show slight differences for the population averages, but further analysis of regional differences, especially highly-anisotropic white matter, will be necessary to understand how the microstructure changes with age.

**References:** [1] Sack, I., et al., NeuroImage, 46, 652–657, 2009. [2] Sack, I., et al., PLoS ONE, 6, e23451, 2011. [3] Guo, J., et al., PLoS ONE, 8, e71807, 2013. [4] Arani, A., et al., NeuroImage, 111, 59–64, 2015. [5] Anderson, A.T., et al., JMBBM, 59, 538–546, 2016. [6] Van Houten EEW, et al., Magn Reson Med, 42(4):779-786, 1999.

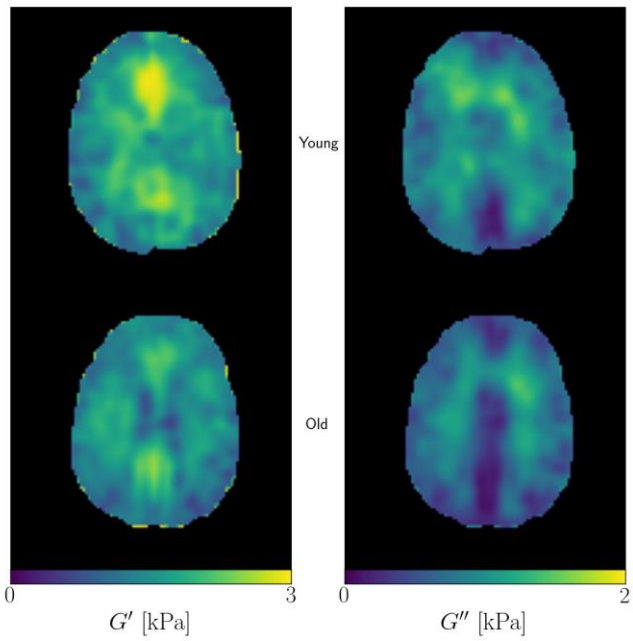


**Figure 1:** An axial slice of the NLI-MRE reconstruction of G' and G'' for a "young" subject (top) and a "old" subject (bottom).

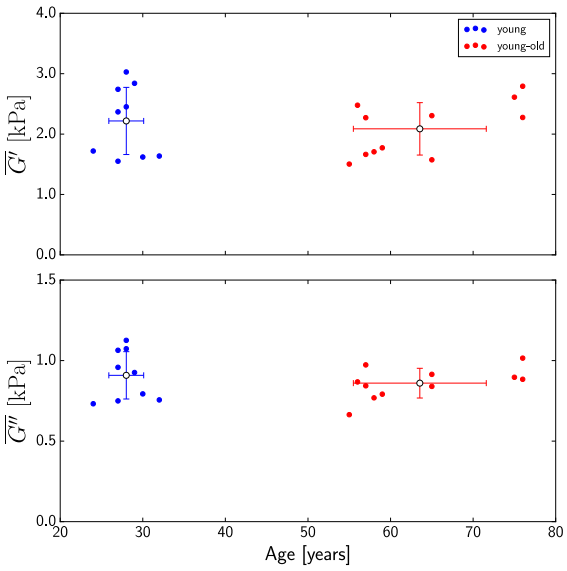


**Figure 2:** Whole brain averages for the reconstructed shear (G') and loss (G'') moduli for the anterior-posterior excitation, separated into two age groups.

## 21 Double Dissociation of Structure-Function Relationships in Memory and Fluid Intelligence Observed with Magnetic Resonance Elastography

CL Johnson[1*], H Schwarb[2*], KM Horecka[2], MDJ McGarry[3], CH Hillman[4], AF Kramer[4], NJ Cohen[2], AK Barbey[2]
*[1]University of Delaware, Newark, DE; [2]University of Illinois at Urbana-Champaign, Urbana, IL; [3]Columbia University, New York, NY; [4]Northeastern University, Boston, MA; * equal contribution*

**Background:** Brain tissue mechanical properties, measured in vivo with magnetic resonance elastography (MRE), have proven to be sensitive metrics of neural tissue integrity[1]. Recently, our group has reported on the positive relationship between viscoelasticity of the hippocampus (HC) and performance on a relational memory task in healthy, young adults[2], which highlighted the potential of sensitive MRE measures for studying brain health and its relation to cognitive function; however, structure-function relationships outside of the HC have not yet been explored.
**Aims:** i) Examine the viscoelasticity of the orbitofrontal cortex (OFC) with MRE and explore its relationship with fluid intelligence in healthy, young adults; and ii) compare HC-relational memory and OFC-fluid intelligence structure-function relationships observed with MRE.
**Methods:** *Subjects:* A sample of healthy, young adults, 18-35 years old, completed MRE scans and cognitive assessment. The final analysis included 53 participants (26M/27F; mean age: 22.8 years) after exclusion for incomplete data or statistical outliers. *MRE:* Displacement data was acquired with a 3D multislab, multishot spiral MRE sequence[3] with 1.6 mm isotropic resolution. Viscoelastic properties in the HC and OFC were estimated using nonlinear inversion (NLI)[4] with soft prior regularization (SPR)[5], as described previously[6]. NLI reconstructs the damping ratio, $\xi = G''/2G'$, and we report $\xi' = 1-\xi$ as in our previous works[2]. *Cognitive Tasks*: Relational memory was assessed using a spatial reconstruction (SR) task (Fig 1b); and fluid intelligence was assessed using a figure series (FS) task (Fig 1c).
**Results:** As in previous works[2], we find a significant, positive relationship between HC $\xi'$ and relational memory from SR task performance ($r$ = 0.41; $p$ = 0.002; Fig 2, top left). We also find a significant, positive relationship between OFC $\xi'$ and fluid intelligence from FS task performance ($r$ = 0.42; $p$ = 0.002; Fig 2, bottom right). Importantly, we also find no significant relationships between HC $\xi'$ and fluid intelligence or OFC $\xi'$ and relational memory. Indeed, the correlations between HC $\xi'$ with SR and FS are significantly different; as are the correlations between OFC $\xi'$ with FS and SR. This indicates a double dissociation.
**Conclusions:** The reported relationship between OFC viscoelasticity and fluid intelligence, and the double dissociation with HC viscoelasticity and relational memory, emphasize the specificity of regional brain MRE measures in support of separable cognitive functions. This is the first report of a structure-function relationship observed with MRE beyond the HC and suggests a future role for MRE as a sensitive neuroimaging technique for brain mapping.

**References:** [1] Hiscox LV, et al., *Phys Med Biol*, 2016, 61(24):R401-R437; [2] Schwarb H, et al., *NeuroImage*, 2016, 132:534-541; [3] Johnson CL, et al., *MRM*, 2014, 71(2): 477-485; [4] McGarry MDJ, et al., *Med Phys,* 2012, 39(10):6388-6396; [5] McGarry MDJ, et al., *IEEE TMI*, 2013, 32(10):1901-1909; [6] Johnson CL, et al., *HBM*, 2016, 37(12):4221-4223.

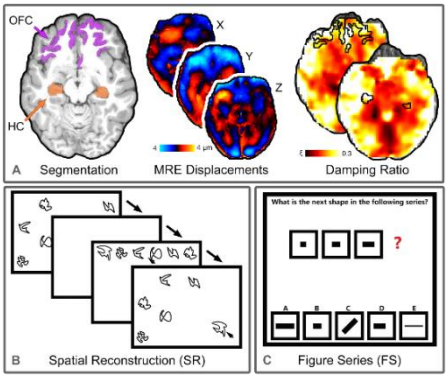


**Figure 1 (above):** A) MRE of the HC and OFC; B) spatial reconstruction task (relational memory); C) figure series task (fluid intelligence).

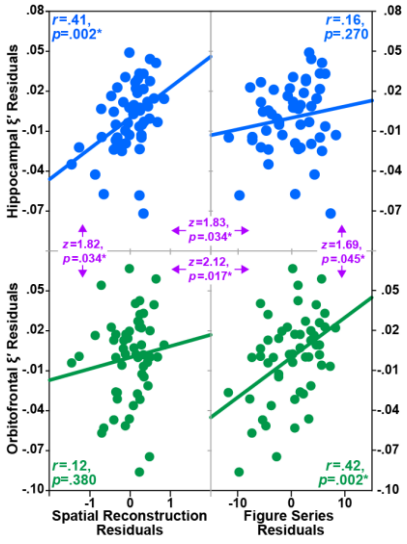


**Figure 2 (right):** Residuals of HC $\xi'$ (top) and OFC $\xi'$ (bottom) plotted against residuals of SR (left) and FS (right).

## 22 Characterization of Pedriatic Brain Viscoelasticity Using Magnetic Elastography

E. Ozkaya[1], G. Fabris[1], J. Martinez[1], F. Macruz[2], K. B. Pauly[2,3], M. Wintermark[2], M. Kurt[1]
*[1]Department of Mechanical Engineering, Stevens Institute of Technology, Hoboken, New Jersey, USA; [2]Department of Radiology, Stanford University, Stanford,California, USA; [3]Department of Bioengineering, Stanford University, Stanford,California, USA*

**Background:** Information on pediatric brain mechanics has been traditionally scarce and hard to obtain in spite of its huge relevance for a range of pathophysiological processes. Understanding the mechanical properties of the human brain during childhood would allow us to not only to better understand normal brain development, but also to develop more targeted preventive measurements against traumatic brain injury (TBI). Magnetic resonance elastography (MRE) is emerging as an *in-vivo* imaging technique allowing to acquire brain tissue mechanical properties in a non-invasive manner thanks to the transmission of shear waves to the skull and brain via a passive driver [1]. The displacements caused by these shear waves in the tissue are then imaged with a phase-contrast imaging method, and after using a direct inversion technique, the frequency dependent characteristic of the pediatric brain can be identified.

**Aims:** i) Understanding the undergoing mechanical changes of the developing brain during childhood
ii) Determining of the viscoelastic properties of the pediatric brain
iii) Observing the variation of viscoelastic properties in deep white matter regions

**Methods:** We have recruited 27 healthy volunteers aged between 7 and 17, in which 13 of them were males and 14 were females. For age group classification the childhood era is divided into three phases which are pre-to early puberty (7-9), early to advanced puberty (10-14) and post puberty (15-17). For these three phases, proper MNI NIHPD templates are being used to register healthy volunteer data to their common age group spaces. Also ICBM template is being used for registering in order to observe the variances in deep white matter areas. Besides registration, pre-processing steps include bias correction, reslicing, skull stripping and smoothening which all are being performed by SPM 12.

While acquiring the brain stiffness maps MRE actuation frequency is varied and the raw data obtained is being moved to a frequency independent domain by fitting the raw data to Zener material model since it expresses the brain tissue response better than Maxwell, Kelvin-Voigt or Springpot material models [2].

**Results:** We have found evidence of brain stiffening until age 14, followed by softening through age 17 (Figure 1). The highest changes were observed for loss modulus values, where we have seen 13% increase through the age 14, followed by a 15% decrease through the age 17. The most significant changes were observed in deep white matter structures, especially corpus callosum, where we observe 23% stiffening through the age 14. (Figure 2).

**Conclusions:** We were able to detect significant differences in the mechanical properties during pre-to early puberty, early to advanced puberty and post puberty, however it should be noted that the sample size was relatively small. The differences between deep white matter structures were the most pronounced.

**References:** [1] Hiscox et al., *Physics in Medicine & Biology*, 61: 401-437. [2] Sack et al., *NeuroImage*, 46:652-657, 2009.

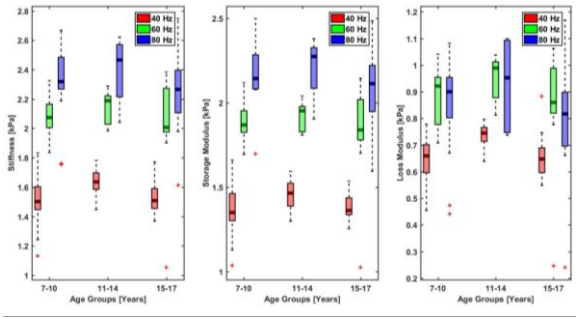


**Figure 1:** Age-dependent changes in the mechanical properties of the pediatric brain.

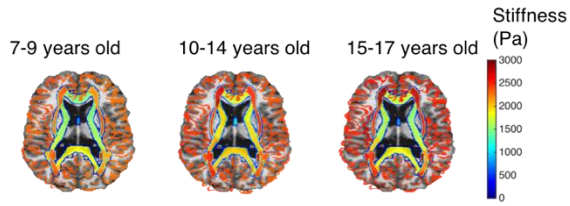


**Figure 2:** Variation of frequency independent parameters in deep white matter regions.

**23 Hippocampal viscoelasticity and episodic memory performance in healthy older adults**

LV Hiscox[1,2], CL Johnson[3], H Schwarb[4], MDJ McGarry[5,6], EJR van Beek[2], N Roberts[2], and JM Starr[1].
*[1]Alzheimer Scotland Dementia Research Centre, University of Edinburgh, UK; [2]Edinburgh Imaging Facility, QMRI, University of Edinburgh, UK; [3]Department of Biomedical Engineering, University of Delaware, DE, USA; [4]Beckman Institute for Advanced Science and Technology, University of Illinois at Urbana-Champaign, IL, USA; [5]Thayer School of Engineering, Dartmouth College, NH, USA; [6]Department of Biomedical Engineering, Columbia University, NY, USA.*

**Background:** Previous work has found a direct relationship between the viscoelastic properties of brain tissue and cognitive function. In particular, microstructural integrity of hippocampal tissue (i.e. damping ratio ξ), assessed using MR Elastography (MRE), has been associated with relational memory performance in healthy young adults[1,2]. The relationship between brain viscoelasticity and cognition in healthy older adults, however, has not been investigated even though standard neuropsychological tests have been shown to have higher sensitivity in this age group. Out of the six major memory systems, disruptions to episodic memory, which refers to the memory system that allows an individual to consciously retrieve a previously experienced episode of life, are among the earliest signs and symptoms of Alzheimer's disease (AD)[3]. An imaging biomarker for episodic memory is therefore a promising avenue for AD early detection.
**Aims:** To investigate the possible relationship between hippocampal viscoelasticity and episodic memory performance in cognitively healthy older adults.
**Methods:** Eighteen older adults (aged 65+) were recruited from the Join Dementia Research database. To be selected as cognitively healthy, subjects were required to score >26/30 on the Montreal Cognitive Assessment (MoCA) as well as perform the National Adult Reading Test (NART). MRE data were acquired using a multi-shot multi-slab spiral sequence[4] and inverted with a FEM-based non-linear inversion (NLI) algorithm incorporating soft prior regularization (SPR)[5]. MRE data quality was measured by OSS-SNR[6]. Masks of the hippocampus and amygdala, a control brain region, were generated with Freesurfer and co-registered to MRE maps using FLIRT within FSL. Outcome MRE measures were shear stiffness, $\mu$ (kPa) and damping ratio ξ. Episodic memory was assessed by using the Verbal Paired Associates subtest (VPA) from the Wechsler Memory Scale-III (WMS-III); the maximum score for immediate recall (VPA-IR) was 24. In total, seven participants were excluded from the final analysis: three subjects had OSS-SNR <3, two subjects scored <26 on the MoCA, one subject had an incidental finding, and one subject scored below the median absolute deviation (MAD) on the VPA-IR. The resulting sample consisted of eleven participants (mean age=69.1 + 2.3 years, 6F/5M).
**Results:** Pearson partial correlation coefficients, $R^2$, with age (years), sex, NART full scale IQ, and ROI volume were used as control variables to investigate how each MRE measure correlated with VPA-IR performance. Age (years), sex, and NART were used as control variables for correlations between ROI volume and memory performance. Results are provided in Table 1 and illustrated in Figure 1. The significance of correlations was determined at $p$<0.05.
**Conclusions:** The results obtained indicate that increased relative viscous-to-elastic behaviour (i.e. higher damping ratio ξ) of the hippocampus is associated with poorer performance on a measure of episodic memory, consistent with previous studies of relational memory[1,2]. The viscoelasticity of a whole brain measure (i.e. cerebrum) and amygdala, however, are not significantly associated with task performance highlighting the specific role of the hippocampus for memory function. Furthermore, hippocampal volume was not associated with memory performance despite the well-established relationship with cognitive decline in ageing[7]. We speculate that increased ξ is likely to reflect the excessive accumulation of damaged proteins, DNA, and membranes due to the known increase in oxidative, metabolic, and ionic stress[8], resulting in disorganized tissue components that more effectively absorb strain energy. Thus, the microstructural measure afforded by ξ outperforms the gross measure of hippocampal atrophy. This preliminary study highlights the importance of high-resolution MRE for studying the cognitive functions of specific brain structures, and provides further support for the relationship between tissue microstructure and functional performance.

**References:** [1] Schwarb et al., Neuroimage,132(3): 534-41, 2016. [2] Schwarb et al., NeuroImage, 153:179:88, 2017. [3] Gold et al., Expert Rev. Neurother, 8(12): 1879-91, 2008. [4] Johnson et al., Magn. Reson. Med., 71:477-85. [5] McGarry et al., Trans Med Imaging, 32:1901-09, 2013. [6] McGarry et al., Phys. Med. Bio., 56:153-64, 2011. [7] Raz et al., Cerb. Cortex, 15:1676-89. [8] Mattson et al., Nature reviews. Neuroscience, 7:278-94, 2006.

*Table 1. Correlation between MRI volumetry and MRE parameters with episodic memory performance.*

| | *Volume ($mm^3$)* | | *Shear stiffness $\mu$* | | *Damping ratio ξ* | |
|---|---|---|---|---|---|---|
| | $R^2$ | P value | $R^2$ | P value | $R^2$ | P value |
| *Cerebrum* | .419 | .302 | -.035 | .941 | .128 | .784 |
| *Hippocampus* | -.191 | .651 | -.181 | .697 | **-.779** | **.039*** |
| *Amygdala* | .079 | .853 | -.077 | .870 | -.742 | .056 |

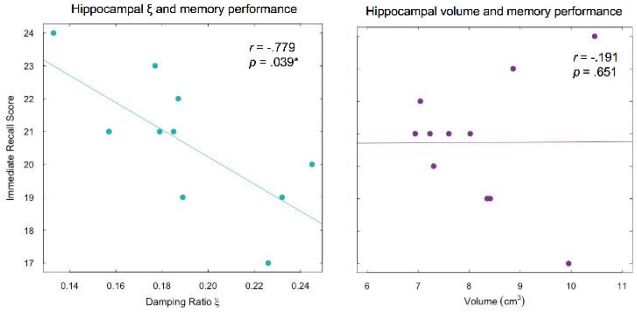


**Figure 1:** Correlation between memory performance and a) hippocampal ξ, and b) hippocampal volume.

**24 Moderate to Severe TBI Studies Using Mixed Model Inversions**

Anthony Romano[1], William Szymczak[1], Ruth Okamoto[2], David Brody[3], Curtis Johnson[4], and Philip Bayly[2]
*[1]Naval Research Laboratory, Acoustics Division, Washington, DC USA; [2]Department of Mechanical Engineering, Washington University, St. Louis, MO USA; [3]Department of Neurology, Washington, University, St. Louis, MO USA; [4]Department of Biomedical Engineering, University of Delaware, Newark, DE USA.*

**Background:** Previously, in collaboration with Charite-Universitatsmedizin, Berlin, Germany, we introduced Waveguide Elastography[1] (WGE) which utilized a fusion of Magnetic Resonance Elastography (MRE), Diffusion Tensor Imaging (DTI), and an anisotropic inversion algorithm for the evaluation of the stiffness coefficients of white matter in the human brain using an Orthotropic model. Here, we utilize a Mixed-Model Inversion[2] (MMI) strategy which uses fractional anisotropy (FA) as a thresholding metric to differentiate between isotropic and anisotropic regions of the brain, thereby dictating whether an isotropic or anisotropic inversion should be implemented. For FA values <~0.2, an isotropic inversion was indicated[3], and for FA values ~>0.2, an Orthotropic inversion was indicated[1]. This allowed for proper segmentation of the differing brain regions such that the appropriate inversion algorithm could be utilized.
**Aims:** The aims of this work are i) to implement the MMI strategy in the evaluation of the elastic properties of both healthy controls and patients who present with moderate to severe TBI and ii) to demonstrate the alterations to the brain structures as a result of insult/injury.
**Methods:** As a proof of concept demonstration below, MRE at 50 Hz excitation and DTI were performed using a 1.5T Siemens scanner on the brains of a healthy 22 year old male and a 44 year female who had suffered moderate to severe TBI due to an automobile accident. The MMI was applied to the data and the isotropic/anisotropic stiffness coefficients were superposed on diffusion ellipsoids provided by the eigenvalues of the DTI data[4].
**Results:** When compared to the healthy control, there was apparent damage to the frontal lobes of the TBI patient with the forceps minor being nearly completely obliterated and replaced with a soft, isotropic encephalomalacia. Additionally, there was disruption to the thalamus of the patient with reduced overall FA and reduced shear stiffness of both gray and white matter when compared to the healthy control.
**Conclusions:** These preliminary studies indicate that the MMI, in concert with diffusion ellipsoids, provides encouraging metrics based on differences in material parameters for differentiation between healthy controls and TBI patients. This work supported by Timothy Bentley, ONR Code 34, Warfighter Protection.

**References:** [1] Romano A.J. et al., MRM, 68, 1410-1422, 2012. [2] Romano A. J. et al., NCA TBI Research Symposium, 2016. [3] Romano A. J. et al., IEEE UFFC,47 (6): 1575-1581, 2000. [4] Basser P.J. ,NMR Biomed; Vol. 8: 333-344, 1995.

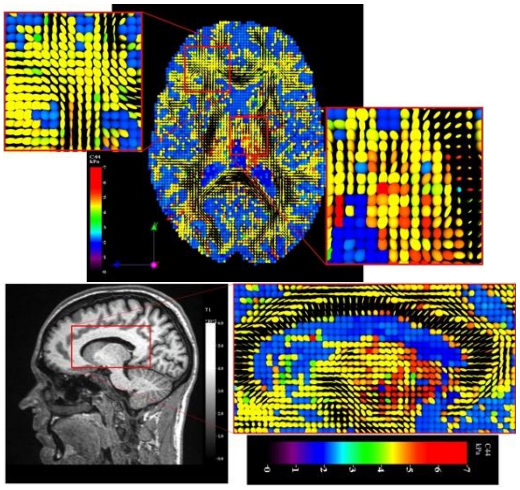

**Upper Left image**, Diffusion ellipsoids colored by shear stiffness coefficient, C44, in healthy control.
**Lower Left image**, T1 and Diffusion ellipsoids of the thalamus region colored by shear stiffness coefficient, C44, in healthy control.

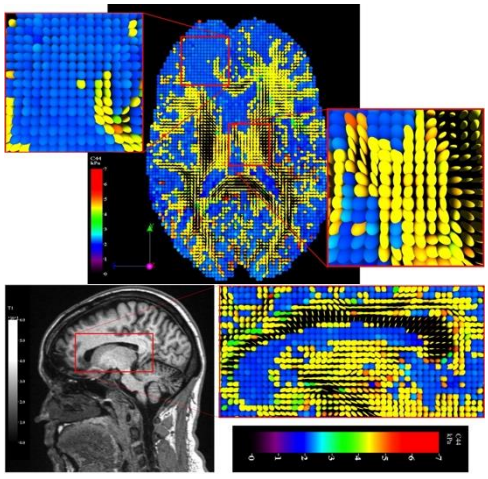

**Upper Right image**, Diffusion ellipsoids colored by shear stiffness coefficient, C44, in TBI patient.
**Lower Right image**, T1 and Diffusion ellipsoids in the thalmaus region colored by shear coefficient, C44, in TBI patient.

## 25 Early-stage analysis of murine models of Familial Alzheimer's disease: Preliminary results

Shreyan Majumdar[1], Rachana Mishra[2], Orly Lazarov[2], Dieter Klatt[1]
*Depts. of Bioengineering[1] and Anatomy & Cell Biology[2], University of Illinois at Chicago, IL, USA*

**Background:** Alzheimer's disease (AD) is the most common form of dementia affecting patients worldwide [1]. Currently, there are no diagnostic or predictive measures for the disease. Magnetic resonance elastography (MRE) revealed decreased brain stiffness in advanced disease stages [2]. However, the sensitivity of MRE to early-stage AD is not fully established [3,4].
**Aim:** To assess the diagnostic potential of brain MRE in two separate mouse models of Familial AD in early disease stages.
**Methods:** We used two different mouse models / groups. 1) Group A: Four APPswe/PS1ΔE9 and four controls; 2) Group B: Five 5xFAD mice and five control mice. All mice were female and in the age group of 3-4 months. A 9.4T pre-clinical MRI scanner at the Research Resources Center of the University of Illinois at Chicago was used to perform the measurements. In the elastography experiments, a vibrating bite bar type actuator induces mechanical shear waves in the mouse brain. Experimental details and SLIM-MRE [5] imaging parameters are as follows: 38 mm volume radiofrequency (RF) coil, 16 mm field of view axial slices, 250 µm isotropic voxel size, TE/TR = 16.24/1000 ms, 3 averages, 1000 Hz actuation frequency, 250 mT/m motion encoding gradient (MEG) strength, 10 MEG cycles, and 8 time steps, with a total scan time of 51 min. 12 secs. Using the curl operator on noise-filtered complex wave images, the complex shear modulus was calculated by the algebraic inversion of the Helmholtz equation. Storage modulus values (real part of the complex modulus) over four region of interests (ROIs) were calculated. ROI-1 is the overall area of the mouse brain (WB) as seen in figure 1 (marked with yellow border). ROIs-2&3 (blue and red highlighted region in figure 1) of the hippocampal area (HC) and the cerebral cortex (CC) were manually segmented from MRI magnitude images. Finally, the rest of the brain (ROB) corresponds to ROI-1 without ROI-2 and ROI-3 and is denoted with ROI-4.
**Results:** For Group A, the median shear stiffness for the APPswe/PS1ΔE9 mice, especially in ROI-2&3 is lower compared to the wild type counterparts (as seen in figure 2). On the other hand, for Group B, the overall stiffness for every ROI in the 5xFAD was higher than their corresponding control values.
**Discussion:** While the results from Group A are in line with reports in the literature [3,4], the higher stiffness in the disease model of Group B presents a surprising and interesting finding. The progression of AD causes cerebral stiffness changes with temporal characteristics that appear to be specific for different disease and control models. Further research will integrate histopathology into the investigation of the stiffness-time behavior for the two AD models.

**References:**

**[1].** Alzheimer's Association. 2015 Alzheimer's disease facts and figures. Alzheimer's Dement. J. Alzheimer's Assoc. 11, 332 (2015). **[2].** Murphy, M. C. et al. Decreased brain stiffness in Alzheimer's disease determined by magnetic resonance elastography. J. Magn. Reson. Imaging 34,494–498 (2011). **[3].** Murphy, M. C. et al. Magnetic resonance elastography of the brain in a mouse model of Alzheimer's disease: initial results. Magn. Reson. Imaging 30, 535–9 (2012). **[4].** Munder, T. et al. MR elastography detection of early viscoelastic response of the murine hippocampus to amyloid b accumulation and neural cell loss due to Alzheimer's disease (2017). doi: 10.1002/jmri.25741. **[5].** Klatt, D. et al. Sample interval modulation for the simultaneous acquisition of displacement vector data in magnetic resonance elastography: theory and application. Phys. Med. Biol. 58, 8663–75 (2013).

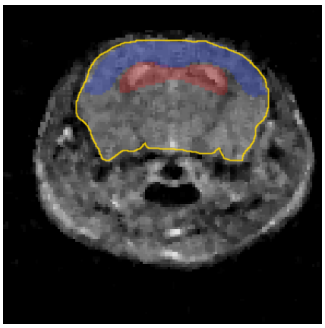

**Figure 1:** Image showing the different ROIs used

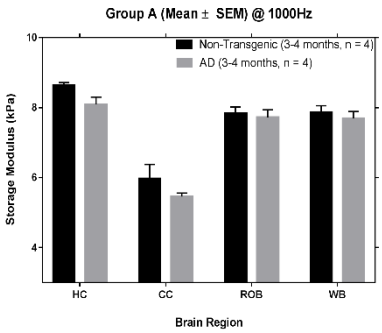


**Figure 2:** Data from APPswe model / group A

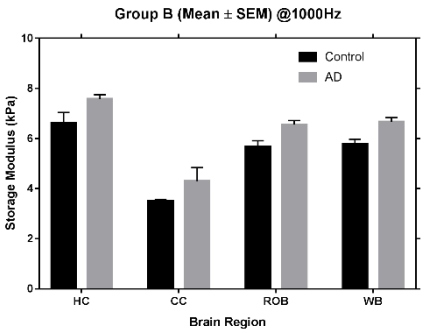


**Figure 3:** Data from 5XFAD model / group B

## 26 An initial experience with high resolution, high frequency, brain MRE with a high performance compact 3T scanner

*A. Arani[1], Z Yin[1], K.J. Glaser[1], M.A. Bernstein[1], R.L. Ehman[1], J. Huston III[1],*
[1]Department of Radiology, Mayo Clinic, Rochester, MN, USA

**Background:** Several groups have investigated the role of magnetic resonance elastography (MRE) in the brain for the diagnosis of neurological diseases and general aging (1-11). A majority of this work has been performed at vibration frequencies ≤ 60Hz due to challenges with having enough phase encoding sensitivity to capture low amplitude, highly attenuated, higher frequency shear waves with traditional scanners and peripheral nerve stimulation limits. Recently, a novel compact 3T MRI scanner with gradients capable of 80mT/m amplitudes and 700 T/m/s slew rates has been developed (12-14). This new hardware development has the potential to measure smaller displacement amplitudes and could allow for the measurement of higher frequency shear waves to be observed in the brain. Furthermore, the added slew rate allows for shorter echo-train lengths, which can be used to increased resolution without introducing any addition image distortions. Real-time correction [15,16] compensates for additional concomitant fields arising from the asymmetric gradient design.
**Aim:** To explore the feasibility of performing brain MRE at a vibration frequency of 80Hz and visually comparing the image quality to 60 Hz exams for brain tumor characterization, stiffness heterogeneity, and tumor adhesion assessment prior to surgery.
**Methods:** With Institutional Review Board approval and written informed consent, 16 patients (7 meningiomas, 3 adenomas, 3 pituitary adenomas, 3 acoustic neuromas) underwent a preoperative MRE exam on a high performance compact 3T scanner. Elastograms and slip interface images (SII) (15) were performed and tumor stiffness heterogeneity, tumor-brain adhesion were assessed. Exams at 60 Hz and 80 Hz were performed on each patient with 3mm and 2.5mm isotropic resolution, respectively.
**Results:** Figure 1 shows an example where high resolution, high frequency MR elastography better demonstrated the adhesive properties of the tumor as assessed by surgical findings.
**Conclusions:** High resolution, high frequency elastography has been shown to be feasible with a high performance compact 3T scanner and preliminary data suggests the opportunity for better depiction of higher frequency and higher resolution brain MRE.

**References:** [1] Xu L et al., Acta radiologica 2007;48:327-30. [2] Hughes JD et al., Neurosurgery 2015;77:653-658. [3] Streitberger KJ et al., NMR in biomedicine 2011;24:385-92. [4] Fattahi N et al. Am J Neuroradiol 2016;37:462-467. [5] Wuerfel J et al., NeuroImage 2010;49:2520-5. [6] Streitberger KJ et al. PloS one 2012;7:e29888. [7] Murphy MC et al., JMRI 2011;34:494-8. [8] Huston J et al., JMRI 2016;43:474-478. [9] Arani A et al. NeuroImage 2015;111:59-64. [10] Sack I et al., NeuroImage 2009;46:652-7. [11] Sack I et al., PloS one 2011;6:e23451. [12] Weavers PT et al., Medical Physics 2016;43:1259-1264. [13] Foo T et al., Orlando, FLA, MHSRS, 2016. [14] Lee SK et al., MRM 2016;76:1939-1950. [15] Tao et al, MRM 77:2250-2262. [16] Weavers et al MRM 2017 doi: 10.1002/mrm.26790. [17] Yin Z et al., JMRI 2017.

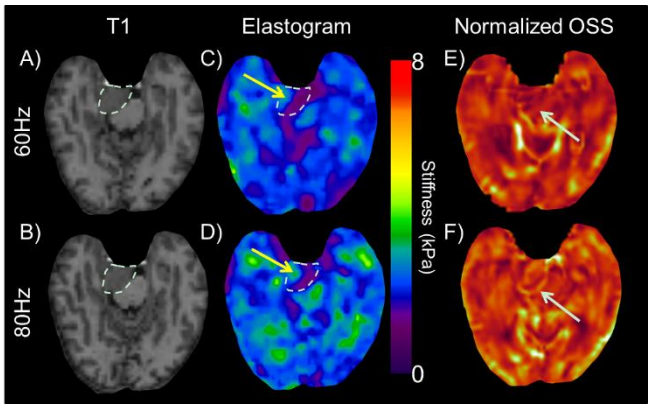


**Figure 1:** T1 images at A) 3mm isotropic resolution and B) 2.5mm isotropic resolution, with corresponding elastograms (C,D) and SII images (normalized octahedral shear strain, E,F). The surgical report stated that the tumor had a firm lateral (yellow arrows in C and D) region, was softer and non-adhesive around the brain stem (white arrow in E and F).

**27 Comparison of Gradient Recalled Echo and Spin-Echo Echo Planar Imaging Sequences in *In Vivo* Aortic MRE**

Huiming Dong[1,2] and Arunark Kolipaka[1,2,3]

*[1]Department of Radiology, The Ohio State University Wexner Medical Center, U.S.A. [2]Department of Biomedical Engineering, The Ohio State University, U.S.A. [3]Department of Internal Medicine, The Ohio State University Wexner Medical Center, U.S.A.*

**Background:** Aortic stiffness is associated with a variety of cardiovascular diseases such as aortic aneurysm, hypertension, etc. [1-2]. Magnetic resonance elastography (MRE) is an excellent non-invasive imaging tool to measure aortic wall stiffness [3]. Currently, gradient recalled echo (GRE) MRE sequences are widely employed for aortic MRE measurements. However, GRE sequences are sensitive to the length of echo time (TE), and also prone to T2* decay of the signal [4].

**Aims:** The goal of this work is to study the feasibility of using spin-echo echo planar imaging (SE-EPI) sequence for in vivo aortic MRE measurements. Specifically, this work aims to compare the mean aortic stiffness obtained using SE-EPI and GRE MRE sequences.

**Methods:** A cardiac-gated SE-EPI MRE sequence was developed in this work. To reduce the effect of aortic flow, the motion encoding gradient (MEG) was designed to be zero- and first-moment-nulled. Unlike the conventional 1-1 bipolar MEG which also encodes constant flow velocity, the designed MEG is less prone to aortic flow: a critical concern in aortic MRE. Subsequently, three healthy volunteers (age: 26 ± 4 years) were recruited for this study. All imaging was performed on a 3T MR scanner (Tim Trio, Siemens Healthcare, Erlangen, Germany) using the developed SE-EPI sequence and a retrospectively pulse-gated GRE sequence. The imaging parameters include: mechanical frequency=70 Hz; MEG frequency=120 Hz; three-directional motion encoding; FOV=400x400 $mm^2$; slice thickness=6 mm; acquisition matrix size=128x64; No. of slices=1; No. of phase offsets=4; TE= 10.18 ms (GRE) and 24.9 ms (EPI); TR = 14.29 ms (GRE) and 600 ms (EPI); EPI factor = 31. Effective aortic stiffness was obtained using local frequency estimation (LFE) via MRElab (Mayo Clinic, Rochester, MN).

**Results:** The SE-EPI sequence yielded higher first harmonic component amplitude and similar stiffness values when compared to the GRE measurement. ***Figure 1*** demonstrated the localizer in sagittal view, amplitude of the first harmonic component and the corresponding mean effective aortic stiffness maps from SE-EPI and GRE sequences in one of the volunteers. ***Table I*** compared the mean effective aortic stiffness of three volunteers obtained using SE-EPI and GRE sequences.

**Conclusions:** It is feasible to perform aortic MRE using SE-EPI sequence. Moreover, SE-EPI demonstrated advantage over GRE in producing stronger first harmonic amplitude, which will be advantageous in imaging patients with high body mass index. Future work will involve accelerated imaging and multi-slice SE-EPI acquisition. The ultimate goal is to perform multi-slice aortic MRE measurement within one breath-hold using SE-EPI sequence.

**References:** [1] Kolipaka, A. et al., J Vasc Surg, 64(4): 966-974, 2016. [2] Dong, H. et al., Magn Reson Med, DOI: 10.1002/mrm.26601. [3] Kenyhercz, W. et al., Magn Reson Med, 75(5): 1920-1926, 2016. [4] Wagner, M. et al., Invest. Radiol, 51(9): 575-581, 2016.

**Acknowledgments:** NIH-R01HL124096 for funding.

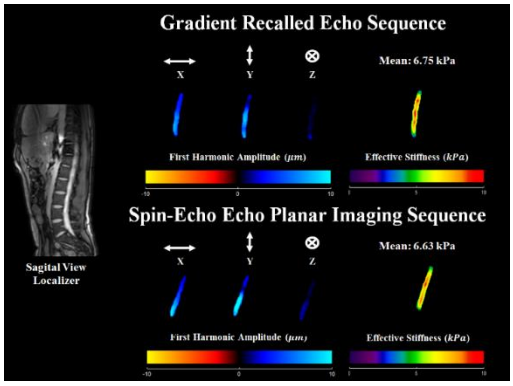


**Figure 1: Aortic MRE Measurements Using GRE and SE-EPI Sequences.** The measurements were performed using a sagtial view to capture the aorta. Amplitudes of first harmonic components from x, y and z directions were demonstrated in the figure. Higher first harmonic component amplitudes (μm) were observed in SE-EPI measurements. The same driver power was employed for both SE-EPI and GRE seqeunces. The z-direction was not the dominant wave propagation direction which explains the low amplitude in both cases. For the volunteer data displayed in the figure, the mean aortic stiffness is 6.75 and 6.63 kPa for GRE and SE-EPI respectively.

| Volunteer No. | SE-EPI | | GRE | |
|---|---|---|---|---|
| | Mean Aortic Stiffness | Standard Deviation | Mean Aortic Stiffness | Standard Deviation |
| 1 | 6.63 kPa | 1.08 kPa | 6.75 kPa | 1.13 kPa |
| 2 | 6.84 kPa | 1.57 kPa | 6.72 kPa | 1.47 kPa |
| 3 | 6.31 kPa | 0.86 kPa | 6.78 kPa | 1.39 kPa |

**Table I:** Comparison of Aortic Stiffness between SE-EPI and GRE Seqeunces

## 28 The Effect of Muscle Loading on Muscle Stiffness

Michiel Simons[1,2], Michael Perrins[1,3], Andre Attard[4], Helen Marshall[1,3], Scott Semple[1], Annette Cooper[1], Colin Brown[5], Leela Biant[6], Edwin van Beek[1] and Neil Roberts[1].

*[1.] Edinburgh Imaging facility, University of Edinburgh, Edinburgh, UK; [2.] Department of Clinical Surgery, University of Edinburgh, Edinburgh, UK; [3.] Centre for Inflammation Research, University of Edinburgh, Edinburgh, UK; [4.] Department of Bioengineering, University of Strathclyde, Glasgow, UK; [5.] The Mentholatum Company Ltd., East Kilbride, UK; [6.] Department of Trauma & Orthopaedic Surgery, University of Manchester, Manchester, UK*

**Background:** Increased muscle stiffness following muscle damage[1,2], knee extension[3] and muscle myopathies[4] has been previously demonstrated using Magnetic Resonance Elastography (MRE). Muscle stiffness changes from muscle loading could have important clinical applications in predicting peak muscle performance, and may aid in patient selection for surgery. In the present study, this is explored using MRE.

**Aim:** To evaluate the sensitivity of MRE for measuring changes in muscle stiffness in response to increasing degrees of muscle loading.

**Methods:** Four participants (age 33.00±9.06 years) were studied. A Resoundant system (Resoundant, Mayo Clinic, Rochester, MN, USA) was used to provide actuation via a non-inflated thigh tourniquet cuff and axial MRE images were acquired at frequencies[3] of 25, 37.5 and 50 Hz. The MRE images were acquired at baseline and at 2kg, 4kg and 8kg of Quadriceps loading using custom designed loading apparatus. Whilst supine, weights were attached to the ankle of participants who were asked to extend the lower leg and sustain the lift for 80 seconds. MRE images were analysed using ESP software and |G*| and axial cross-sectional area (CSA) were computed for ROI's corresponding to the individual muscles of the thigh. Furthermore, pixel-wise mapping[5] analysis was performed on co-registered images.

**Results:** Repeated measures ANOVA showed a significant increase in |G*| in response to increased loading ($p$<.000), from baseline (1.93 [±.42] kPa), to 2kg (2.50 [±.64] kPa), 4kg (2.60 [±.67] kPa) and 8kg (2.93 [±.63] kPa). A significant correlation between |G*| and the weight of muscle loading was observed ($R^2$ =.71, $p$=.002).

**Conclusions:** Muscle loading has shown a strong correlation with increases in muscle stiffness as measured using MRE. This suggests that MRE can be used as a sensitive tool for measuring muscle engagement.

**References:** **[1]** Kennedy et al., JMRI, 2017. **[2]** Perrins et al., ISMRM: Singapore, 2016. **[3]** Barnhill et al., Phys. Meas., 2013. **[4]** Basford et al., Arch. Phys. Med. Rehabil., 2002. **[5]** Papazoglou et al., MRM, 2006. **[6]** Barnhill et al., MRM, 2015.

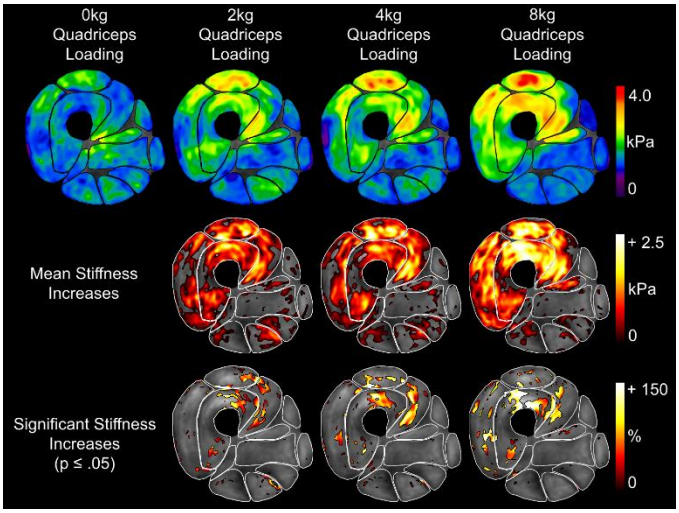


**Figure 1.** Statistical mapping of |G*| in response to increased muscle loading.

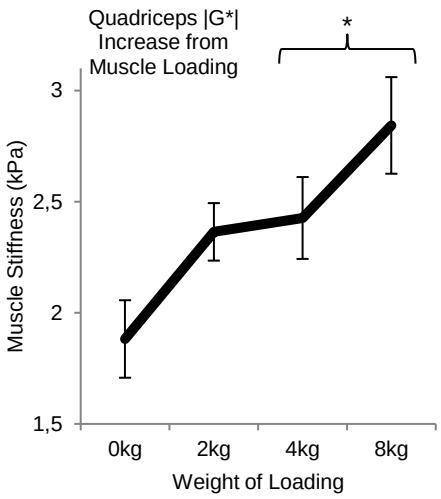


**Figure 2.** Increase in muscle stiffness with increase in muscle loading. * Indicates significant difference (p<.05)

**29** **Assessing tumor mechanical properties and blood perfusion with MRE and FAIR MRI at different strain levels**

G. Pagé[1], M. Tardieu[1], P. Garteiser[1], B.E. Van Beers[1,2],

*[1]Laboratory of Imaging Biomarkers, UMR1149, INSERM-University Paris Diderot, Paris, France; Department of Radiology Beaujon University Hospital Paris Nord, Clichy, France*

**Background:** The tissue mechanical properties are determined by a static component that is mainly related to extracellular tissue composition, and a dynamic component that is affected by vascular pressure [1]. The influence of the structural and dynamic components in the high pressure of malignant tumors remains debated [2-3].

**Aims:** To assess at MRI the changes of the mechanical properties and blood perfusion with increasing compression in xenografted tumors.

**Methods:** MRI examinations were performed in-vivo in 5 SCID mice with subcutaneous tumors (patient derived hepatocellular carcinoma xenografts) implanted in the left flank. The examinations were repeated in 3 mice after euthanasia (ex-vivo examinations). A 7T MRI scanner (Pharmascan, Bruker, Germany) with a volume resonator and a 25mm diameter receiver coil was used. Mechanical vibrations were generated with an electromagnetic shaker and transmitted to the tumor via a flexible carbon fiber rod linked to the plastic insert in contact with the tumor [4]. An inflatable balloon was placed on the abdomen to apply a load to the tumor. MRE and perfusion acquisitions were performed at basal strain, and at increasing compression levels. Mechanical excitations were performed at 600 Hz and synchronized with a sinusoidal motion-encoded spin echo sequence. MRE acquisition parameters were: matrix = 87 x 67 x 9, resolution = 0.30 x 0.30 x 0.35 mm, TR/TE = 1007/18 ms and scan time of 4 min 30 s for each of three acquired spatial direction, including 4 times steps. Maps of G' were obtained by inversion of the Helmholtz wave equation [5]. MR FAIR perfusion parameters were: TR/TE = 12000/35 ms, slice selective thickness = 4.5 mm, resolution = 0.3 x 0.3 x 1.5 mm, inversion times = 30 + n × 250 ms (n = 1 … 21), acquisition time = 8 min 54 s. Moreover, for each strain level, an anatomical map was acquired (sequence: ultra-fast-SE, matrix = 150 x 150 x 40, resolution = 0.2 x 0.2 x 0.5 mm, TR/TE = 9000/60 ms). Anatomical images were used to calculate the tumor octahedral shear strain (OSS) between basal strain state and each strain level.

**Results:** Relative difference values between tumor G' measured at increasing strain levels are plotted in Figure 1. This graph shows similar increase of G' with strain in-vivo and ex-vivo. Figure 2 shows the decrease of tumor perfusion in-vivo at increasing strain.

**Conclusions:** Our results show that with increasing compression and strain, the tumor elasticity increases similarly in-vivo and ex-vivo. This increase has been previously shown ex-vivo in the liver with MRE [6]. We observed that this elasticity increase occurs in-vivo despite a decrease of tumor blood perfusion. These results suggest that high intra-tumor pressures are generated predominantly by solid stress and elevated pressure within the interstitial hyaluroninan-rich gel-fluid phase rather than by intravascular and interstitial free fluid phase pressure [7-8].

**References:** [1] Yin M *et al.*, Radiology, 2017, 160622,. [2] Chauchan *et al.* Cancer Cell, 2014 26(1) : 14-15 [3] DelGiorno *et al.* Cancer Cell, 2014, 26(1) : 16-17. [4] Ronot M *et al.*, Plos One, 2014 9(4):94679. [5] Sinkus R *et al.,* Magn Res Imaging, 2005, 23:159-165. [6] Clarke E C *et al.* J Biomech, 2011; 44(13): 2461-2465, [7] DuFort CC *et al.*, Biophys J, , 2016; 110(9): '2106-2119. [8] Perepelyuk M *et al.,* Plos One 11(1): e0146588, 2016.

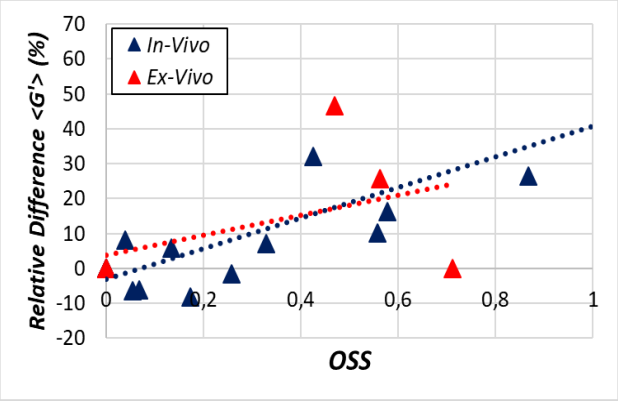


**Figure 1:** Evolution of mean values of tumor G' relative to OSS measured in-vivo in 5 mice and ex-vivo in 3 mice.

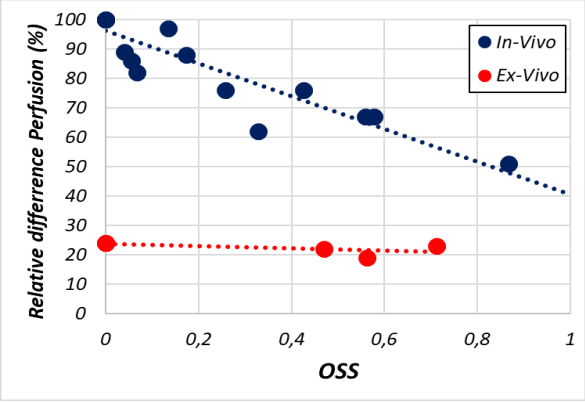


**Figure 2:** Evolution of tumor perfusion relative to OSS in-vivo in 5 mice and ex-vivo in 3 mice.

**30 MRE Study of Muscle Recovery Following Time Spent in an Intensive Care Unit (ICU)**

Michael Perrins[1,2], Michiel, Simons[1,3], Helen Marshall[1,2], Lucy Hiscox[1], Calum Grey[1], Scott Semple[1], Annette Cooper[1], Lucy Barclay[3], Rachael Kirkbride[3], Lisa Salisbury[3], Colin Brown[4], Timothy Walsh[2,4], Edwin van Beek[1], Neil Roberts[1] and David Griffith[2,4].

*[1.] Edinburgh Imaging facility, The University of Edinburgh, Edinburgh, UK; [2.] Centre for Inflammation Research, The University of Edinburgh, Edinburgh, UK; [3.] Department of Clinical Surgery, University of Edinburgh, Edinburgh, UK; [4.] Anaesthesia, Critical Care and Pain Medicine, The University of Edinburgh, Edinburgh, UK; [5.] The Mentholatum Company Ltd., East Kilbride, UK.*

**Background:** Muscle weakness following time spent in an Intensive Care Unit (ICU) is a common observation in immobile patients, particularly muscle atrophy[1,2] and significant loss of muscle strength[3,4] within the first week of admission.
**Aims:** To use Magnetic Resonance Elastography (MRE) to measure changes in the muscle mechanical properties and morphology as a result of time in ICU, and whether these effects are reversed following a period of convalescence.
**Methods:** The participants comprised 7 discharged ICU patients (46.9 [±18.6] years), of whom 3 patients returned following convalescence (43.0 [±15.5] years) and 8 age-matched controls (46.0 [±11.6] years). ICU patients were scanned at discharge and after a period of convalescence (126.00 [±33] days). A multi-frequency MRE[5] sequence (25, 37.5, 50, 62.5Hz) was analysed using ESP[6] to create high-resolution muscle stiffness maps. Twelve individual muscles were manually segmented to enable ROI analysis of muscle cross-sectional area (CSA) and computation of the average value of |G*| for each muscle. The MRE images were also co-registered[7] to produce stiffness elastograms for group averages.
**Results:** MANOVA revealed a significant difference in muscle |G*| and CSA ($p$=.042) ($p$<.000) between groups. In particular, compared to healthy controls, |G*| was significantly greater (1.6 [±.5]kPa) than in ICU patients (Figure 1) following discharge (1.3 [±.6]kPa; -20%; $p$=<.000) and convalescence (1.4 [±.3]kPa; -15%; $p$=.05; Figure 2) and average muscle CSA (9.5 [±7.4]cm$^2$) was significantly lower for patients at ICU discharge (7.3 [±5.4]cm$^2$, -23%, $p$=.05) but not following convalescence (8.8 [±7.1]cm$^2$, -7%, $p$ = .447). In healthy controls there was a significant positive correlation between muscle CSA and |G*| ($R^2$=.242, $p$=0.17), however these two factors were not significantly correlated following either ICU discharge ($R^2$=.017, $p$=.872) or convalescence ($R^2$=-.015, $p$=.930).
**Conclusions:** This first use of MRE in an investigation of muscle recovery following time spent in ICU has shown that whilst muscle CSA recovered following convalescence, there were long-term effects on the muscle stiffness. The findings of this research have implications for using MRE in understanding and supporting the musculoskeletal system recovery process following trauma.

**References: [1]** Gruther et al., J.Reh.Med., 2008. **[2]** Reid et al., Clin.Nut., 2004. **[3]** Schweickert et al., Chest, 2007. **[4]** Appell, Sports Medicine, 1990. **[5]** Papazoglou et al., MRM, 2006. **[6]** Barnhill et al., MRM, 2015. **[7]** Barnhill et al., Phys. Meas., 2013.

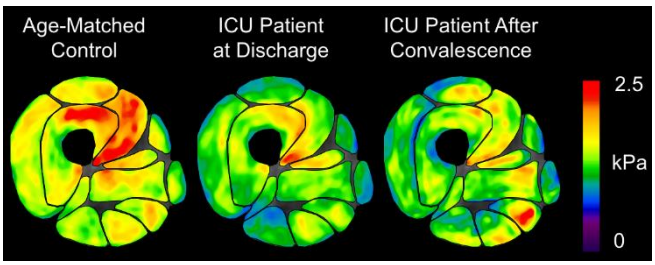


**Figure 1.** |G*| decrease following ICU discharge

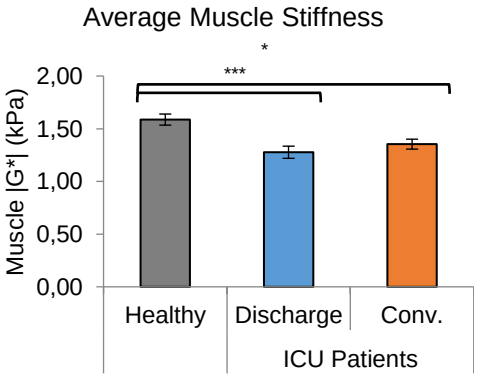


**Figure 2.** |G*| compared to healthy controls for ICU patients at discharge and following convalescence. * = p<.05; *** =p<.000

## 31 Monitoring of High Intensity Focused Ultrasound (HIFU) ablations in real time using interventional MR Elastography (MRE)

J. Vappou[1], K.S. Kim[1], A. Gangi[1,2], E. Breton[1]

*[1]ICube, UMR 7357, CNRS, Université de Strasbourg, 1 place de l'hôpital, Strasbourg, France ;[2] Dpt. of Interventional Radiology, Hôpitaux Universitaires de Strasbourg, FRANCE*

**Background:** Tissue elasticity has been shown to be a promising biomarker for monitoring thermal ablations [1-3]. Interventional MR Elastography (iMRE) has been developed recently for this purpose. iMRE includes specific features such as: (1) Interventional-friendly, compact mechanical exciters that use the interventional needle as an internal exciter, (2) Interactive, real-time MRE pulse sequences that allow simultaneous MR Thermometry and MRE measurements, and (3) Online reconstruction of elastograms in real time (~ 1 Hz) [3]. The capability of the method for monitoring MR-guided laser ablations has been demonstrated in vivo in swine liver [3-4].

**Aims:** In this study, the iMRE method is adapted to the monitoring of HIFU ablations. The main originality of this study is the use of the HIFU transducer as mechanical exciter, through the use of the acoustic radiation force, during and after the ablation. Feasibility is demonstrated in vivo in porcine muscle tissue.

**Methods:** A MR-compatible HIFU system (Image Guided Therapy, France) including a 256-element transducer driven at 1 MHz and 285 W is used. The signal transmitted to the transducer is modulated by a square wave at 50 Hz (duty cycle 50%), allowing for simultaneous heating and mechanical excitation through an oscillating pseudo-harmonic acoustic radiation force. The HIFU transducer is positioned using an orientable MR-compatible structure on the thigh of a 52kg swine (fig.1). Acoustic coupling is realized through the use of a degassed water-filled balloon. MRI experiments are conducted in a 1.5T MRI system (MAGNETOM Aera, Siemens). A spoiled, interactive, interventional MRE GRE sequence is used for encoding displacements resulting from this excitation. Main MRI parameters are: TR/TE 20ms/13ms, MSG frequency 90 Hz, FOV 400 mm × 400 mm, 128 px × 128 px, 3 phase shifts with opposite MSG, total acquisition time per slice 2.5 s. Both elasticity and temperature maps are reconstructed simultaneously using a LFE-based approach and the Proton Resonance Frequency (PRF) method, respectively [4]. A HIFU heating phase of 150 s was followed by a relaxation phase of 250 s.

**Results:** Shear waves could be clearly observed emerging from the focal region (fig.2). Tissue stiffness was found to increase consistently, along with temperature, during tissue ablation. As expected, tissue temperature decreased back to 37°C after HIFU was turned off, while tissue stiffness changes were definitive (fig.3).

**Conclusions:** These preliminary results suggest that tissue elasticity is an interesting biomarker directly related to permanent, irreversible tissue damage, as opposed to temperature. This method allows for simultaneous HIFU ablation and MRE, without the use of additional excitation devices.

**References:** [1] Mariani et al., J. Surg. Res., 188:37-43, 2014. [2] Chen et al., Magn. Reson. Med., 1: 59-67, 2014. [3] Corbin et al., Magn. Reson. Med., 75(3): 1110-8, 2015. [4] Corbin et al., ISMRM 2015, Toronto, Canada.

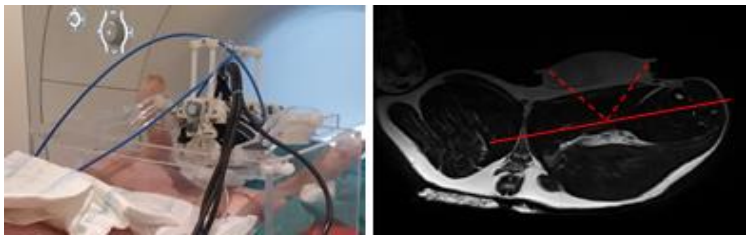

**Figure 1:** Experimental setup showing the positioning device and the HIFU transducer (left). Anatomical image showing the HIFU focus and the imaging plane (red) used for MRE. The coupling water balloon is visible (hypersignal) below the transducer.

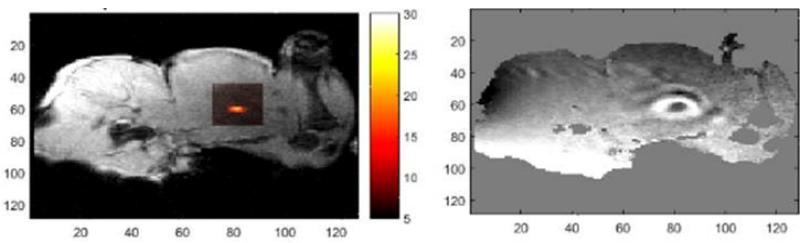

**Figure 2:** Temperature map showing the HIFU focus (left), and wave images during the ablation (right) in the thigh of a swine.

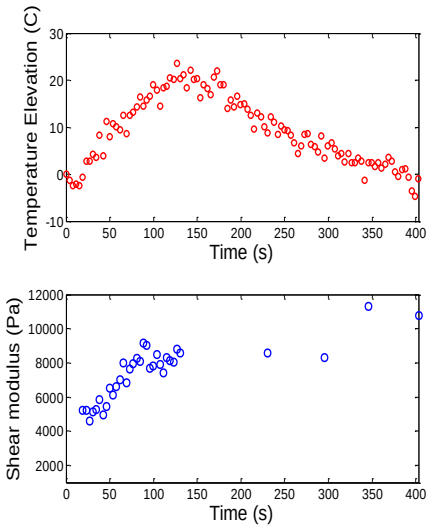


**Figure 3:** Temperature and elasticity vs. time during and after the HIFU ablation (first 150 s).

## 32 Evidence from MRE that Muscle Engagement Strategy Influences Occurrence of Oedema Following an Exercise Induced Muscle Damage (EIMD) Protocol

Michael Perrins[1,2], Helen Marshall[1,2], Michiel Simons[2,3], Paul Kennedy[4], Lucy Hiscox[2], Lewis MacGregor[5], Angus Hunter[5], Colin Brown[6], Edwin van Beek[2] and Neil Roberts[2].

*[1.] Centre for Inflammation Research, University of Edinburgh, Edinburgh, UK; [2.] Edinburgh Imaging facility, University of Edinburgh, Edinburgh, UK; [3.] Department of Clinical Surgery, University of Edinburgh, Edinburgh, UK; [4.] Translational and Molecular Imaging Institute (TMII), Icahn School of Medicine at Mount Sinai, New York, USA; [5.] School of Sport, University of Stirling, Stirling, UK; [6.] The Mentholatum Company Ltd., East Kilbride, UK.*

**Background:** Repeated eccentric knee extensions were shown to increase the stiffness of the Quadriceps[1] following an Exercise Induced Muscle Damage (EIMD) protocol. In addition, was observed in almost half of participants and interpreted to be due to a build up of additional free calcium ($Ca^{2+}$) as a result of significant damage[2]. The musculoskeletal system employs co-contraction of muscle groups in order to avoid muscle strain[3] and we have investigated whether MRE is able to distinguish different muscle co-contraction patterns in participants with and without oedema[4].

**Aim:** Investigate whether oedema induced muscle damage is due to a specific muscle co-contraction strategy.

**Methods:** Fourteen healthy male participants (24.79[±4.00] years) were studied using T2-weighted (T2w) MRI and Magnetic Resonance Elastography (MRE) before and two days after the EIMD paradigm. For MRE, a carbon fibre rod attached to a loudspeaker was connected to an actuator cuff around the thigh using multi-frequency MRE[5] (25, 37.5, 50 and 62.5Hz) and ESP post-processing[6] for axial (n=14) and sagittal (n=10) images. Maximum Voluntary Contraction (MVC), workload and number of repetitions were also measured.

Analysis of the T2w images by Kennedy et al (2017) revealed the occasional presence of oedema following EIMD (axial n=8; sagittal n=7), which was used to group participants. Subsequently, statistical mapping[7] of |G*| increase following EIMD was used to identify which muscles had been significantly involved in the muscle damage protocol.

**Results: T**here were no significant differences in workload ($p$=.282) or number of repetitions ($p$=.239) between groups, however the oedema group showed significantly lower MVC following EIMD ($p$=.035). Average muscle CSA of the Oedema group increased by 40% following EIMD. Statistical mapping of axial MRE images revealed that the No Oedema group (Figure 1) showed increased |G*| in Rectus Femoris ($p$=.001) and Semimembranosus ($p$=.002), where as the Oedema group (Figure 2) showed increased |G*| in Gracilis ($p$=.001). Further, analysis of the sagittal MRE images showed a 55% increase in CSA (p=.003) and 71% |G*| increase ($p$=.019) of Rectus Femoris in the Oedema group.

**Conclusions:** We interpret that the No Oedema group employed a balanced co-contraction of Rectus Femoris and Semimembranosus in performing the EIMD protocol. The Oedema group, however, engaged Rectus Femoris and Gracilis, and due to the Gracilis not able to produce as much force as the Semimembranosus[8] meant there was a greater dependency on the Quadriceps to produce force during eccentric contractions, resulting in Oedema. Analysis of the sagittal MRE images further revealed that the less ideal muscle combination used by the Oedema group resulted in increased |G*| at the muscle-tendon junction, a key factor in the reduced MVC.

**References: [1]** Kennedy et al., JMRI, 2017. **[2]** McMahon et al., AJR, 2010. **[3]** Faulkner, J. App. Phys., 2003. **[4]** Perrins et al., ISMRM: Singapore, 2016. [**5**] Papazoglou et al., MRM, 2006. **[6]** Barnhill et al., MRM, 2015. **[7]** Barnhill et al., Phys. Meas., 2013. **[8]** Lieber et al., CORR, 2001.

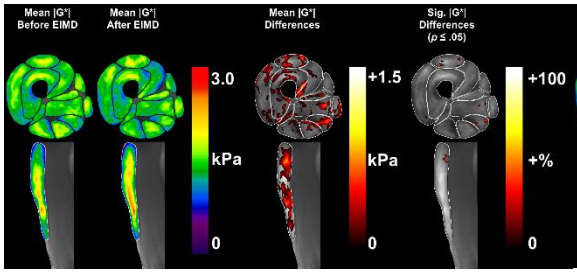


**Figure 1.** Co-contraction of the Rectus Femoris and Semimembranosus: Anterior knee extensions.

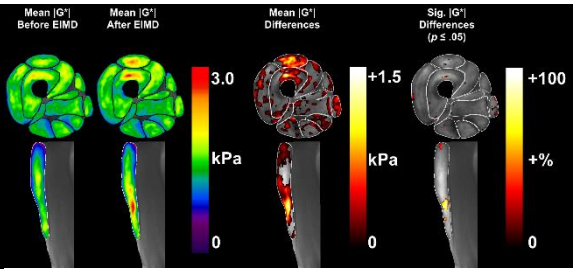


**Figure 2.** Co-contraction of the Rectus Femoris and Gracilis: Medial-Anterior knee extensions.

## 33 Change in Mechanical Properties and Cross Sectional Area (CSA) of Thigh Muscles Following Total Knee Replacement (TKR) Surgery

Michiel Simons[1,2], Michael Perrins[1,3], Gwenllian Tawy[4], Helen Marshall[1,3], Colin Brown[5], Edwin van Beek[1], Neil Roberts[1] and Leela Biant[6]

*[1.] Edinburgh Imaging facility, University of Edinburgh, Edinburgh, UK; [2.] Department of Clinical Surgery, University of Edinburgh, Edinburgh, UK; [3.] Centre for Inflammation Research, University of Edinburgh, Edinburgh, UK; [4.] Department of Bioengineering, University of Strathclyde, Glasgow, UK; [5.] The Mentholatum Company Ltd., East Kilbride, UK; [6.] Department of Trauma & Orthopaedic Surgery, University of Manchester, Manchester, UK*

**Background:** The outcome of Total Knee Replacement (TKR) surgery is dependent on the accuracy of surgical implantation[1]. However, patient engagement with muscle rehabilitation programmes plays a crucial role in achieving the best possible outcome[2]. Osteoarthritis (OA) is a joint deforming disease process which may lead to altered joint biomechanics. This in turn can affect the mechanical properties and morphology of surrounding stabilising musculature.
**Aim:** To investigate the impact of Total Knee Replacement (TKR) surgery on thigh muscle mechanical properties and morphology.
**Methods:** Five TKR Patients (65.80[±10.38] years old) attended a Magnetic Resonance Elastography (MRE) scanning session pre-operatively and then 138.2 (±51.2) days post TKR surgery. A Resoundant system (Resoundant, Mayo Clinic, Rochester, MN, USA) was used to provide actuation via a non-inflated thigh tourniquet cuff. Axial MRE images were acquired at frequencies[3] of 25, 37.5 and 50 Hz before and after surgery for the following two conditions (i) knee flexion and (ii) knee extension sustained for 80 seconds. MRE images were analysed using ESP software and |G*| and axial cross-sectional area (CSA) were computed for ROI's corresponding to the individual muscles of the thigh. Furthermore, pixel-wise mapping[5] analysis was performed on co-registered images.
**Results:** Following TKR |G*| was significantly greater in the Adductors (+67%; $p$<.000), Hamstrings (+28%; $p$=.016), and Quadriceps (+17%; $p$=.006; Figure 1) in the flexed knee condition. Interestingly, |G*| of the Quadriceps increased by 57% upon knee extension pre-operatively but by only 18% ($p$=.040; Figure 2) post-operatively. Significant muscle atrophy was also observed with decreases in muscle CSA occurring individually in Quadriceps (-19%, $p$<.000), Hamstrings (-29%; $p$=.016) and Adductors (-26%; $p$=.002).
**Conclusions:** After TKR surgery average muscle stiffness of the whole thigh increased significantly (p<.000) and CSA decreased significantly (p<.000). Furthermore, pixel-wise mapping showed that knee extension caused a significantly less increase in |G*| post-operatively compared to pre-operatively. This work has demonstrated a potential clinical role for muscle MRE in measuring the effect of joint surgery on individual muscles and which could in future be used to support the development of personalised rehabilitation programmes following surgery.

**References:** **[1]** Jeffrey et al., J Bone Jt Surg Br 1991. **[2]** Artz et al., BMC Musculoskelet Disord. 2015 **[3]** Papazoglou et al., MRM, 2006. **[4]** Barnhill et al., MRM, 2015. **[5]** Barnhill et al., Phys. Meas., 2013.

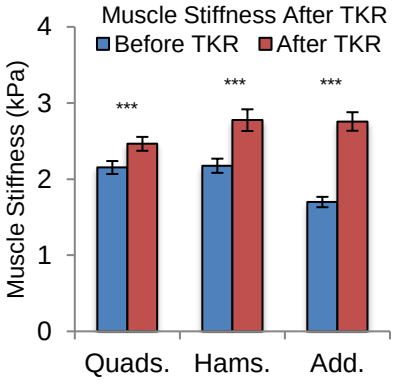


**Figure 1.** Muscle group |G*| comparison between scans with averaged loading. *** Indicates significant difference (p<.01).

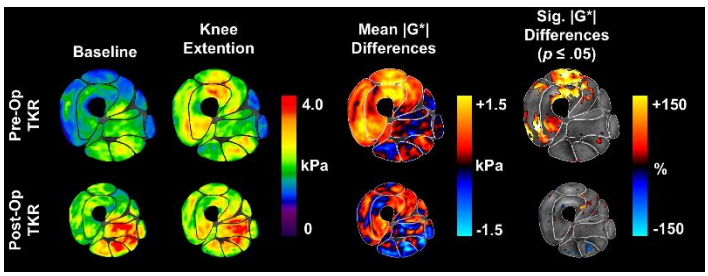


**Figure 2.** Pixel Mapping of significant |G*| changes in the thigh following TKR.

**34 MR elastography for assessing hepatic fibrosis and steatosis in pediatric non-alcoholic fatty liver disease**

Jing Guo[1], Christian Hudert[2], Susanna Wiegand[2], Birgit Rudolph[3], Heiko Tzschätzsch[1], Jürgen Braun[4], Ingolf Sack[1]

*[1]Department of Radiology, [2]Center for Chronically Sick Children, [3]Institute of Pathology, [4]Institute of Medical Informatics, all at Charité - Universitätsmedizin Berlin*

**Background:** Non-alcoholic fatty liver disease (NAFLD) is the most common chronic liver disease in children and adolescents today. Liver biopsy is still the gold standard for the diagnosis of NAFLD, despite its invasiveness and limited organ coverage. MR elastography (MRE) is a noninvasive imaging technique (1) used to probe the biomechanical properties of soft tissues in vivo. MRE has been of great value in diagnosing liver fibrosis and could be useful for diagnosis and characterization of pediatric NAFLD.

**Aims:** The aim of the study is to use multifrequency MRE (MMRE) to detect changes in liver stiffness and damping properties associated with NAFLD and to discriminate low-grade fatty liver disease from advanced fibrosis in children.

**Methods:** 51 overweight or obese patients (age range 14±2 years, mean BMI: 33.8 kg/m$^2$) with elevated ALT and/or AST values (>50 U/l for at least 3 months) were investigated after liver biopsy. MMRE (1) was conducted in a 1.5-T scanner (Siemens, Magnetom Sonata) using 7 mechanical frequencies (30 to 60 Hz, 5 Hz increment) by the abdominal MRE setup described in (2). The 3D wave field was recorded using a single-shot EPI sequence with motion-encoding gradients (MEG). Total acquisition time for 9 consecutive slices of 2.7×2.7×5mm$^3$ resolution, 7 frequencies, 8 wave dynamics was approx. 5min. MRE data was reconstructed by wavenumber recovery as detailed in (3), yielding parameter maps of shear wave speed (*c*) and penetration rate (*a*). Hepatic fat fraction (HFF) was estimated by the Dixon method.

**Results:** Based on histological staging, 28 subjects had no or early fibrosis, 15 subjects with stage 0 (F0), 13 with stage 1 (F1). 9 subjects had stage 2 (F2) moderate fibrosis and 14 subjects had advanced fibrosis with stage 3 (F3). Based on the steatosis grade, the patients are divided into 3 groups, with 11, 17 and 23 subjects having steatosis grade 1, 2 and 3 (S1, S2 and S3), respectively. Fig.1 shows magnitude image, shear wave image, map of shear wave *c* and penetration rate *a* in a patient with F1 obtained from the MRE scan. *c* was significantly higher in patients with F3 (Fig.2a). *c* was could detect any fibrosis (F≥1), moderate fibrosis (F≥2) and advanced fibrosis (F≥3) with AUROC-values of 0.82, 0.91 and 0.90, respectively (Fig.2d). *a* was significantly lower in the S3 group (Fig.2b) while HFF was elevated with increasing steatosis (Fig.2c). *a* and HFF could detect moderate steatosis (S ≥ 2) with AUROC values of 0.86 and 0.92, respectively (Fig 2e). *a* and HFF were negatively correlated (R=-0.58, P<0.0001).

**Conclusions:** MMRE-derived mechanical parameters *c* and *a* are independently responsive to pathological feature of pediatric NAFLD such as fibrosis and steatosis. While *c* can differentiate moderate from advanced fibrosis, *a* can detect moderate steatosis. Both mechanical parameters can potentially serve as complementary imaging markers for the noninvasive assessment of liver fibrosis and steatosis in young patients with NAFLD.

**References:** [1] Muthupillai R et al. Nat Med. 1996;2(5):601-3. [2] Guo J et al. Invest Radiol. 2015;50(5):347-51. [3] Tzschatzsch H et al. Med Image Anal. 2016;30:1-10.

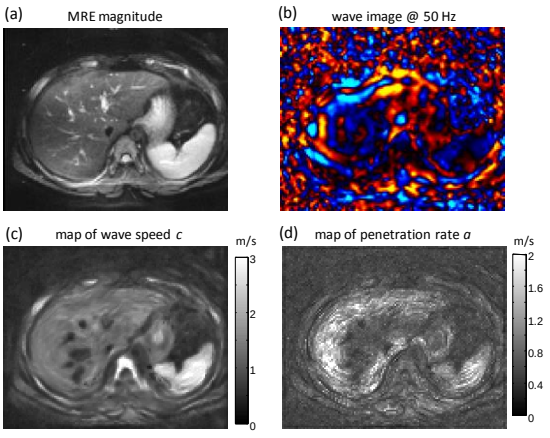


**Fig.1:** Magnitude of the MRE signal (a), wave image at 50 Hz vibration frequency (b), map of wave speed (c) and penetration rate (d) in a central slice of one patient with F1.

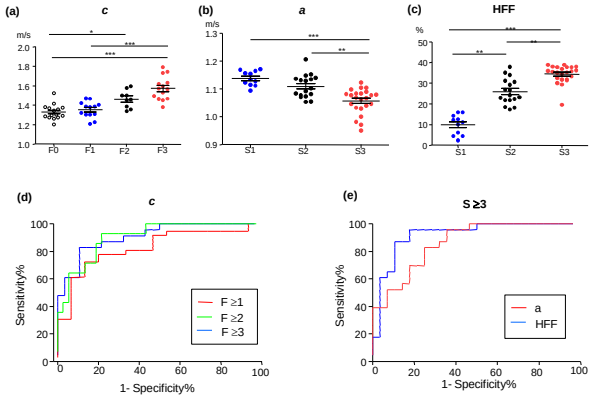


**Fig.2:** Mean values of *c* (a), *a* (b) and HFF (c) in patients from all fibrosis and steatosis groups. ROC curves of *c* in detecting different fibrosis stages (d) and ROC curves of *a* and HFF in detecting advanced steatosis stage (S ≥ 2).

## Poster contributions

**P01** **Viscoelasticity of rat liver tissue in native, lysed and decellularized states measured by 0.5 T tabletop magnetic resonance elastography (MRE)**

Angela Ariza de Schellenberger[1,3], Hannah Everwien[2], Nils Haep[2], Igor Sauer[2], Heiko Tzschätzsch[1], Jürgen Braun[3,] Ingolf Sack[1]

*[1] Elastography, Department of Radiology; Charité - Universitätsmedizin, Charitéplatz 1, 10117 Berlin, Germany; [2] Chirurgische Klinik; Charité - Universitätsmedizin, Augustenburger Platz 1, 13353 Berlin, Germany; [3] Department of medical informatics, Charité - Universitätsmedizin, Hindenburgdamm 30, 12200 Berlin, Germany*

**Background:** The search of the ideal matrix for tissue and organ regeneration is one of the big challenges in regenerative medicine. Ideally, a 3D non-immunogenic biomatrix that supports cell survival and functionality is required for tissue recellularization and proper function for organ transplantation. Characterization of 3D decellularized tissue scaffolds is commonly approached by histological and quantitative chemical analysis. The mechanical ECM properties depend on the complex mechanical interactions of entangled components which are poorly characterized in the literature due to the lack of volume-based mechanical test methods such as MRE.

**Aims:** To measure the viscoelastic properties of 3D tissue scaffolds from rat livers after complete removal of cells in comparison with native rat livers and rat liver tissue previously frozen (lysed) to destroy the integrity of cell walls.

**Methods:** Livers were harvested from Lewis rats and animal protocols were approved by the State Office of Health and Local Affairs (LAGeSo, Berlin, Germany; Reg. No L 0421/12). Each rat liver sample was introduced into the cylindrical glass capillary and prepared for MRE. Native samples were prepared immediately after animal dead. Lysed samples from the same rat were embedded in PBS and overnight frozen at -20°C to destroy cells without removing cell debris. The samples were thawed at next day at 4°C. Decellularized livers were prepared from additional rats and detailed procedure have been published somewhere else [1].

A compact MRE tabletop device with a 0.5-T permanent-magnet based MRI system was used for the MRE experiments. Details of the system are described elsewhere [2, 3]. MRE was performed in native, lysed and decellularized rat liver samples (B x H: 1cm). The shear modulus dispersion functions were acquired at 300-1200 Hz. Two viscoelastic models were fitted to the data: i) the powerlaw springpot model (SP) comprising a shear modulus $\mu_{SP}$ and powerlaw exponent $\alpha$ and ii) the Kelvin-Voigt (KV) model comprising a shear modulus parameter $\mu_{KV}$ and a viscosity parameter $\eta$.

**Results:** Decellularized tissue shows a rich collagen matrix with cavities due to the removed cells in SEM images. Cell lysis and complete cell removal drastically changed the mechanical properties of the liver. Overall, liver stiffness progressively decreased and the powerlaw coefficient $\alpha$ increased due to cell lysis or cells removal (Figure 1). The fit residue $\sigma$ indicating the quality of the fit was lower for the KV-model, but best fit decellularized tissue (mean $\sigma$ SP decellularized, lysed, native: 0.08 ± 0.04, 0.17 ± 0.04, 0.31 ± 0.03). Conversely, the SP-model similarly matched the viscoelastic properties of all three tissue states (mean $\sigma$ SP decellularized, lysed, native: 0.11 ± 0.04, 0.12 ± 0.03, 0.11 ± 0.04).

**Conclusions:** Tabletop MRE can reproducibly measure the change of viscoelastic properties in liver tissue due to cell removal or modification of cellular integrity. Overall, decellularized tissue is much softer than native tissue and the degree of reduction of stiffness is similar to what is obtained by freezing the tissue. However, the parameter change with frequency, i.e. the viscoelastic dispersion function was distinct in all three investigated tissue states. While the viscoelastic properties of intact liver tissue are determined by cells giving rise to a powerlaw behavior, decellularized tissue has more solid-like properties which are better described by the KV-model.

**References:** [1] Struecker B.et al. J. tissue engineering and regenerative medicine 2017. [2] Ipek-Ugay S. et al. J. Magnetic Resonance 2015 [3] Braun J. et al. Magnetic resonance in Medicine, 2017

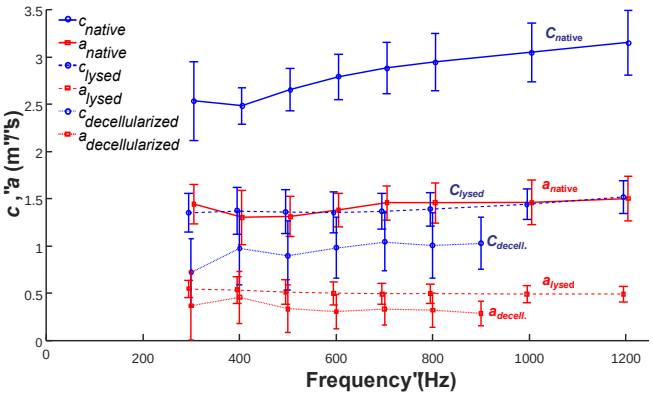


**Figure 1:** Average for shear wave (*c*) and penetration rate (*a*) for native, lysed and decellularized rat liver acquired at 300-1200Hz

**P02** **Tomoelastography of the mouse brain**

Gergely Bertalan[1] , Jing Guo[1], Jürgen Braun[2], Ingolf Sack[1]

*[1]AG Elastography, Experimental Radiologie, Charité - Universitätsmedizin Berlin, Berlin, Germany; [2]Institute of Medical Informatics, Charité - Universitätsmedizin Berlin, Berlin, Germany*

**Background:** Despite the significant advancements of in vivo MRE elastography (MRE) of the brain in the last two decades, high resolution elasticity maps of the mouse brain are still lacking in the literature. Tomoelastography is a full-field-of-view multifrequency MRE technique based directional filtering and noise-robust wavenumber recovery. Albeit feasible in vivo in abdominal organs, tomoelastography is limited in the human brain due to the prevalence of sulci and slip interfaces.

**Aims:** The mouse brain has relatively smooth boundaries which favors tomoelastography. We therefore aim to generate high resolution stiffness maps of in vivo murine brain. To this end fast single-shot multifrequency EPI-MRE with SLIM-encoding was developed.

**Methods:** 11 healthy female C57BL-6 mice were investigated. Experiments were executed with a 7T pre-clinical scanner (Bruker PharmaScan 70/16, Ettlingen, Germany). Two MRE sequences were developed based on single-shot (EPI-MRE) and multi-shot (MS-MRE) spin echo techniques. The mouse brain was mechanically stimulated with a custom built actuator shown in Figure 1 by 6 frequencies from 900 to 1400 Hz. Wave speed (*c*-) maps were reconstructed by *k*-MDEV as detained in [6]. Three experiments were performed: (1) Singel *c*-map experiments by EPI-MRE in 10 mice (10 min total measure time for each animal); (2) 5 slice-MS-MRE in a single mouse in vivo (approx. 1.5 h measure time). (3) the same as (2) but ex vivo brain fixed and embedded in agarose gel. The following regions were analyzed: whole brain (b), isocortex (ic), hippocampus (h), corpus calosum (cc), brain stem (st), midbrain (mb) and thalmus (th).

**Results:** Figure 2 shows MRE magnitude images and *c*-maps from tomoelastography. Mean *c* of the entire brain was 3.76 ±0.33 m/s in (1), 3.66 ±1.16 m/s in (2) and 7.8 ±3.76 m/s in the fixed state (3). In vivo c decreased in the order of h > st > ic > cc as quantified in Figure 3. *c*-maps of (1), (2) and (3) show similar stiffness features of mouse brain anatomy.

**Discussion/Conclusions:** The distribution of in vivo stiffness as seen in *c*-maps reflects mouse brain anatomy. Tissue consisting of mainly white matter (eg. corpus calosum) was softer than tissue with both gray and white matter. This finding contradicts reports from in vivo MRE of the human brain [7] but agrees to micro-indentation measurements of mouse brain tissue [5]. The hippocampus was measured stiffer and isocortex softer than in [1]. Median stiffness of the entire brain was lower than in [2] and higher than in [3] and [4]. These discrepancies are probably due to differences in the used frequency range, mechanical stimulation and inversion method.

**References:** [1] Macé E et al., IEEE Transaction on Medical Imaging, 30(3): 550-58, 2011. [2] Murphy CM et al., Magn Reson Imaging, 30(4): 535–539, 2012. [3] Atay M et al., J Biomech Eng, 130:021013, 2008. [4] Clayton E.H et al., Phys Med Biol, 56(8): 2391–2406, 2011. [5] Christ A. F et al., J Bio Mech, 43(15):2986-92, 2010. [6] Tzschätzsch H et al., Medical Image Analysys, (30):1-10, 2016. [7] Hirsch S et all. Magnetic Resonance Elastography: Physical Background And Medical Applications: Wiley-VCH 2017

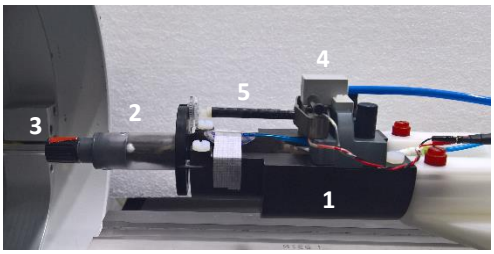


**Figure 1:** Custom built animal holder with the vibration unit: (1) animal holder, (2) anesthesia coin, (3) bite bar, (4) piezo actuator, (5) transducer rode.

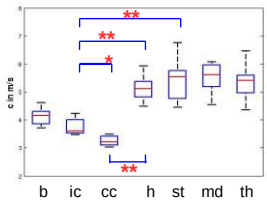


**Figure 3:** Mean stiffness of brain regions averaged over 10 animals (*p < 0.02, **p < 0.005).

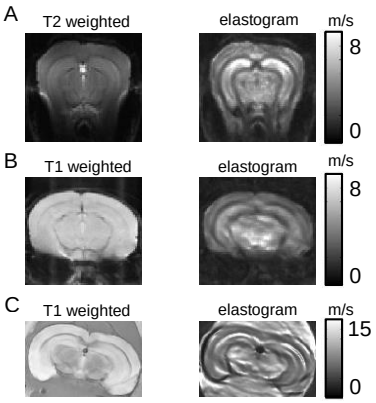


**Figure 2**: Coronal *c*-maps and corresponding magnitude images of the mouse brain. (A) In vivo EPI-MRE: 150 µm in-plane resolution. (B) In vivo MS-MRE: 150 µm in-plane resolution. (C) Ex vivo MS-MRE: 100 µm in-plane resolution.

**P03** **Correlating Relative Myelin Content And Dissipative Properties Of Human Brains: An In-Vivo Mri Study**

G. Fabris (1), E. Ozkaya (1), J. Martinez (1), Z. M. Suar (1), F. Macruz (2), K. B. Pauly (2,3),M. Wintermark (2), M. Kurt (1)

*[1]Department of Mechanical Engineering, Stevens Institute of Technology, Hoboken, New Jersey, USA; [2]Department of Radiology, Stanford University, Stanford,California, USA; [3]Department of Bioengineering, Stanford University, Stanford,California, USA*

**Background:** Magnetic resonance elastography (MRE) is emerging as a non-invasive means to measure material properties of biological tissues that would be otherwise inaccessible. This phase-contrast based imaging technique almost mimics the act of "palpating" the brain, allowing for examination of the local brain stiffness properties *in-vivo.* In previous *ex-vivo* studies, it was shown that myelin content contributes to the stiffness of bovine brain white matter. Also, in the first 18 months after birth, myelination peaks dramatically [1]. With these two ideas in mind, we sought to use the MRE to investigate the correlation between myelin content in the developing brain and stiffness.

**Aims:** i) Extracting myelin content data and correlating it with brain stiffness maps acquired from MRE

ii) Identifying the best mechanical parameter to be used as a diagnostic marker of demyelination

**Methods:** A 3T MRI Scanner (GE Healthcare) and a custom designed MRE protocol with a single actuator frequency operated at the frequency values of 40, 60 and 80 Hz (Mayo Clinic, Rochester, MN) were used to retrieve the data used to determine correlations between relative myelin content and brain stiffness maps. For this study, we recruited 27 volunteers aged from 7 to 17, of which 13 were male and 14 were female. To create the myelin maps for the subjects, at first T1-weighted and T2- weighted images were acquired, each containing 160 and 48 slices respectively. The images were then sent through a pre-processing pipeline consisting of bias correction, image registration, skull stripping, and smoothening steps. All of the preprocessing was performed on the software platform SPM12. After pre-processing, the conventional MRI scans were divided pixelwise, T1-w/T2-w, to retrieve the myelin maps [2,3]. This was followed by pixelwise Pearson correlation value calculation between the myelin maps and brain stiffness maps.

**Results:** Correlation values between the brain stiffness maps with respect to the relative myelin content spanned values of 0.5 to 0.9, with the highest correlates observed for the loss modulus. Interestingly, a higher correlation was observed for low actuation frequencies compared to high MRE actuation frequencies. This might indicate that the myelin plays a role during the low frequency responses of the brain tissue under external loading. Also, when comparing the data on an age-by-age basis, no statistically significant difference was observed, indicating the robustness of the loss modulus as a biomechanical marker capable of predicting demyelination among different age groups.

**Conclusions:** By identifying the loss modulus as the best correlate to relative myelin content, our data indicate that myelin imaging can be exploited as a substitute for MRE stiffness maps. Loss moduli can therefore be used as a mechanical predictor of demyelination, with far-reaching clinical implications.

**References:** [1] Duhaime et al., J. Neurosurgery, 93:445-462, 2000. [2] Duhaime et al., J. Neurosurgery, 93:445-462, 2000. [3] Ganzetti, M et al.,G et al., *Neuroradiology*, 57:917-928, 2015.

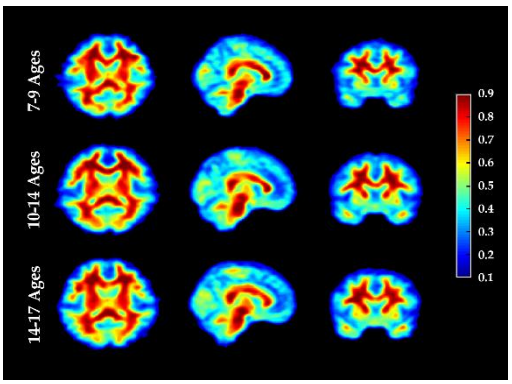


**Figure 1:** Percentile myelin distribution as estimated from T1-w/T2-w ratio imaging for different age groups.

| | MRE 40 Hz | MRE 60 Hz | MRE 80 Hz |
|---|---|---|---|
| Stiffness | $0.89 \pm 0.18$ | $0.83 \pm 0.26$ | $0.57 \pm 0.40$ |
| Storage Moduli | $0.79 \pm 0.25$ | $0.62 \pm 0.45$ | $0.61 \pm 0.37$ |
| Loss Moduli | $0.91 \pm 0.31$ | $0.95 \pm 0.07$ | $0.80 \pm 0.37$ |

**Table 1:** Average correlation values for the all volunteers.

**P04** **Development of a Tissue-Mimicking Visco-elastic Phantom for Quantitative Assessment of MRE**

Koki Ishii[1], Mikio Suga[1,2,3], Riwa Kishimoto[3], Eika Hotta[3], and Takayuki Obata[3]

*[1]Graduate School of Science and Engineering, Chiba University, Chiba, Japan; [2]Center for Frontier Medical Engineering, Chiba University, Chiba, Japan; [3]Hospital, National Institute of Radiological Sciences, QST, Chiba, Japan.*

**Background:** Magnetic Resonance elastography (MRE) is a non-invasive technique for quantitatively measuring tissue viscoelasticity [1]. The measured viscoelasticity can be used as an imaging biomarker. A quantitative phantom is required to assess the accuracy and repeatability of MRE systems. We have previously developed tough and stable polyacrylamide (PAAm) gel phantoms for this purpose. We have also achieved to make a phantom which viscosity was close to that of living tissue using glycerin as a solvent. In this study, we compared the mechanical properties of our phantoms with those of living tissue.

**Aims:** i) To compare frequency dependence of mechanical properties between our phantoms and living tissue. ii) To confirm the temporal changes in moduli.

**Methods:** We made two gel phantom sheets with different loss moduli (G”). The phantom sheets were designed to have a storage modulus (G’) of 1.5 kPa at 60 Hz, one having a loss tangent (tan δ = G”/G’) greater than 0.2 (high viscosity phantom) and the other, less than 0.02 (low viscosity phantom). The storage and loss moduli of each phantom and fresh bovine liver (diameter: 50 mm, slice thickness: 2.0–2.7 mm) were measured using a parallel disc rheometer (MCR302, Anton-Parr). We repeated the measurements on these three samples with the strain amplitude set to 1%. High viscosity phantom (diameter: 120 mm, height: 150 mm) was examined by multi-frequency MRE at four driving frequencies (30, 40, 50, and 60 Hz). To compare the mechanical properties at low frequencies, we applied spring-pot model fitting to the measured MRE data [2]. To evaluate temporal changes, the phantom which was designed to have storage modulus of 3 kPa was examined by MRE for a year (driving frequency: 62.5 Hz).

**Results:** Figures 1a and 1b show the storage and loss moduli obtained with MRE, the rheometer, and the fitted curves according to the spring-pot model for the MRE data. In the high viscosity phantom and bovine liver, the storage and loss moduli increased with the frequency, which were different from changes in the low viscosity phantom. Figure 2 shows the change in the mechanical properties of the phantom over a year. The change in storage elastic modulus during the one year period was within ± 3%.

**Conclusions:** Similar frequency characteristics were found in the storage and loss moduli of the high viscosity phantom and bovine liver by multi-frequency MRE and rheometer measurements. There was minimal change in the mechanical characteristics of the tissue-mimicking phantom over time. It is considered that the developed phantoms can be used for the quantitative assessment of MRE system.

**References:** [1] R. Muthupillai, et.al. *Science*, 269:1854-1857, 1995. [2] D. klatt, et.al. *Biorheology*, 47:133-141, 2010.

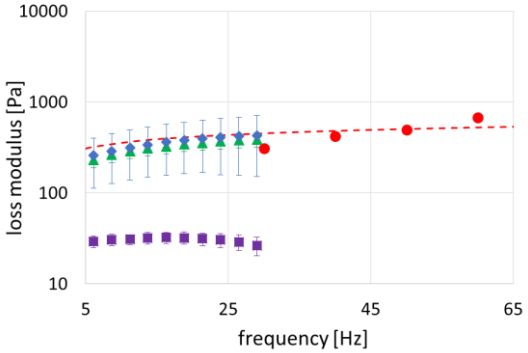


**Figure 1a:** Relationship between frequency and storage modulus

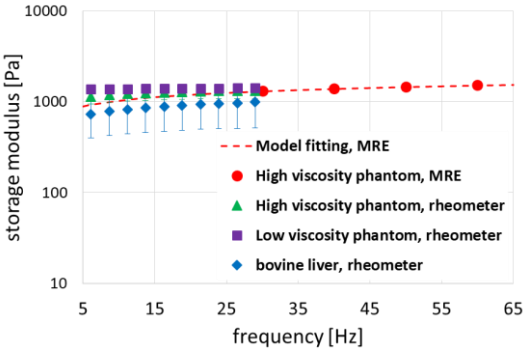


**Figure 1b:** Relationship between frequency and loss modulus

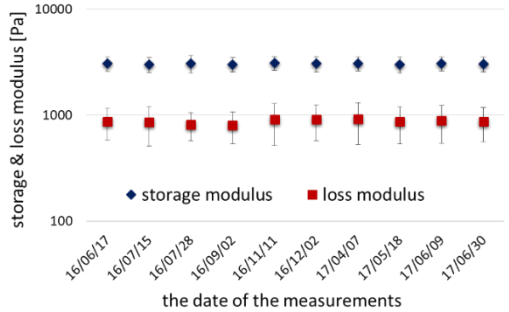


**Figure 2:** Changes in the mechanical properties over time

**P05** **Multislice interventional MR Elastography using simultaneous image refocusing (SIR)**

K.S. Kim[1], E. Breton[1], A. Gangi[1,2], J. Vappou[1]

*[1]ICube, UMR7357, Université de Strasbourg, CNRS, 1 place de l'Hôpital, Strasbourg, France; [2]Dpt. of Interventional Radiology, Hôpitaux Universitaires de Strasbourg, France.*

**Background:** Interventional MR Elastography (MRE) has been developed to monitor changes in biomechanical properties induced by thermal ablations [1]. Based on a GRE sequence, it allows to simultaneously derive both elasticity and thermometry maps (Proton Resonance Frequency) in a single slice [2]. However, real-time monitoring of thermal ablations requires the acquisition of multiple contiguous slices in order to cover spatially the ablation area with high temporal resolution.

**Aims:** This paper proposes the use of the Simultaneous Image Refocusing (SIR) technique [3] for the simultaneous MRE encoding and acquisition of 2 slices in a single acquisition.

**Methods:** As shown in Fig. 1, two consecutive RF excitations are used to selectively excite 2 non-contiguous slices in a single TR. The combination of 2 pre-dephasing readout gradients creates 2 sequential echo formations, one per slice, each slice having its specific TE [3]. Using minimal fractional encoding, it is possible to acquire the echoes for 2 slices with TR = 2 mechanical periods ($T^{exc}$). Experiments are conducted in a 1.5 T MRI scanner (MAGNETOM Aera, Siemens, Germany). Table 1 shows the main acquisition parameters, and a comparison of the proposed SIR-GRE MRE sequence with GRE MRE sequences in terms of acquisition time per slice and fractional encoding. The phantom consists of a 9% inclusion within 7% gelatin background. Elastograms are reconstructed by calculating the temporal Fourier transform with 3 phase offsets and by using a local frequency estimation (LFE)-based algorithm. Motion is encoded through slice, and 2 acquisitions of 2 slices (slice gap 100% between 2 simultaneously acquired slices) allow covering the whole inclusion, with no space between slices.

**Results:** A total of 4 slices are acquired with the SIR-GRE sequence, with an elasticity update rate of 1.6 s. Mean and standard deviation calculated respectively in the inclusion and the background are: slice 1 10.7±0.7 / 4.2±0.1 kPa, slice 2 10.5±0.5 / 4.3±0.1 kPa, slice 3 8.8±0.7 / 4.0±0.1 kPa, slice 4 11.2±0.8 /3.9±0.05 kPa. As shown in Table 1, at 125 Hz, conventional GRE-MRE sequence with TR = $T^{exc}$ requires high fractional motion encoding, while GRE MRE with TR = $2T^{exc}$ requires longer acquisition time for each single slice. The SIR GRE-MRE sequence allows the acquisition of 2 slices with TR = $2T^{exc}$ and limited fractional encoding.

**Conclusions:** This preliminary experiment shows that SIR-GRE MRE can provide stiffness values in multiple contiguous slices, while minimizing the loss in terms of temporal resolution.

**References:** [1] Corbin et al., Magn. Reson. Med., 75(3): 1110-8, 2015 ; [2] Yuan L et al., Magn. Reson. Med. 55:700-05, 2006; [3] David F et al., Magn. Reson. Med. 48(1):1-5, 2002.

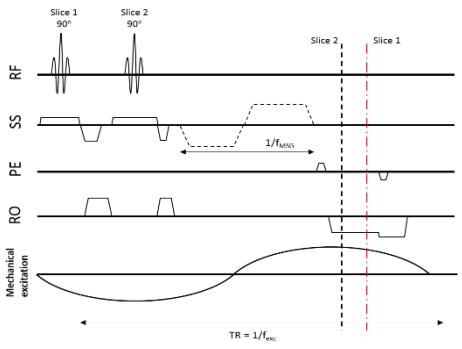


**Figure 1:** Chronogram of the SIR-GRE MRE sequence. Black dash line and red dot-dash line point out the echo formation of slices 1 and 2, respectively.

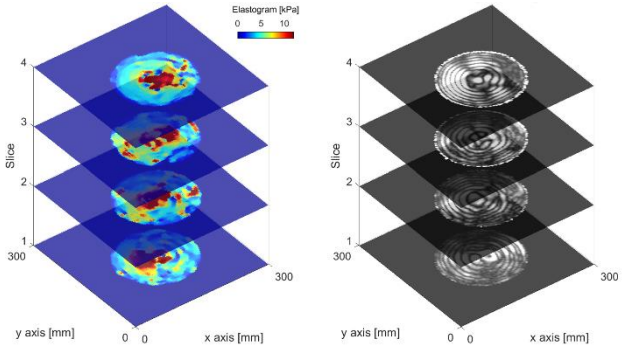


**Figure 2:** Multislice elastogram (left) and wave propagation images (right) at 125 Hz in an inhomogeneous gelatin phantom. A total of 4 slices are acquired, in twice the acquisition time necessary for a single slice (slices 1&3, then 2& 4).

**Table 1:** Acquisition parameters for SIR-GRE and conventional GRE MRE sequences at 125Hz. The SIR-GRE MRE sequence uses TR = $2T^{exc}$, $T^{exc}$ being the mechanical period. The GRE MRE sequence can be used either with/out fractional encoding, with TR = $T^{exc}$ or TR = $2T^{exc}$, respectively.

| Parameter | SIR-GRE MRE | GRE MRE (1 $T^{exc}$) | GRE MRE (2 $T^{exc}$) |
|---|---|---|---|
| Excitation frequency (1/$T^{exc}$) | 125 Hz | 125 Hz | 125 Hz |
| TR | $2T^{exc}$ (16 ms) | $T^{exc}$ (8 ms) | $2T^{exc}$ (16 ms) |
| TE | 9 ms – 10.7 ms | 5.87 ms | 9.92 ms |
| MSG frequency | 138 Hz | 255 Hz | 125 Hz |
| Acquisition Time | 800 ms for 2 slices | 400 ms per slice | 800 ms per slice |

*Bandwidth 1502 Hz/Px, FoV/matrix 300 mm × 300 mm / 128 × 128 (80% phase), slice thickness 7 mm, Grappa ×2, partial Fourier 6/8*

**P06** **An investigation of the relationship between the grid dimensions and wave** shapes of an anisotropic fiber phantom: preliminary results

H. Palnitkar[1], P. Lewis[3], M. Hammersley[3], R.N. Shah[3], T. J. Royston[1,2] , D. Klatt [2]

*[1] Mechanical and Industrial Engineering; [2] Bioengineering, UIC, Chicago, IL.; [3] Materials Science and Engineering, Northwestern University, Chicago, IL.*

**Background:** The mechanical behavior of biological tissue, such as brain white matter and muscle, is anisotropic due to a preferred direction imposed by fibers. Anisotropic tissue phantoms enable the study of wave propagation in tissue more realistically. Anisotropic wave field inversion has been performed assuming homogeneous material characteristics[1]. However, anisotropic phantoms composed of fibers and a gel matrix are heterogeneous on smaller scales.

**Aim:** To investigate the relationship between the structure of an anisotropic fiber phantom and the wave shapes in order to identify parameter ranges, in which homogenization techniques may be applied for wave field inversion.

**Method:** An anisotropic fiber phantom was constructed by immersing a 3D-printed 15% w/v water based gelatin fibrous phantom into a 10% w/v water-based gelatin medium inside a glass tube, as shown in fig. 1. MRE experiments were performed on this anisotropic fiber phantom at five frequencies, namely 1.5 kHz, 2 kHz, 3 kHz, 5 kHz and 6 kHz using geometrically focused mechanical excitation technique[2] and a gradient echo based Sample Interval Modulation (SLIM) pulse sequence[3].

**Results:** Figure 2 presents a comparison of wave images obtained during MRE experiments of the anisotropic fiber phantom. Elliptical wave shapes are visible at 2 kHz that vary in orientation for different mechanical phases. At smaller ratios of wave length over grid dimensions (1.2 and below), the wave fronts deviate from regular elliptical shapes presumably due to diffraction effects.

**Conclusions:** The observations indicate that homogenization techniques may be applied below a certain ratio limit of wave length over grid dimensions, which was 1.2 in the present study. An extension of the current work will be to determine a measure for when homogenization is possible based on the correlation of experimental wave images of fiber phantoms and images from simulations using homogeneous anisotropic structures.

**References:**

[1] Romano, A. et al., In Vivo Waveguide Elastography of White Matter Track in the Human Brain. *MRM*, **68**(5), 1410-22 (2012); [2] Yasar, T.K. et al. Wideband MR Elastography for viscoelasticity model identification. *MRM*. **70** (2): 479 – 489 (2013); [3] Klatt, D. et al. Sample Interval Modulation for the simultaneous acquisition of displacement vector data in magnetic resonance Elastography: theory and application. *Phys. Med. Biol.* **58,** 8663 – 8675 (2013).

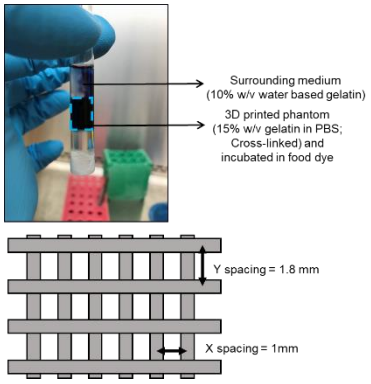


**Figure 1:** Microstructure of the anisotropic fiber phantom

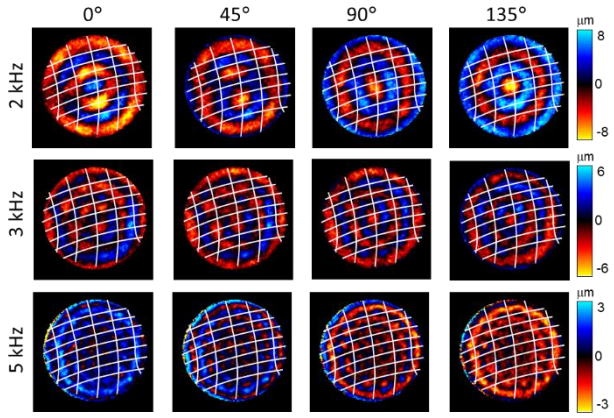


**Figure 2:** Snaphots of wave propagation (out-of-plane) at four mechanical phases for three excitation frequencies. The fiber orientation is highlighted with white lines. The ratio of wave length over grid dimension was 1.9, 1.2 and 0.6 in the experiment using 2 kHz, 3 kHz and 5 kHz, respectively.

**P07** **MR Elastography on polymer networks: a proof of concept for collagen gels**

Frank Sauer[1], Linda Oswald[2], Angela Ariza de Schellenberger[3], Heiko Tzschätzsch[3], Jürgen Braun[4], Josef A. Käs[2], Claudia T. Mierke[1], Ingolf Sack[3]

*[1]Biological Physics Division, [2]Soft Matter Physics Division, Peter Debye Institute for Soft Matter Physics, Linnestr. 5, Leipzig, Germany; [3]Department of Radiology, [4]Institute of Medical Informatics, Charité-Universitätsmedizin, Charitéplatz 1, Berlin, Germany*

**Background:** Magnetic resonance elastography (MRE) allows for the measurement of intrinsic material parameters by inducing shear waves within a bulky sample with a piezo actuator and measuring their propagation with the help of medical imaging (MRI).

**Aims:** MRE of small tissue samples covers a frequency range which usually exceeds that of standard rheology [1]. Collagen polymer networks are of great interest in biophysical research since they provide 3D matrices for cell experiments and can simulate the cellular environment in biological tissues. We test the applicability of multifrequency MRE to characterize collagen polymer gels by their shear modulus dispersion functions and powerlaw behavior using a tabletop MRE device.

**Methods:** 3.0 g/l collagen gels consisting of a 2:1 mixture of type 1 bovine skin and type 1 rat tail collagen [2] were crosslinked with 0.2 % glutaraldehyde for 1 hr [3]. Elastography measurements were carried out with a recently introduced 0.5 T tabletop MRE device [1].

**Results:** In a frequency range of 200 - 2000 Hz, collagen treated with glutaraldehyde for one hour was stiffer and more elastic than untreated collagen with $\mu = 1032 \pm 83$ Pa and $\alpha = 0.124 \pm 0.018$ versus $\mu = 36.5 \pm 4.5$ Pa and $\alpha = 0.381 \pm 0.022$. The crosslinking of the collagen gels led to a 28-fold increase in $\mu$ and a 3-fold reduction of $\alpha$.

**Conclusions:** Tabletop MRE is a suitable method to reproducibly characterize viscoelastic constants of collagen gels over a wide frequency range which cannot be examined by standard oscillatory rheology. Shear moduli obtained by MRE and rheology are in a similar range, although a different frequency dependence of G* is expected in the so far non-overlapping measurement frequencies of both methods [4]. The crosslinking of collagen due to treatment with glutaraldehyde was well detectable by an increased shear modulus and reduced powerlaw constant.

**References:** [1] Braun, J. et al. A compact 0.5 T MR elastography device and its application for studying viscoelasticity changes in biological tissues during progressive formalin fixation. Magn. Reson. Med. 0, 1–9 (2017); [2]Kunschmann, T. et al. Integrin-linked kinase regulates cellular mechanics facilitating the motility in 3D extracellular matrices. Biochim. Biophys. Acta - Mol. Cell Res. 1864, 580–593 (2017); [3] Lang, N. R. et al. Biphasic response of cell invasion to matrix stiffness in three-dimensional biopolymer networks. Acta Biomater. 13, 61–67 (2015); [4] Shayegan, M. et al. Microrheological Characterization of Collagen Systems: From Molecular Solutions to Fibrillar Gels. PLoS One 8, e70590 (2013).

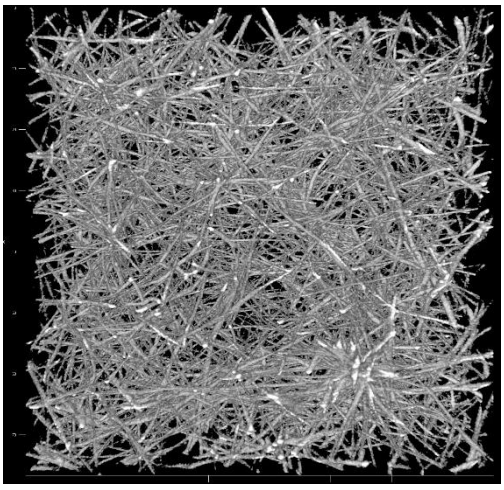

**Figure 1:** Confocal stack of a 3.0 g/l collagen gel (TAMRA-SE) with an average pore size of 3.5 µm. Image section: 80 µm x 80 µm x 50 µm

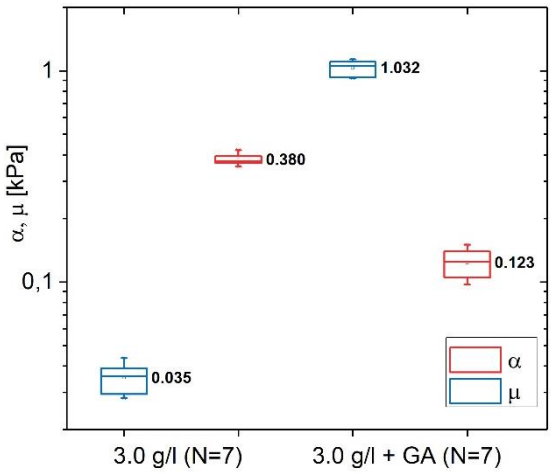


**Figure 2:** Spring pot fit model constants µ and α for untreated (3.0 g/l) and glutaraldehyde crosslinked collagen gels (3.0 g/l + GA).

**P08** **Heparin as MRE phantom material with viscoelastic powerlaw properties similar to soft biological tissues**

Felix Schrank[1], Heiko Tzschätzsch[1], Angela Ariza de Schellenberger[1], Jürgen Braun[2], Ingolf Sack[1]
*[1]Department of Radiology, [2]Institute of Medical Informatics, Charité - Universitätsmedizin Berlin, Berlin, Germany*

**Background:** The viscoelastic springpot model is a powerlaw which describes the mechanical properties of many biological tissues across a wide range of frequencies [1]. In the literature, springpot-based viscoelastic constants of in-vivo organs have been reported with a shear modulus of μ = 4.63 ± 0.91 kPa and a dimensionless powerlaw exponent α = 0.27 ± 0.01 for liver tissue and μ = 5.58 ± 0.90 and α = 0.29 ± 0.01 for brain tissue [1]. The present study is motivated by the need for phantom materials in MRE which reproduce the viscoelastic powerlaw behavior of biological tissues in a wide dynamic range.
**Aims:** To introduce heparin as a new viscoelastic phantom material for MRE investigations and to demonstrate its powerlaw behavior over more than 6 octaves dynamic range by multifrequency MRE at different systems. Furthermore, heparin will be compared to commercially available phantoms which have been used for MRE investigations.
**Methods:** Heparin gel (Ratiopharm, Ulm, Germany), the CIRS Model-049 phantom (CIRS, Norfolk, Virginia, USA) and the Resoundant MRE phantom (Resoundant Inc., Rochester, Minnesota, USA) were investigated. MRE measurements were performed in a 1.5-T clinical scanner and a 0.5-T tabletop MRE scanner [2]. The CIRS and Resoundant phantoms were investigated in a frequency range from 60 Hz to 150 Hz in the clinical system while heparin was investigated between 10 and 1000 Hz in both systems. Parameter reconstruction was based on waveform fitting which has been demonstrated less susceptible to noise and discretization artifacts than direct inversion [2]. The resulting shear modulus dispersion functions are fitted by the springpot powerlaw model. Fit tolerances were given as standard mean error.
**Results:** The figure shows the shear modulus dispersion functions for the three investigated phantom materials. The resulting springpot constants are, (i) heparin: μ = 0.56 ± 0.01 kPa, α = 0.27 ± 0.01, (ii) CIRS phantom: μ = 5.60 ± 0.50 kPa, α = 0.00 ± 0.04 and, (iii) Resoundant phantom: μ = 3.29 ± 1.42 kPa, α = 0.06 ± 0.02.
**Conclusions:** Heparin features an almost ideal springpot powerlaw behavior in a wide frequency range. The derived springpot constants reveal that heparin is softer than human liver and brain tissue, while it has similar dispersion properties as encountered in both types of tissue by in-vivo MRE. In contrast, the CIRS and Resoundant phantoms have higher storage moduli but do not show a powerlaw behavior. Heparin could be used as MRE phantom material to simulate viscosity of in vivo biological soft tissues.

**References:** [1] I. Sack et al. Soft Matter, vol. 9, no. 24, pp. 5672–5680, May 2013; [2] J. Braun et al. Magnetic Resonance in Medicine, vol. 68, no. 2, p. 041914, Mar. 2017.

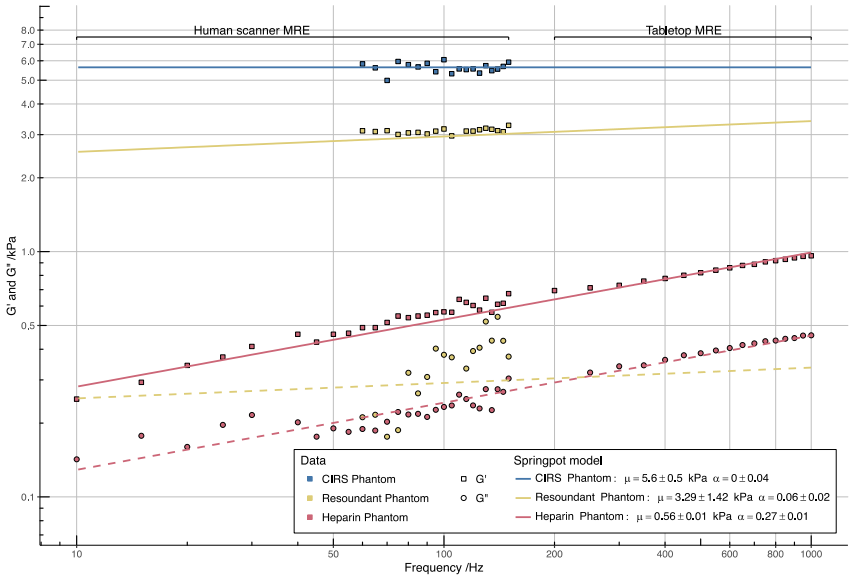


**Figure 1** Shear modulus dispersion functions and related springpot fits of the investigated MRE phantoms.

**List of participants**

| # | Name | Institute | Country | Email |
|---|---|---|---|---|
| 1 | Anderson, Aaron T. | Mechanical Science & Engineering Department, Beckman Institute for Advanced Science & Technology, University of Illinois at Urbana-Champaign, Urbana | United States | aandrsn3@illinois.edu |
| 2 | Arani, Arvin | Department of Radiology, Mayo Clinic, Rochester | United States | arani.arvin@mayo.edu |
| 3 | Ariyürek, Cemre | UMRAM, National Magnetic Resonance Research Center, Bilkent University Main Campus, Ankara | Turkey | cemre@ee.bilkent.edu.tr |
| 4 | Assili, Sanam | BIOQIC, Institute for Radiology, Charité Berlin, Berlin | Germany | sanam.assili@gmail.com |
| 5 | Bayly, Philip | Mechanical Engineering and Materials Science, Washington University in Saint Louis, Saint Louis, MO | United States | pvb@wustl.edu |
| 6 | Bertoglio, Cristobál | Johann Bernoulli Institute, University of Groningen, Groningen | The Netherlands | c.a.bertoglio@rug.nl |
| 7 | Bigot, Mathilde | CREATIS – site CPE, Villeurbanne | France | Mathilde.Bigot@creatis.insa-lyon.fr |
| 8 | Bolster, Bradley | Siemens Healthineers, Siemens Medical Solutions USA, Inc., Malvern | USA | bradley.bolster@siemens-healthineers.com |
| 9 | Caiazzo, Alfonso | WIAS Berlin, Berlin | Germany | caiazzo@wias-berlin.de |
| 10 | Chaopathomkul, Bundit | Department of Radiology, King Chulalongkorn Memorial Hospital, Thai Red Cross Society, Chulalongkorn University, Bangkok | Thailand | bchaopathomkul@hotmail.com |
| 11 | Chatelin, Simon | ICube, University of Strasbourg – CNRS, S/s IRCAD, Strasbourg | France | schatelin@unistra.fr |
| 12 | de Arcos Rodríguez, José Fernando | St Thomas Hospital, London | United Kingdom | jose.dearcos@kcl.ac.uk |
| 13 | Detroux, Thibaut | Stevens Institute of Technology, Department of Mechanical Engineering, Hoboken | United States | tdetroux@ulg.ac.be |
| 14 | Dong, Huiming | Department of Radiology, The Ohio State University Wexner Medical Center, Columbus | United States | dong.449@osu.edu |
| 15 | Fabris, Gloria | Stevens Institute of Technology, Department of Mechanical Engineering, Hoboken | United States | gfabris@stevens.edu |
| 16 | Fakhouri, Faisal | The Ohio State University, Columbus | United States | fakhouri.3@osu.edu |
| 17 | Fovargue, Daniel | Department of Biomedical Engineering, King's College London, London | United Kingdom | daniel.fovargue@kcl.ac.uk |
| 18 | Garteiser, Philippe | Inserm UMR1149 Center For Research on Inflammation, Paris | France | philippe.garteiser@inserm.fr |
| 19 | Guenthner, Christian | Institute for Biomedical Engineering, University and ETH Zurich, Zurich | Switzerland | guenthner@biomed.ee.ethz.ch |
| 20 | Hiscox, Lucy | Edinburgh Imaging Facility QMRI, University of Edinburgh, Edinburgh | United Kingdom | l.v.hiscox@sms.ed.ac.uk |
| 21 | Hockings, Paul | Antaros Medical | Sweden | paul.hockings@antarosmedical.com |
| 22 | Hwang, Darryl H. | Department of Radiology, University of Southern California, Los Angeles | United States | Darryl.Hwang@med.usc.edu |
| 23 | Ishii, Koki | Chiba University, Chiba | Japan | adca2218@chiba-u.jp |
| 24 | Johnson, Curtis L. | Department of Biomedical Engineering, University of Delaware, Newark | United States | clj@udel.edu |
| 25 | Joldersma-Bakker, W.T. | University Medical Center Groningen, Groningen | The Netherlands | w.bakker@umcg.nl |
| 26 | Kim, Kisoo | ICube laboratory, CNRS-Université de Strasbourg, Strasbourg | France | kisoo.kim@unistra.fr |
| 27 | Klatt, Dieter | UIC Bioengineering (MC 063), Chicago | United Stated | dklatt@uic.edu |
| 28 | Kreis, Roland | University Bern, AMSM, Bern | Switzerland | roland.kreis@insel.ch |

| | | | | |
|---|---|---|---|---|
| 29 | Kupriyanova, Yuliya | Deutsches Diabetes-Zentrum (DDZ), Düsseldorf | Germany | yuliya.kupriyanova@ddz.uni-duesseldorf.de |
| 30 | Lefebvre, Pauline M. | Laboratoire CREATIS - La Doua, Villeurbanne | France | pauline.lefebvre@creatis.insa-lyon.fr |
| 31 | Lilaj, Ledia | BIOQIC, Institute for Radiology, Charité Berlin, Berlin | Germany | ledia.lilaj@charite.de |
| 32 | Manduca, Armando | Department of Physiology & Biomedical Engineering, Mayo Clinic, Rochester | USA | manduca.armando@mayo.edu |
| 33 | Marshall, Helen | Centre for Inflammation Research, Edinburgh Imaging Facility, University of Edinburgh, Edinburgh | United Kingdom | helenmarshall93@hotmail.co.uk |
| 34 | McGarry, Matthew | Thayer School of Engineering, Hanover | United States | mattmcgarrynz@gmail.com |
| 35 | McGrath, Deirdre | Nottingham NIHR BRC, Sir Peter Mansfield Imaging Centre, Queens Medical Centre, Nottingham | UK | Deirdre.mcgrath@nottingham.ac.uk |
| 36 | Mohtashamdolatshahi, Azadeh | BIOQIC, Institute for Radiology, Charité Berlin, Berlin | Germany | Azadeh.Mohtashamdolatshahi@charite.de |
| 37 | Pagé, Gwenaël | UMR 1149 Inserm, Paris | France | gwenael.page@inserm.fr |
| 38 | Paulsen, Keith D. | Thayer School of Engineering at Dartmouth, Hanover | United States | Keith.D.Paulsen@dartmouth.edu |
| 39 | Perrins, Michael | Centre for Inflammation Research, Edinburgh Imaging Facility, University of Edinburgh, Edinburgh | United Kingdom | M.Perrins@ed.ac.uk |
| 40 | Potze, Jan Hendrik | University Medical Center Groningen, Groningen | The Netherlands | jhpotze60@gmail.com |
| 41 | Prieur, Fabrice | Department of Informatics, University of Oslo, Oslo | Norway | fabrice@ifi.uio.no |
| 42 | Roberts, Neil | Edinburgh Imaging Facility, Queen's Medical Research Institute, University of Edinburgh, Edinburgh | United Kingdom | neil.roberts@ed.ac.uk |
| 43 | Romano, Anthony | Naval Research Laboratory, Washington, DC | United States | Anthony.romano@nrl.navy.mil |
| 44 | Ropele, Stefan | Department of Neurology, Medical University of Graz, Graz | Austria | Stefan.ropele@medunigraz.at |
| 45 | Sauer, Frank | Peter Debye Institute for Soft Matter Physics, Biological Physics Division, University of Leipzig, Leipzig | Germany | sauer@physik.uni-leipzig.de |
| 46 | Simons, Michiel | Edinburgh Imaging Facility, University of Edinburgh, Edinburgh | United Kingdom | msimons@nhs.net |
| 47 | Strasser, Johannes | Department of Neurology, Medical University of Graz, Graz | Austria | Johannes.strasser@medunigraz.at |
| 48 | Sudakova, Jelizaveta | St Thomas Hospital, London | United Kingdom | jelizaveta.sudakova@kcl.ac.uk |
| 49 | Tse Ve Koon, Kevin | CREATIS, Villeurbanne | France | kevin.tsevekoon@creatis.insa-lyon.fr |
| 50 | Uca, Yavuz Oguz | BIOQIC, Experimental Radiology, Charité Berlin, Berlin | Germany | Yavuz-oguz.uca@charite.de |
| 51 | Van Houten, Elijah | Département de genie méchanique, Université de Sherbrooke, Québec | Canada | eew.vanhouten@usherbrooke.ca |
| 52 | Vappou, Jonathan | ICube laboratory, CNRS-Université de Strasbourg, Strasbourg | France | jvappou@unistra.fr |
| 53 | Venkatesh, Sudhakar K. | Department of Radiology, Mayo Clinic, Rochester | United States | Venkatesh.sudhakar@mayo.edu |
| 54 | Webb, Jessica | King's College London, London | United Kingdom | Jessica.webb@kcl.ac.uk |
| 55 | Weber, David Paul | Department of Radiology, Charité Berlin, CBF, Berlin | Germany | david-paul.weber@charite.de |
| 56 | Werner, Patrick | BIOQIC, Leibnitz-Institut für Molekulare Pharmakologie, Berlin | Germany | werner@fmp-berlin.de |
| 57 | Wuerfel, Jens | MIAC (Medical Image Analysis Center), Basel | Switzerland | ceo-office@miac.ch |

## Map of social events